August 1987

UILU-ENG-87-2251
DC-96

COORDINATED SCIENCE LABORATORY
College of Engineering
Decision and Control Laboratory

LINEAR AND NONLINEAR CONTROLLER DESIGN FOR ELASTIC JOINT MANIPULATORS

Markus Albert
Mark W. Spong

UNIVERSITY OF ILLINOIS AT URBANA-CHAMPAIGN

Approved for Public Release. Distribution Unlimited.

REPORT DOCUMENTATION PAGE

1a. REPORT SECURITY CLASSIFICATION Unclassified	1b. RESTRICTIVE MARKINGS None
2a. SECURITY CLASSIFICATION AUTHORITY	3. DISTRIBUTION / AVAILABILITY OF REPORT Approved for public release; distribution unlimited
2b. DECLASSIFICATION / DOWNGRADING SCHEDULE	
4. PERFORMING ORGANIZATION REPORT NUMBER(S) UILU-ENG-87-2251 (DC-96)	5. MONITORING ORGANIZATION REPORT NUMBER(S)
6a. NAME OF PERFORMING ORGANIZATION Coordinated Science Lab University of Illinois	6b. OFFICE SYMBOL (If applicable) N/A
6c. ADDRESS (City, State, and ZIP Code) 1101 W. Springfield Avenue Urbana, IL 61801	7a. NAME OF MONITORING ORGANIZATION National Science Foundation 7b. ADDRESS (City, State, and ZIP Code) 1800 G Street, N.W. Washington, D.C. 20550
8a. NAME OF FUNDING / SPONSORING ORGANIZATION National Science Foundation	8b. OFFICE SYMBOL (If applicable)
8c. ADDRESS (City, State, and ZIP Code) 1800 G Street, N.W. Washington, D.C. 20550	9. PROCUREMENT INSTRUMENT IDENTIFICATION NUMBER NSF DMC 85-16091
	10. SOURCE OF FUNDING NUMBERS PROGRAM ELEMENT NO. / PROJECT NO. / TASK NO. / WORK UNIT ACCESSION NO.

11. TITLE (Include Security Classification)
LINEAR AND NONLINEAR CONTROLLER DESIGN FOR ELASTIC JOINT MANIPULATORS

12. PERSONAL AUTHOR(S)
Markus Albert and Mark W. Spong

13a. TYPE OF REPORT	13b. TIME COVERED	14. DATE OF REPORT (Year, Month, Day)	15. PAGE COUNT
Technical	FROM _____ TO _____	August 1987	100

16. SUPPLEMENTARY NOTATION

17. COSATI CODES			18. SUBJECT TERMS (Continue on reverse if necessary and identify by block number)
FIELD	GROUP	SUB-GROUP	joint elasticity, controller design, robot manipulators

19. ABSTRACT (Continue on reverse if necessary and identify by block number)

The problem of joint elasticity in robot manipulators is important to consider if rapid cycle-time is desired. Recent experimental work indicates that the resonant modes due to joint elasticity are a major factor limiting the closed loop bandwidth and hence arm cycle-time. In this report we describe a controller design for a single link manipulator taking into account the joint elasticity. Both linear and nonlinear models are analyzed using frequency domain, state space, and singular perturbation design techniques.

20. DISTRIBUTION / AVAILABILITY OF ABSTRACT ☒ UNCLASSIFIED/UNLIMITED ☐ SAME AS RPT. ☐ DTIC USERS	21. ABSTRACT SECURITY CLASSIFICATION Unclassified
22a. NAME OF RESPONSIBLE INDIVIDUAL	22b. TELEPHONE (Include Area Code) / 22c. OFFICE SYMBOL

TABLE OF CONTENTS

1. INTRODUCTION

In typical industrial manipulators the cycle time is limited due to flexibility in the robot structure. The reason is that structural vibrational modes of the arm may be excited if the acceleration of the arm is too high. Experimental work has shown that compliance in the structure arises mainly from the joints while the link compliance is relatively insignificant (in common robot designs, 2-20% of the total compliance arises from the link, dependent on the structure)[1]. Sources for joint elasticity can be gears, belts, tendons, bearings and hydraulic lines. One encounters considerable compliance especially when harmonic drives are used for speed reduction of the motors.[2] These harmonic drives are popular because of their compact design, high torque transmission and low backlash.[3]

The common approach is to use a rigid robot model for the controller design and to determine in an experimental worst-case study the maximum controller gain. However, in order to optimize cycle-time for every arm position and arm load, the joint flexibility has to be considered in the controller design.

The following report describes an analysis of a model of a single link elastic joint manipulator. We first discuss a classical PD-control of a linear model with feedback of the motor position, compare it with feedback of the link position, and discuss the trade-offs among controller gain, cycle-time, joint compliance, link inertia and damping. Our simulations show that the joint compliance in the structure severely limits the maximum speed of response attainable with PD-control, due to oscillations or instability which occurs as the compensator gain is increased.

Using a state space description of our model, we then show how the cycle-time can be considerably decreased if full state feedback is allowed. We design a linear, quadratic optimal controller which increases the speed of response by more than a factor of four without significantly increasing the input torque requirement. Since we assume only the link position is measured we construct a linear observer to estimate the full state from the measured output.

Using the insight gain from the linear design we then treat the nonlinear problem in section 5. We design a nonlinear state feedback controller based on the feedback linearization result of Su [4] and a nonlinear observer using the result of Krener and Isidori [5]. Our simulations show that the linear behavior of the system achieved in section 4 is exactly recovered in the nonlinear case by our nonlinear

observer/nonlinear state feedback controller.

In section 6. we show with a singular perturbation approach how to separate fast dynamics arising from the joint flexibility from the overall system behavior. This allows us to treat the design problem for the flexible joint, which is represented as a fourth order system, as one for a rigid joint which is of second order.

2. THE SINGLE LINK MODEL

For our analysis we use the single link models shown in Figures 2.1 and 2.2. The joint fixtures at the actuator (motor) side are represented by an inertia J_m. In the nonlinear model in Figure 2.1, the manipulator link including the load is modeled as a mass M whose center is at a distance l from the axis of rotation and through an inertia J_l about the axis of rotation. Since the contribution of the link to the overall compliance can be neglected, as is mentioned above, we consider only the joint compliance which is modeled as a linear spring of stiffness k, connecting the rotor and the link. On the actuator side as well as on the link side, damping coefficients B_m and B_l are considered.

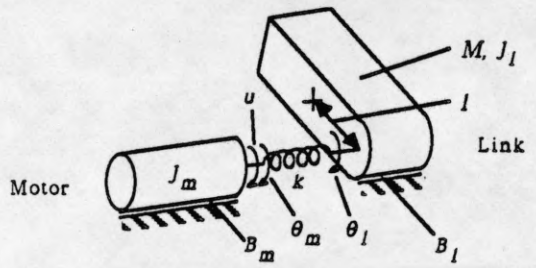

Figure 2.1 Nonlinear model of a single link elastic joint manipulator

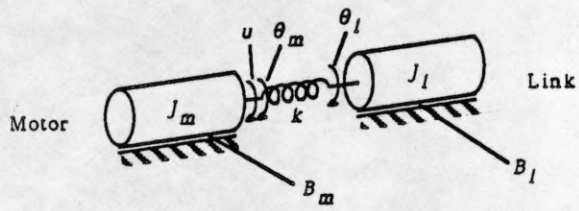

Figure 2.2 Lumped linear model of a single link elastic joint manipulator

The equations of motion for the nonlinear system of Figure 2.1 are easily shown to be

$$J_l \ddot{\theta}_l + B_l \dot{\theta}_l + Mgl \sin\theta_l + k(\theta_l - \theta_m) = 0 \tag{2.1}$$

$$J_m \ddot{\theta}_m + B_m \dot{\theta}_m - k(\theta_l - \theta_m) = u \tag{2.2}$$

where θ_l, θ_m are the link angle and motor shaft angle, respectively, and u is the input torque applied to the motor shaft. Because of the gravitational torque $Mgl \cdot \sin\theta_l$ the system is nonlinear.

The equations of motion for the lumped linear system of Figure 2.2 are

$$J_l \ddot{\theta}_l + B_l \dot{\theta}_l + k(\theta_l - \theta_m) = 0 \tag{2.3}$$

$$J_m \ddot{\theta}_m + B_m \dot{\theta}_m - k(\theta_l - \theta_m) = u \tag{2.4}$$

which are written in the frequency domain as

$$(J_l\, s^2 + B_l\, s + k)\cdot\theta_l(s) = k\,\theta_m(s)\,. \tag{2.5}$$

and

$$(J_m\, s^2 + B_m\, s + k)\cdot\theta_m(s) - k\,\theta_l(s) = u(s)\,, \tag{2.6}$$

The system (2.3) - (2.4) represents the nonlinear system (2.1) - (2.2) in the absence of the gravitational torque $Mgl\cdot\sin\theta_l$. The reason for considering the system (2.3) - (2.4) rather than a linearized (Taylor series) approximation of (2.1) - (2.2) will become clear in section 5.

3. CLASSICAL DESIGN

3.1. PD-control

3.1.1. Feedback of motor position θ_m

In common controller designs for industrial robot arms the motor angle is usually fed back for the simple reason that it is easier to measure than the link position. Figure 3.1 shows a PD-control for the linear system (2.5) - (2.6) with feedback of motor position.

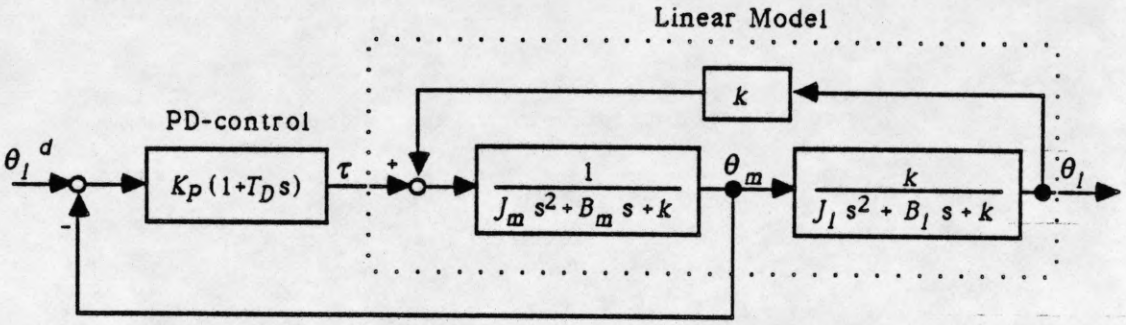

Figure 3.1 Block diagram for PD-control and motor position feedback

The open loop transfer function of this system is given by

$$G_{om} = K_p \cdot (1 + T_D\, s) \cdot \frac{\dfrac{1}{J_m\, s^2 + B_m\, s + k}}{1 - \dfrac{k^2}{(J_m\, s^2 + B_m\, s + k)(J_l\, s^2 + B_l\, s + k)}}$$

$$= K_p \cdot (1 + T_D\, s) \cdot \frac{J_l\, s^2 + B_l\, s + k}{(J_m\, s^2 + B_m\, s + k)(J_l\, s^2 + B_l\, s + k) - k^2} \qquad (3.1)$$

The corresponding root locus shown in Figure 3.2 allows conclusions about the system behavior.

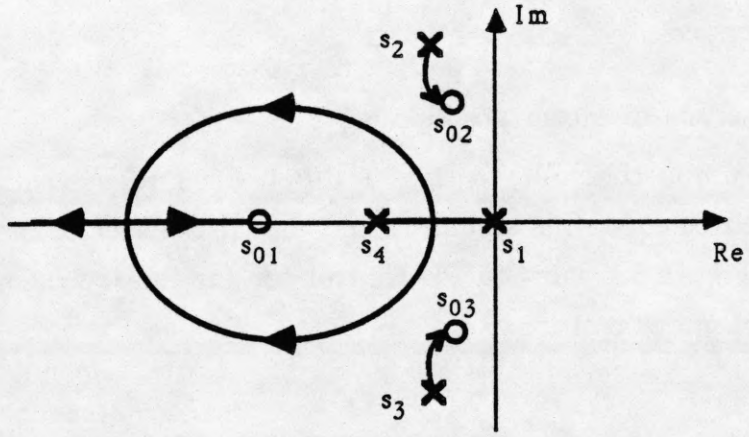

Figure 3.2 Root locus for PD-control and motor position feedback

G_{om} has poles at

$$s_1 = 0,\ s_2, s_3 \text{ and } s_4. \tag{3.2}$$

Poles s_2, s_3 are complex and s_4 is real.

Zeros of G_{om} are at

$$s_{01} = -\frac{1}{T_D},\quad s_{02}, s_{03} = -\frac{B_l}{2J_l} \pm \left(\frac{B_l^2}{4J_l^2} - \frac{k}{J_l} \right)^{\frac{1}{2}}. \tag{3.3}$$

The zeros s_{02}, s_{03} are complex because the link damping B_l is usually small in relation to the stiffness k.

Equation (3.3) shows that as the stiffness k increases the zeros s_{02}, s_{03} move towards higher frequencies. A plot of zero and pole locations in dependency of the stiffness k (Figure 3.3) confirms this and reveals furthermore that the same happens to the poles s_2, s_3. Hence, the complete outer branches of the root locus move towards higher frequencies. This means that resonant modes move towards higher frequencies and are less likely to be excited.

Pole s_4 moves towards the right for an increase in stiffness. Consequently, the poles of the closed loop system with the lower frequency become more dominant towards the higher frequency poles. This means for the transient response that oscillations of higher frequency diminish for an increasing stiffness. For an infinite

stiffness, the system is of second order and equivalent to one without consideration of joint compliance.

A plot of zero and pole locations in dependency of the link damping B_l shown in Figure 3.4 indicates that the whole root locus will move towards the left for an increase in link damping. This implies that oscillations in the system response become more and more damped.

Hence, we are likely to obtain faster responses with less oscillations for higher stiffness and for higher link damping. We note here that the system is stable for all values $K_p > 0$ of the controller gain. (The system parameters for Figures 3.3 and 3.4 are chosen as in section 3.2.)

3.1.2. Feedback of the link position θ_1

In later control designs we find more and more a feedback of the link position because it allows the achievement of a tighter control over the link angle. Therefore we analyze in the following the corresponding system behavior and take θ_l also as the output for the remainder of the report. The block diagram in Figure 3.5 shows a PD-control of the system (2.5) - (2.6) with feedback of link position.

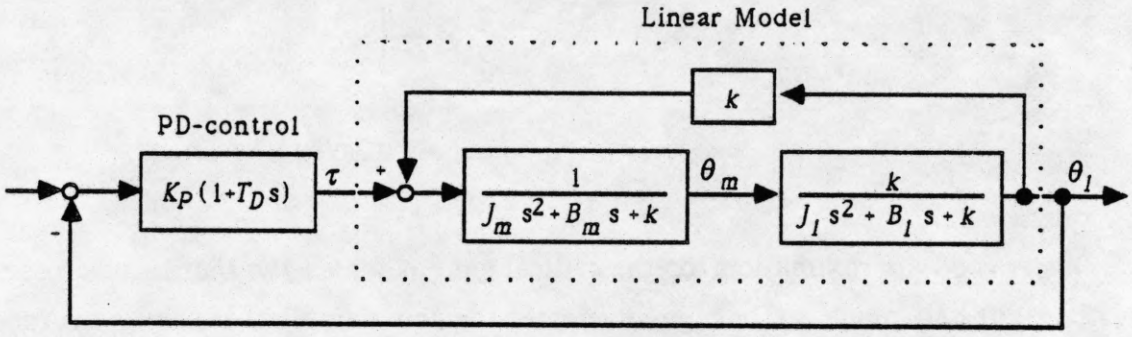

Figure 3.5 Block diagram for PD-control and link position feedback

The open loop transfer function of this system is given by

$$G_{ol} = K_p \cdot (1 + T_D\, s) \cdot \frac{\dfrac{k}{(J_m\, s^2 + B_m\, s + k)(J_l\, s^2 + B_l\, s + k)}}{1 - \dfrac{k^2}{(J_m\, s^2 + B_m\, s + k)(J_l\, s^2 + B_l\, s + k)}}$$

$$= K_p \cdot (1 + T_D\, s) \cdot \frac{k}{(J_m\, s^2 + B_m\, s + k)(J_l\, s^2 + B_l\, s + k) - k^2} \qquad (3.4)$$

The corresponding root locus in Figure 3.6 reveals, that the system is unstable for large gains K_p.

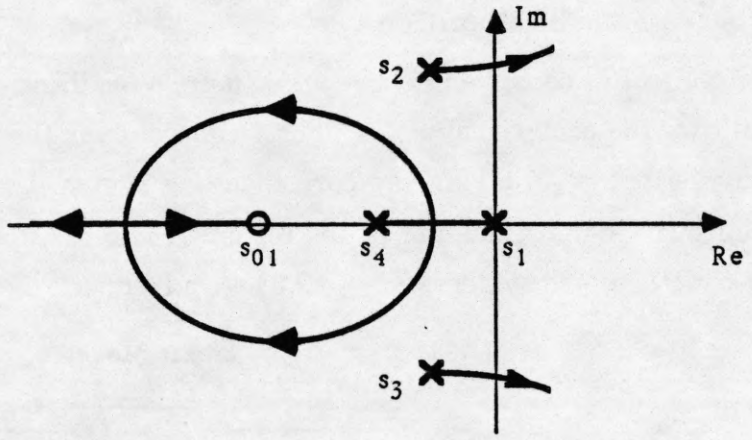

Figure 3.6 Root locus for PD-control and link position feedback

A good approximation for the critical gain at which the root locus crosses into the right half plane is (for high stiffnesses and low damping) as shown in Appendix I

$$K_{p_{crit.}} = \frac{1}{T_D} \cdot \left(\frac{J_l}{J_m} B_m + \frac{J_m}{J_l} B_l \right). \qquad (3.5)$$

The critical gain is independent of the stiffness (for $k >> B_m B_l / (J_m + J_l)$). Large gains can be implemented for large damping in the joint and large load and link inertias. However, an increase in the gain following an enlargement of these parameters does not induce automatically a high cycle-time, because then the

system becomes more inert towards an input signal.

3.2. Simulations

With the following simulations we demonstrate on a realistic model of a single joint manipulator the limits of an applied PD-control. The system parameters are the same as the one of a model used by Good/Sweet[2] and have the following values:

$k = 0.8\ \text{Nm/rad}$ $\qquad$ $B_m = 0.015\ \text{Nms/rad}$

$J_m = 0.0004\ \text{Nms}^2\text{/rad}$ $\qquad$ $B_l = 0.0\ \ \text{Nms/rad}$

$J_l = 0.0004\ \text{Nms}^2\text{/rad}$

The implemented controller is of the form $K_p \cdot (1 + T_D\ s)$. The parameter T_D is chosen to be 0.005 s for all simulations since it turns out to be convenient.

From the frequency responses of the open loop system shown in Figures 3.7 and 3.8 we can see that the system has a strong resonant/anti-resonant behavior especially for feedback of the motor position. The magnification curve for feedback of θ_m has a relative maximum at $f_r^m = 9.87\ \text{Hz}$ while that maximum is $f_r^l = 9.07\ \text{Hz}$ for feedback of θ_l. These resonant peaks mean a limit to an increase of the controller gain. If the gain is chosen too high, resonant modes are excited.

Figures 3.9 and 3.10 show the exact root loci for the above system parameters. The zero s_{01} lies at -200 and is therefore not included in the plots. Although the shapes of the root loci differ slightly from Figures 3.2 and 3.6 because of the parameter configuration, it is still equivalent to the shape derived theoretically. Figure 3.10 shows clearly the crossing of the root locus into the right half plane for high gains while the root locus for feedback of θ_m (Figure 3.9) only approaches the imaginary axis without crossing it.

The highest possible gain for a unit step response without overshoot is found experimentally to be $K_p = 0.105$ for a feedback of θ_l. From the corresponding response shown in Figure 3.12 a rise time of $T_r = 0.219\ \text{s}$ and a settling time of $T_s = 0.312\ \text{s}$ is measured. If we increase K_p from the critical value of 0.105 by 50% and 100% the step response shows slight oscillations of higher frequencies, as

we predicted already (Figure 3.13). Figure 3.14 shows the torque u corresponding to the step response for $K_p = 0.105$. The input for these responses is a step of θ_l^d from 0 rad to 1 rad, and the pole locations for the closed loop system are at $s_1, s_2 = -10.73 \pm j\,5.83$ and $s_3, s_4 = -8.02 \pm j\,58.67$.

Figure 3.12 shows that θ_m oscillates slightly about the link position. This originates from the joint flexibility and link inertia which introduce a certain delay and damping of the movements of θ_l related to θ_m.

The transient response for feedback of the motor position shown in Figure 3.11 is almost identical to the response for feedback of θ_l and is therefore not analyzed in detail.

3.2.1. Trade-off between gain and stiffness

Since the natural frequency of our model is given by $f_n = \sqrt{k \,/\, J_{eff}}$ [6] we expect that an increase of the stiffness k results in the movement of resonant modes towards higher values. This is confirmed by simulations of the frequency response of the system for a stiffness of $k = 4.0$ Nm/rad. Figures 3.15 and 3.16 show that the relative maxima in the magnification curves increased to $f_r = 16.55$ Hz for both feedback of motor position and feedback of link position.

The root locus plots in Figures 3.17 and 3.18 confirm this, too. The outer branches move towards higher frequencies while the inner branches remain close to their previous frequencies.

However, this does not imply a higher possible controller gain, as equation (3.5) already suggests. Since the stiffness is higher, the load side of the manipulator is coupled more directly with the motor side and with the input torque. An experimental approach confirms this. For an increase of k to 4.0 Nm/rad the maximum value for K_p remains 0.105 as it is derived for $k = 0.8$ Nm/rad. Figure 3.20 shows that rise and settle time of the unit step response also remain almost unchanged at $T_r = 0.232$ s and $T_s = 0.316$ s.

If we raise the gain K_p by about 50% and 100% from the critical value of 0.105 we obtain an overshoot similar to the one for $k = 0.8$ Nm/rad (Figure 3.21). The only difference here is that the higher frequency oscillations almost disappear, as frequency responses and root loci already suggested.

Figure 3.20 also shows that the variations between motor and link position observed previously for a smaller stiffness disappeared which is due to a stiffer coupling between motor and link.

The transient response for feedback of the motor position shown in Figure 3.19 is again very similar to the response for feedback of θ_l.

3.2.2. Trade-off between gain and inertia

An increase of the manipulator load to $J_l = 0.0012$ Nms^2/rad results in lower frequencies of the relative maxima in the magnification curve, as simulations of our system shown in Figures 3.22 and 3.23 indicate. The relative maximum for feedback of θ_l almost even disappears. The relative maxima for feedback of the motor position lies now at $f_r^m = 7.64$ Hz as does the corner frequency for feedback of θ_l. This leads to the conclusion that the controller gain K_p has to be kept smaller in order to not excite resonant modes.

The root locus plots in Figures 3.24 and 3.25 show, however, that the higher frequency poles of the closed loop system are now less dominant than before as the pole s_4 moved towards the right. This allows the second conclusion that even though the resonant modes are at lower frequencies they are not more likely to become excited because the lower frequency poles dominate for all gains K_p.

The unit step response for the system with a larger load inertia of $J_l = 0.0012$ Nms^2/rad has an overshoot of about 8.3% for the critical gain of $K_p = 0.105$ which we have derived previously for $J_l = 0.0004$ Nms^2/rad (Figure 3.26). An experimental approach shows that the maximum value for K_p without overshoot is here 0.045 for the larger load inertia. Figure 3.28 shows the unit step response for the reduced controller gain with a rise time of $T_r = 0.527$ s and a settle time of $T_s = 0.75$ s.

Also, the step response is now free of the oscillations that the system had for the smaller load inertia. The oscillations of the motor angle about the link angle positions in the step response also disappeared except for a minor displacement in the beginning of the angle change. This is a result of the higher inertia of the system which leads to smoother changes in the link position and consequently less oscillations on the motor side of the arm.

In Figure 3.27 the transient response for feedback of the motor position is given. It shows no difference to the step response for feedback of θ_l.

3.2.3. Trade-off between gain and damping

An increase of the damping B_l in the gears and at the end of the manipulator arm leaves the frequencies of the relative maxima/corner frequency in the magnification curves almost unchanged at $f_r^m = 9.71$ Hz and $f_r^l = 10.35$ Hz (Figures 3.29 and 3.30). The anti-resonance/resonance behavior is not as strong anymore as for a damping of $B_l = 0$, and the relative maxima for feedback of θ_l disappeared again.

The higher damping lets the root loci as a whole move towards the left (Figure 3.31 and 3.32), as we predicted before. This suggests that although the resonant modes remain unchanged in their frequencies they become more damped due to the increase in damping.

Because the damping B_l decouples motor and link position more in comparison to the case where B_l equals zero, it is now possible to raise the controller gain K_p to higher values without inducing an overshoot of the link position. In an experimental approach, K_p could be increased up to 0.35 for a feedback of the link position. The corresponding rise and settle times $T_r = 0.121$ s and $T_s = 0.182$ s, determined from the plot in Figure 3.33, indicate that not only resonant modes are less likely excited for a higher link damping but also much faster responses can be achieved.

The decoupling between motor and link position also leads to a remarkable difference in the time response between the system with feedback of θ_m and the system with feedback of θ_l. For the former system, the controller gain K_p can even be raised to 0.5 with corresponding times of $T_r = 0.11$ s and $T_s = 0.164$ s as shown in Figure 3.34. However, the tracking accuracy is then smaller because only θ_m is measured.

Figure 3.35 shows the price we have to pay for the increase in response speed. The link damping leads to a relatively large displacement between motor and link position which causes in the worst case damage in the gears or even breaks the arm.

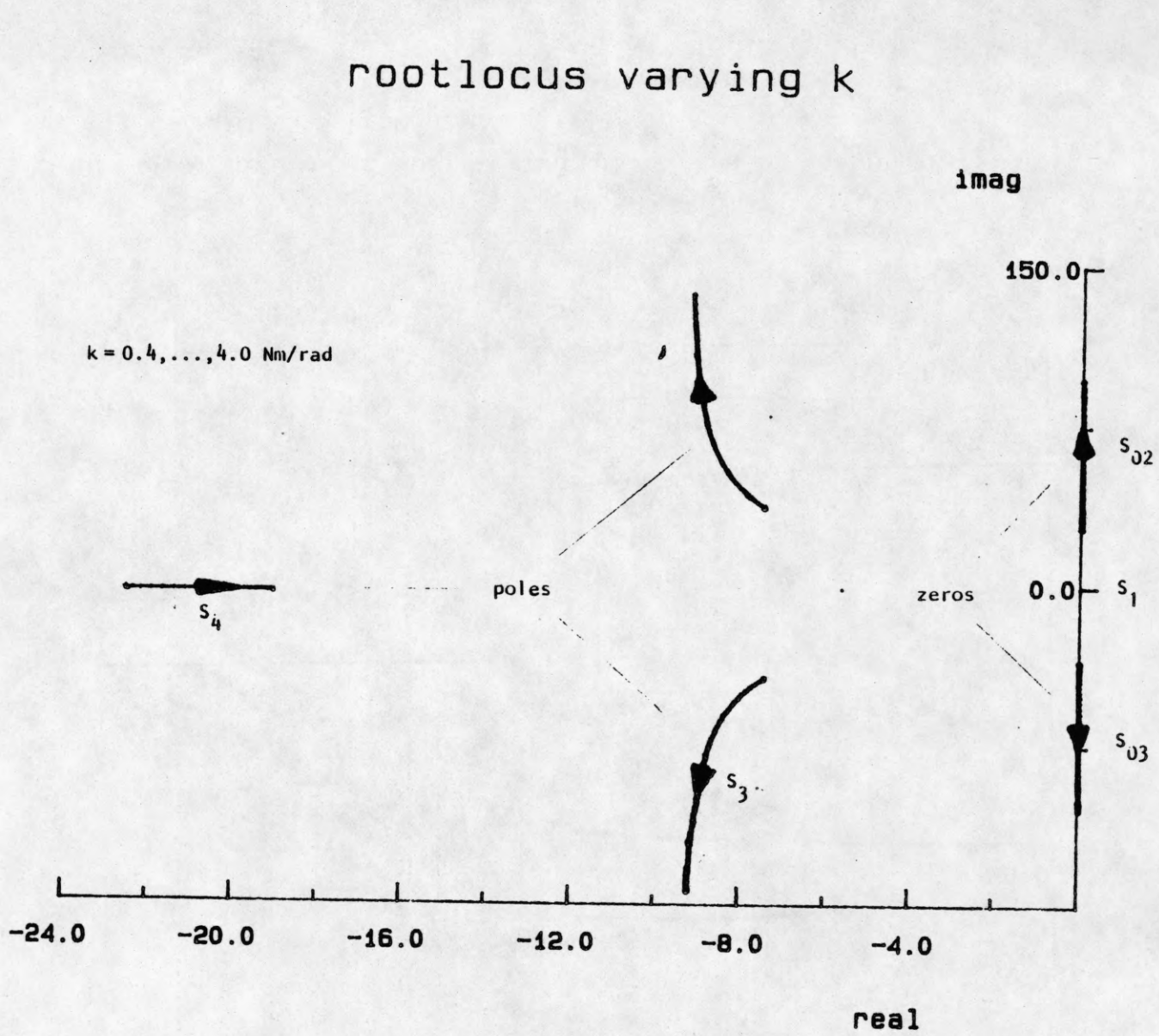

Figure 3.3 Rootlocus for PD-controlled system and variation of the stiffness

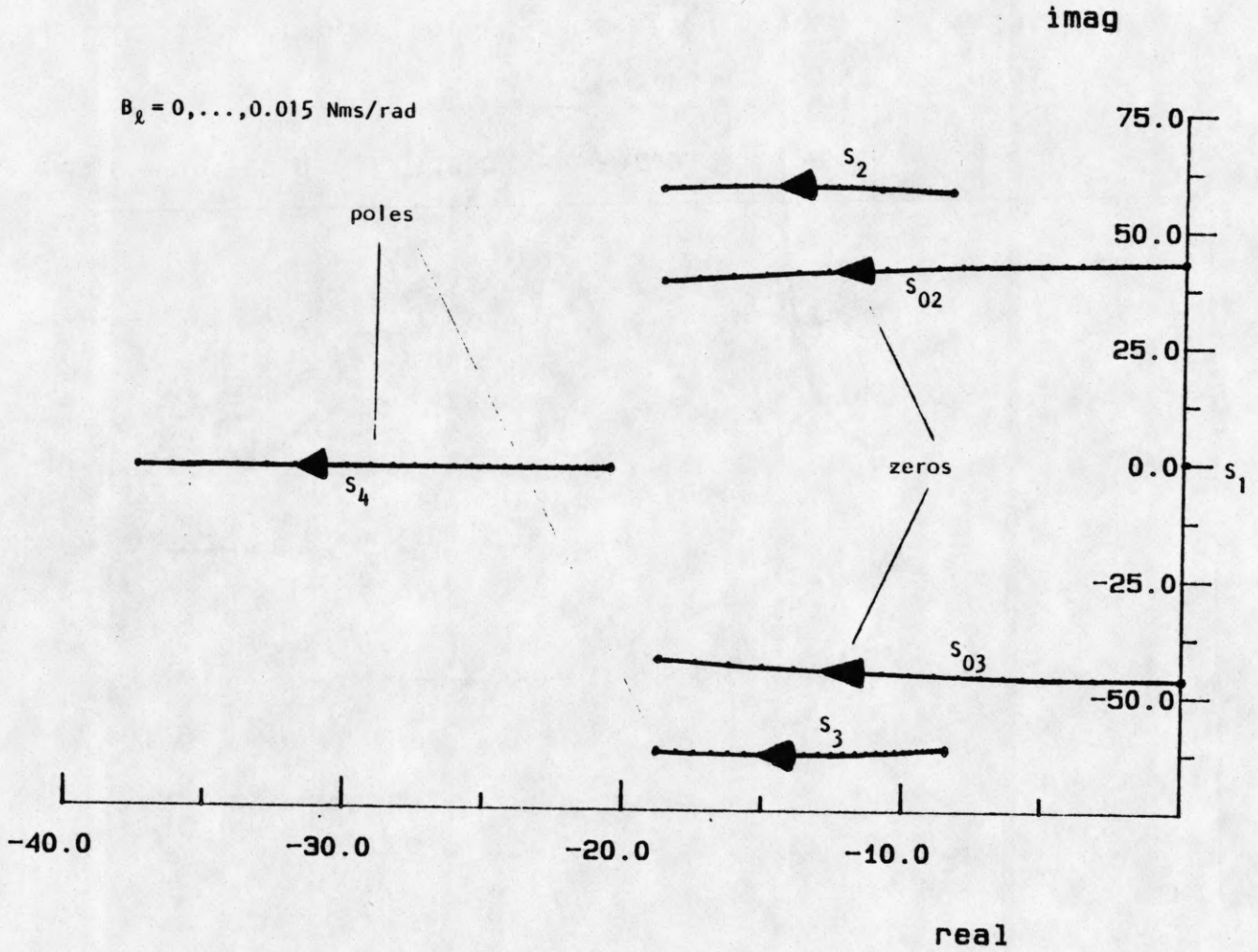

Figure 3.4 Rootlocus for PD-controlled system and variation of the link damping

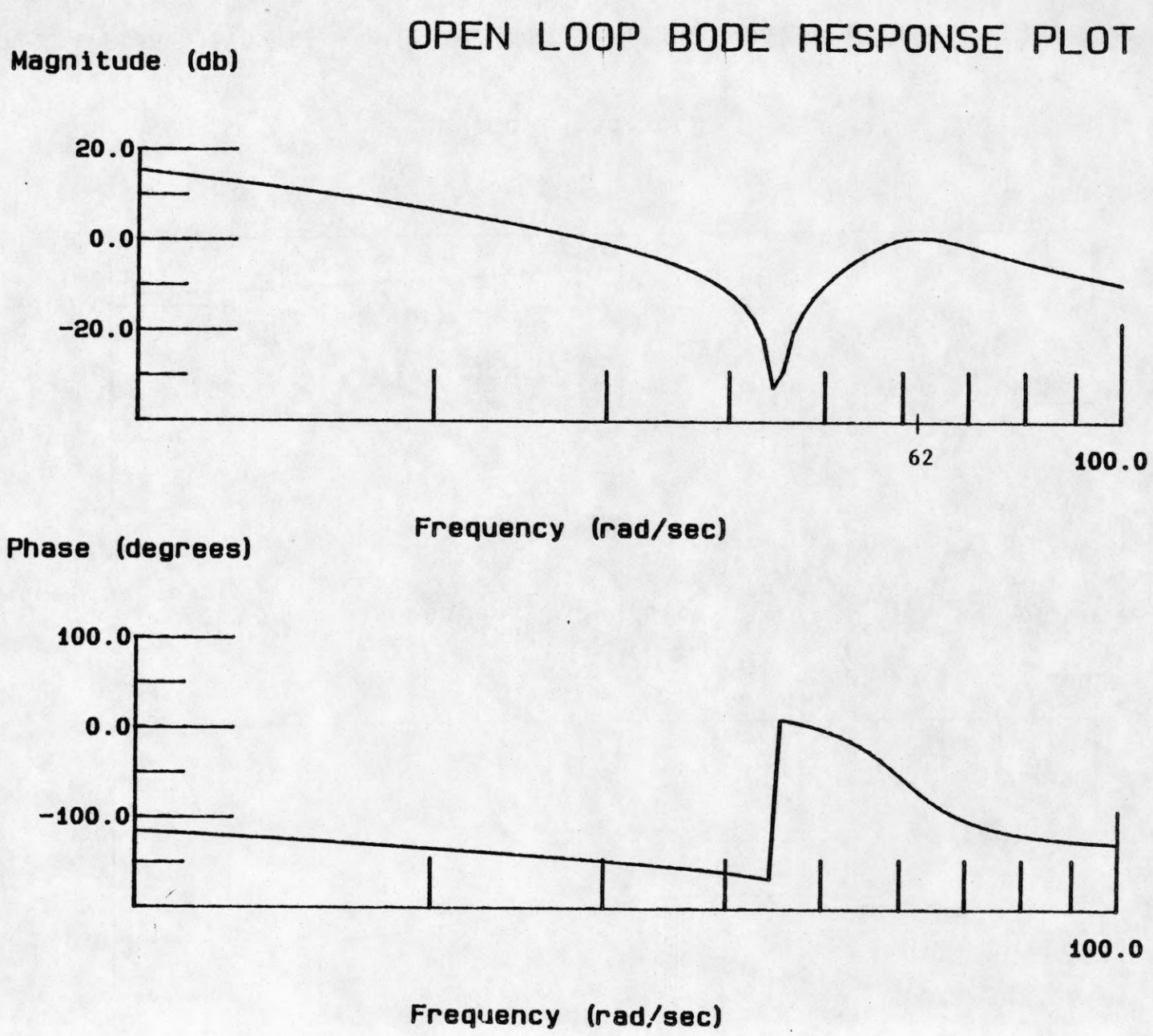

Figure 3.7 Bode plot for PD-controlled system, motor position feedback, k = 0.8 Nm/rad

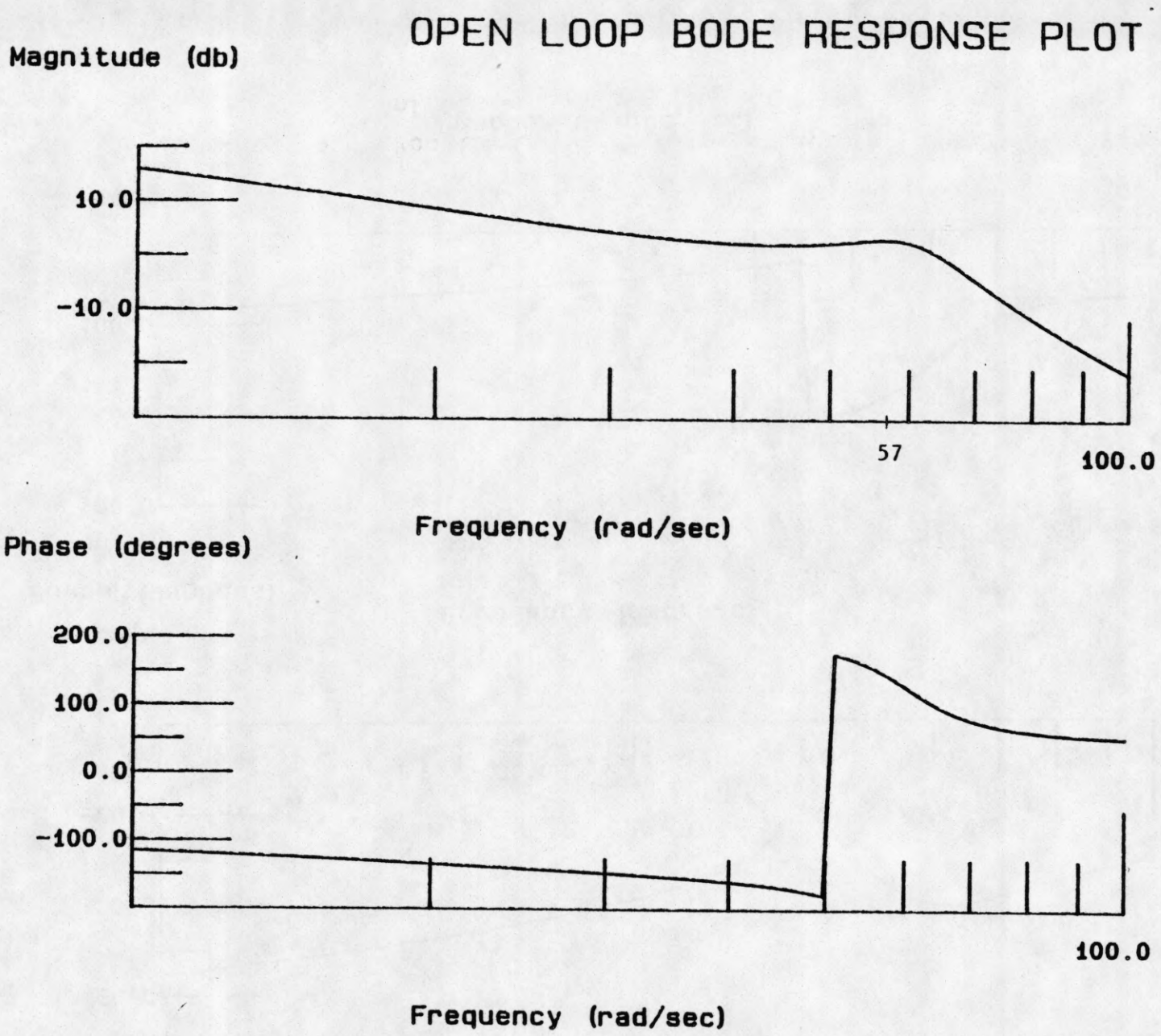

Figure 3.8 Bode plot for PD-controlled system, link position feedback, k = 0.8 Nm/rad

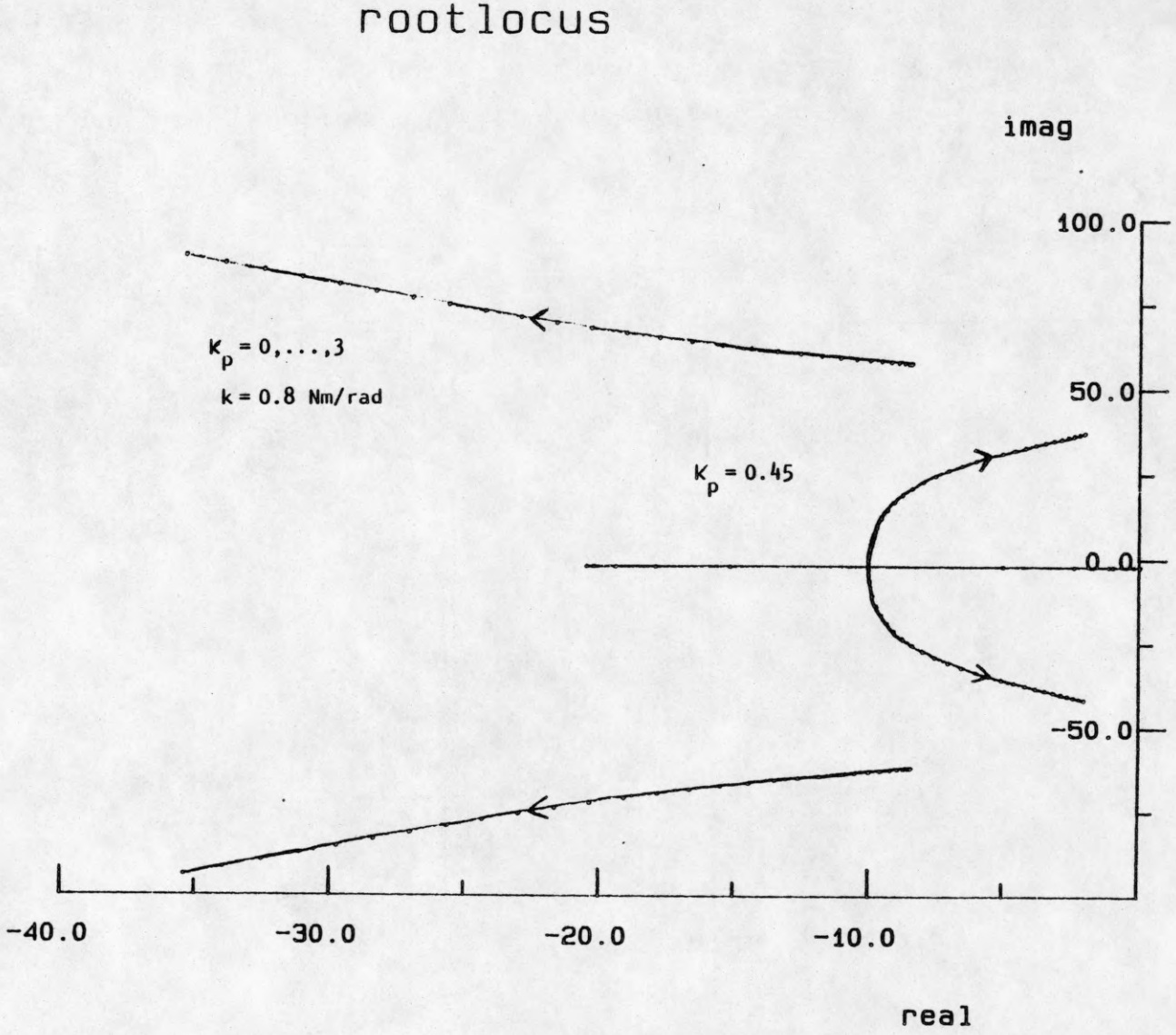

Figure 3.9 Rootlocus for PD-controlled system and variation of the controller gain, motor position feedback

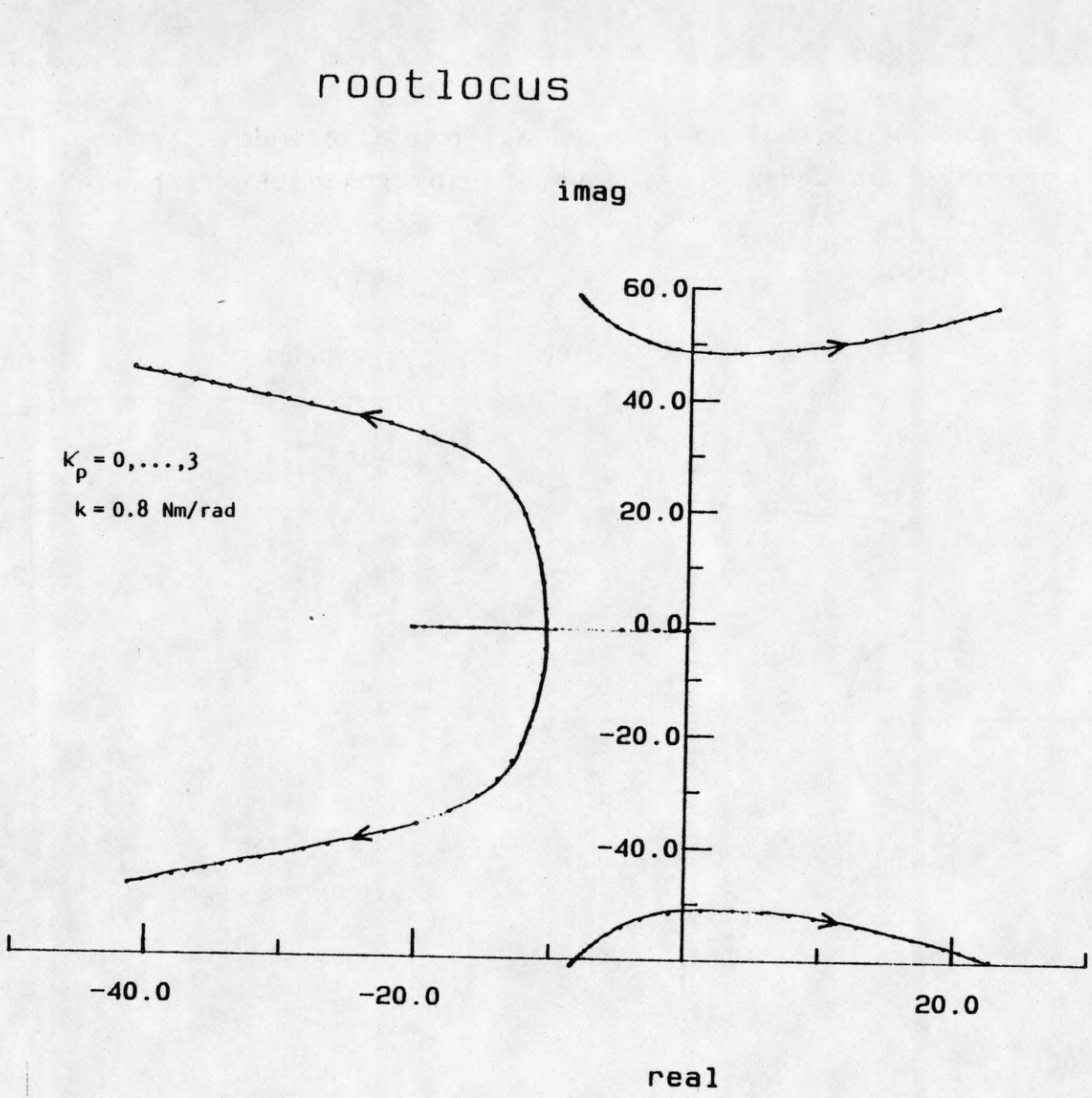

Figure 3.10 Rootlocus for PD-controlled system and variation of the controller gain, link position feedback

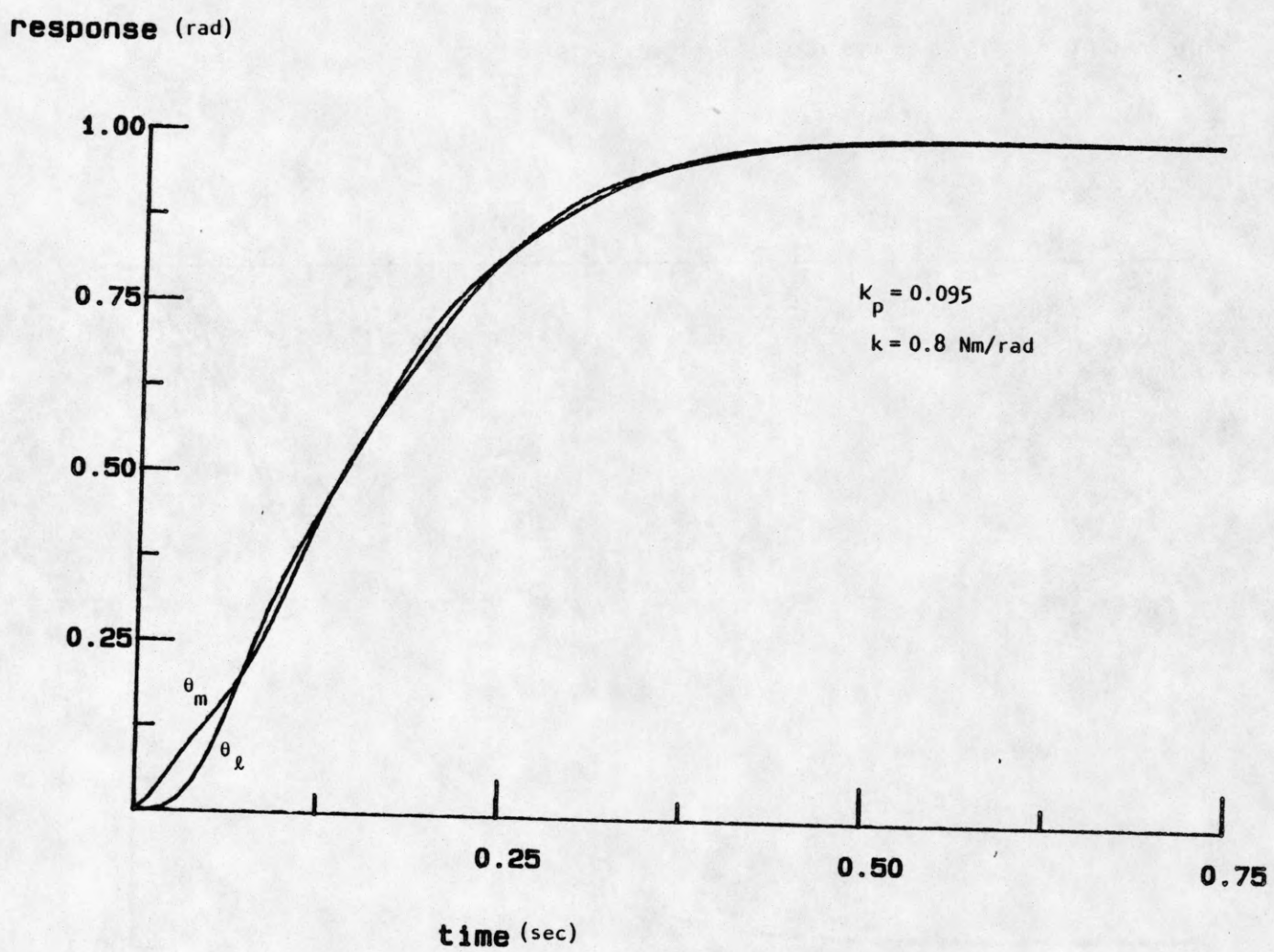

Figure 3.11 Step response for PD-controlled system, motor position feedback

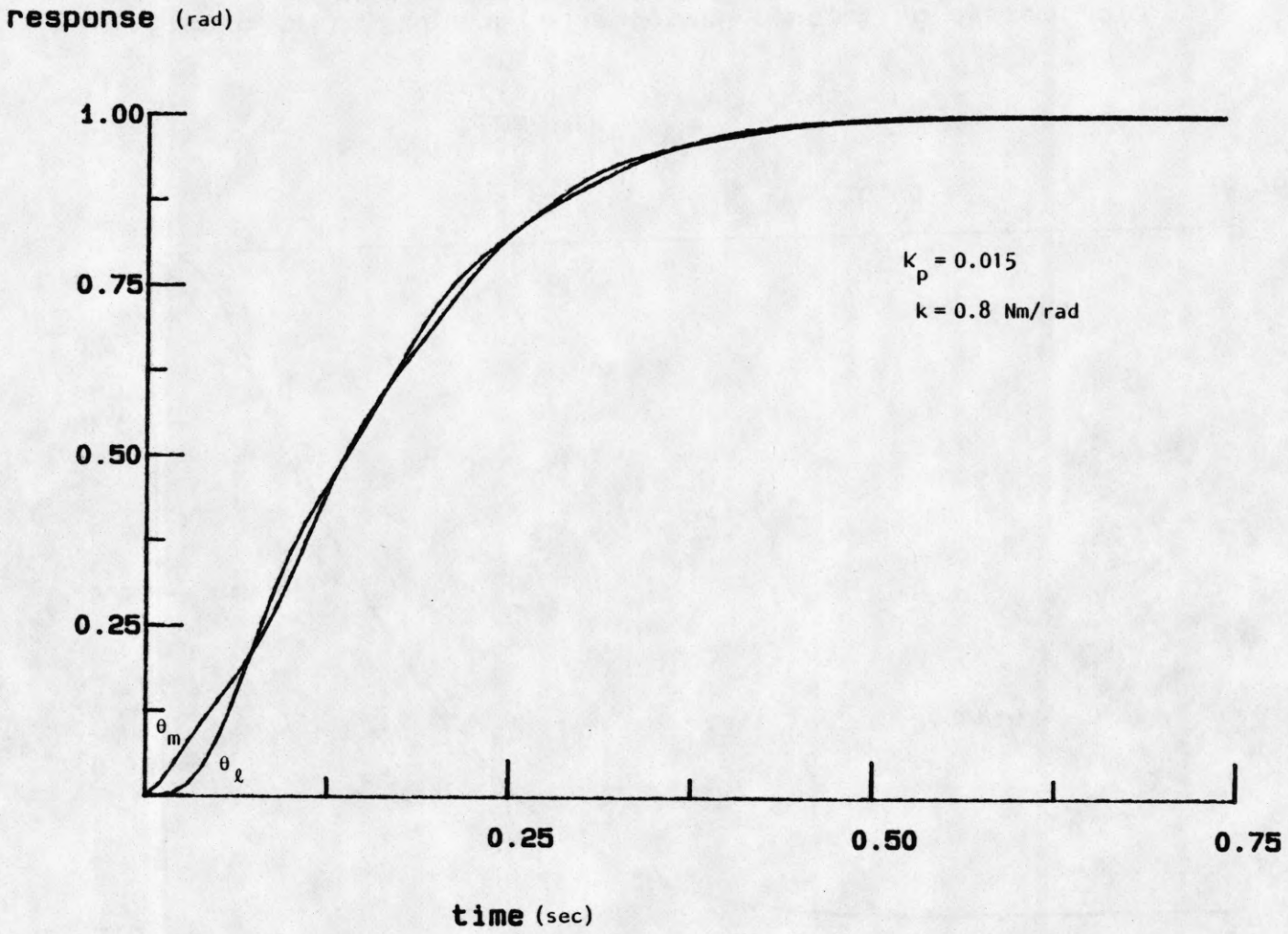

Figure 3.12 Step response for PD-controlled system, link position feedback

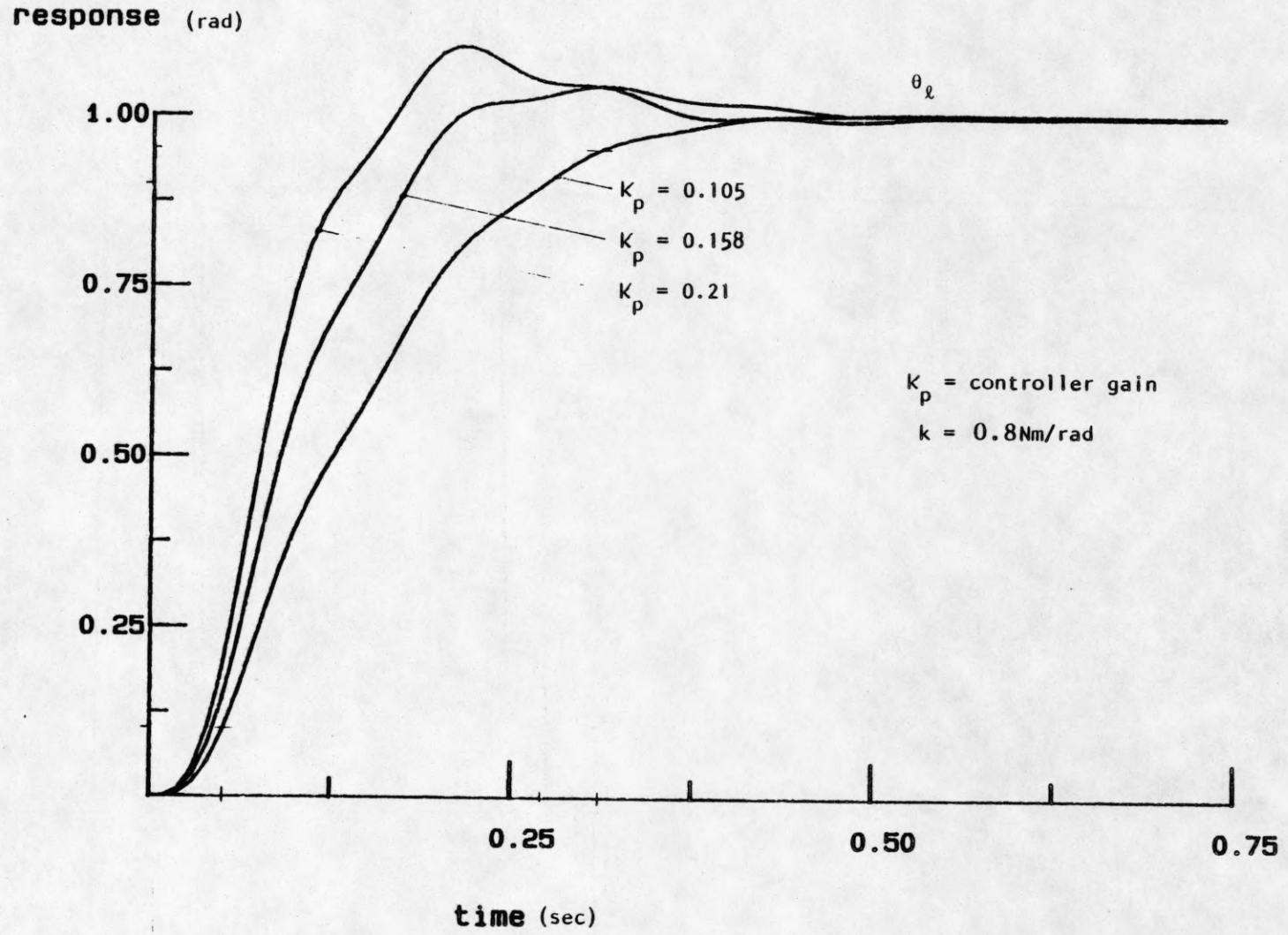

Figure 3.13 Step response for PD-controlled system, link position feedback

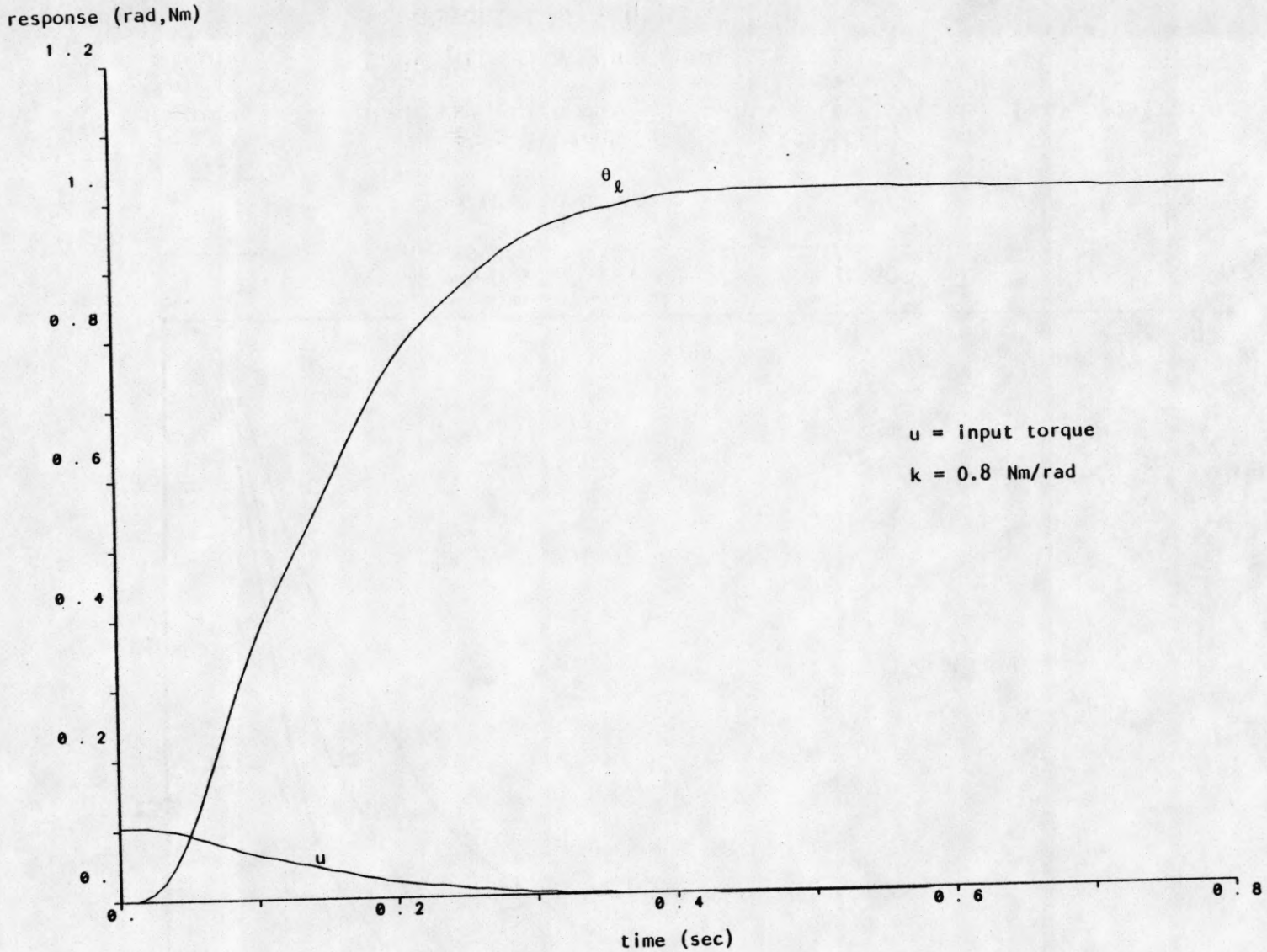

Figure 3.14 Input torque for PD-controlled system, link position feedback

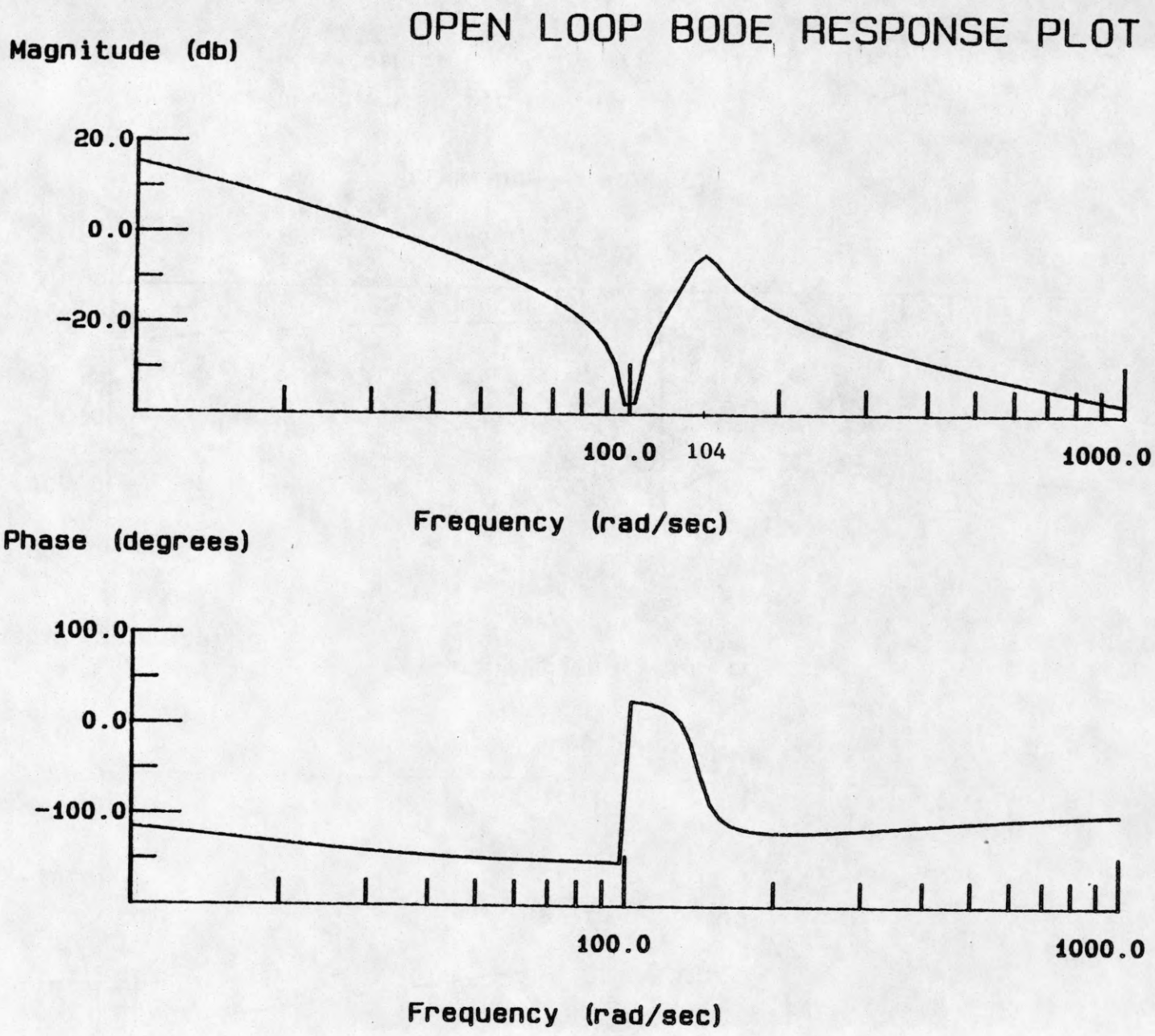

Figure 3.15 Bode plot for PD-controlled system, motor position feedback, k = 4.0 Nm/rad

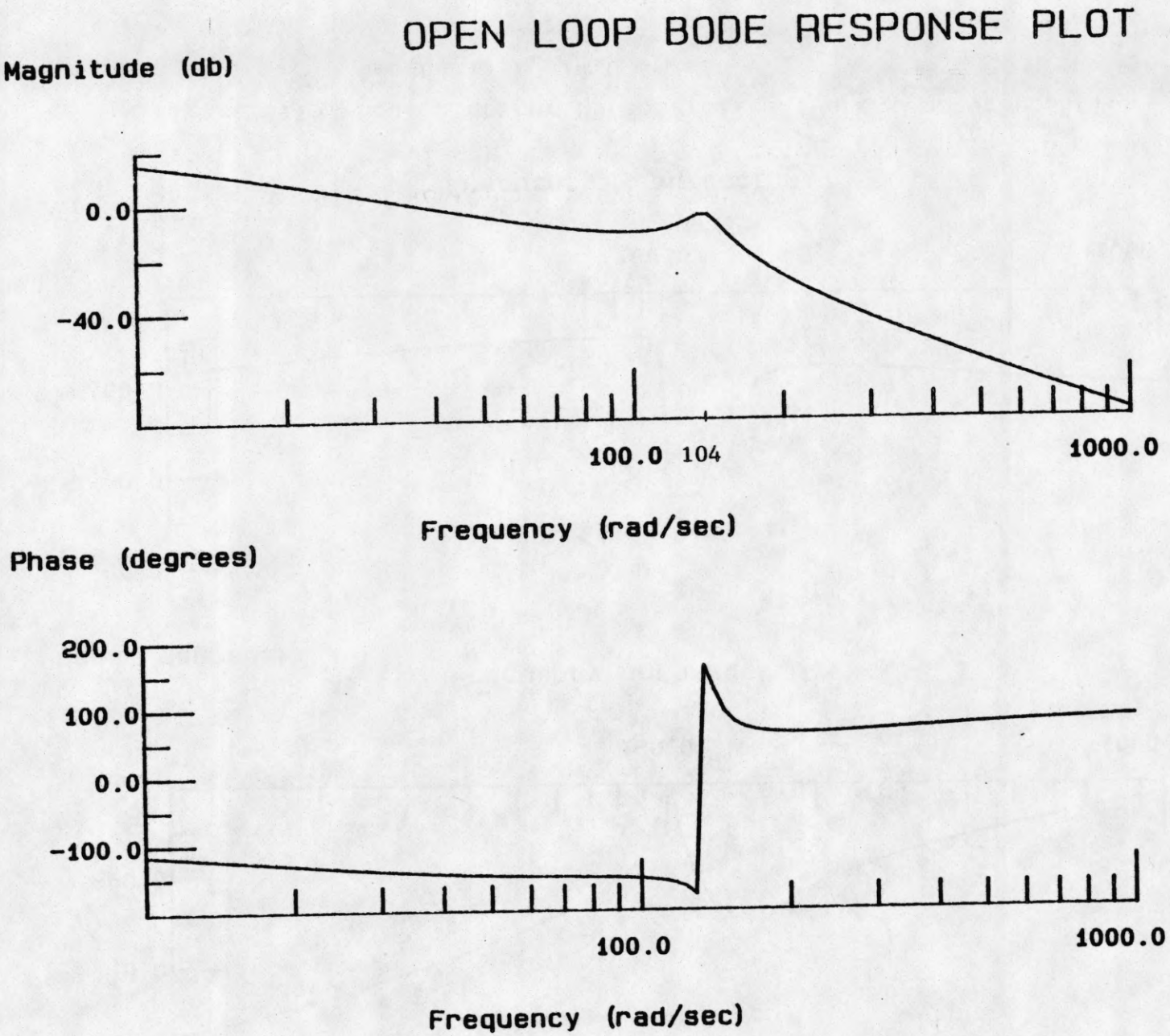

Figure 3.16 Bode plot for PD-controlled system, link position feedback, k = 4.0 Nm/rad

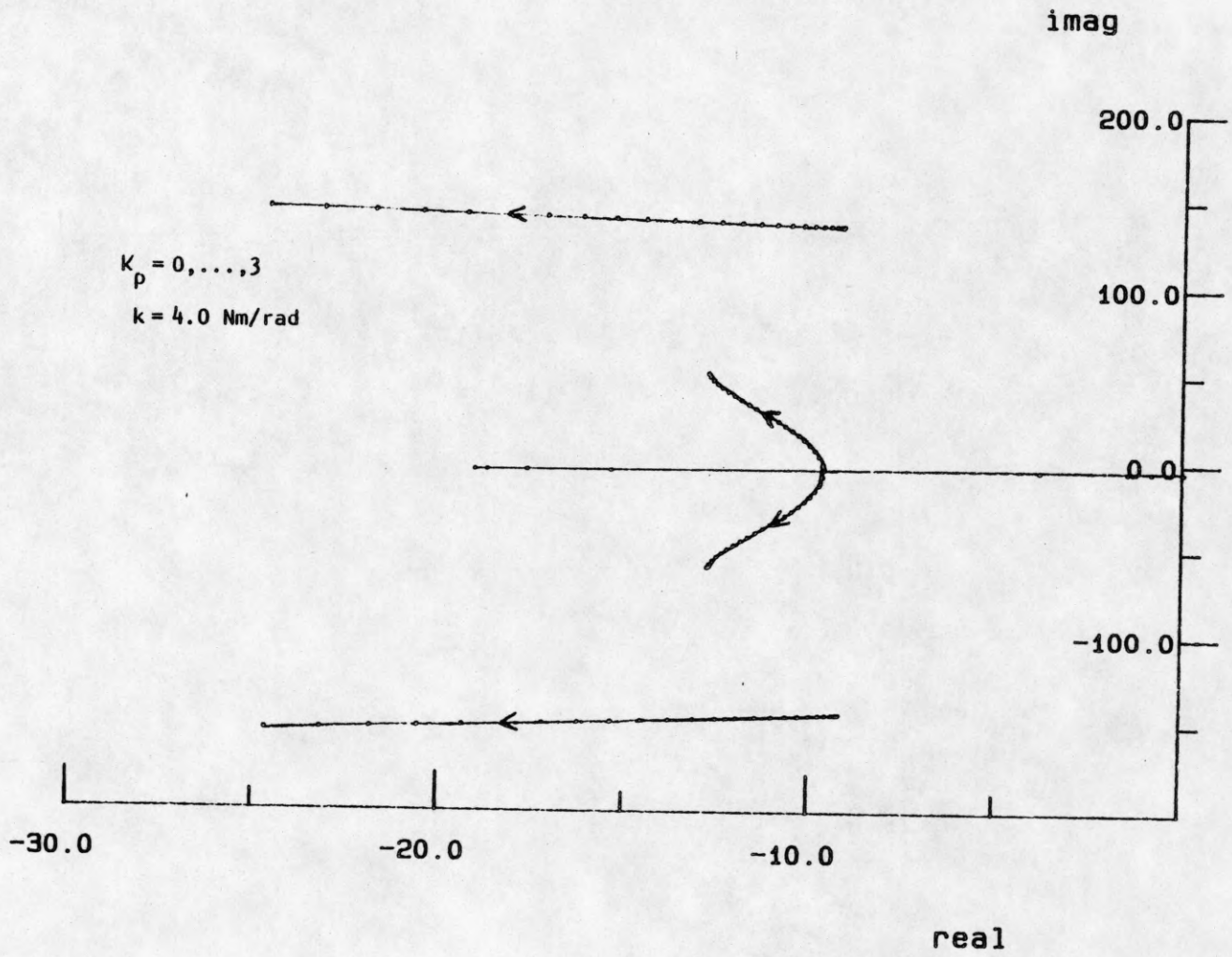

Figure 3.17 Rootlocus for PD-controlled system and variation of controller gain, motor position feedback

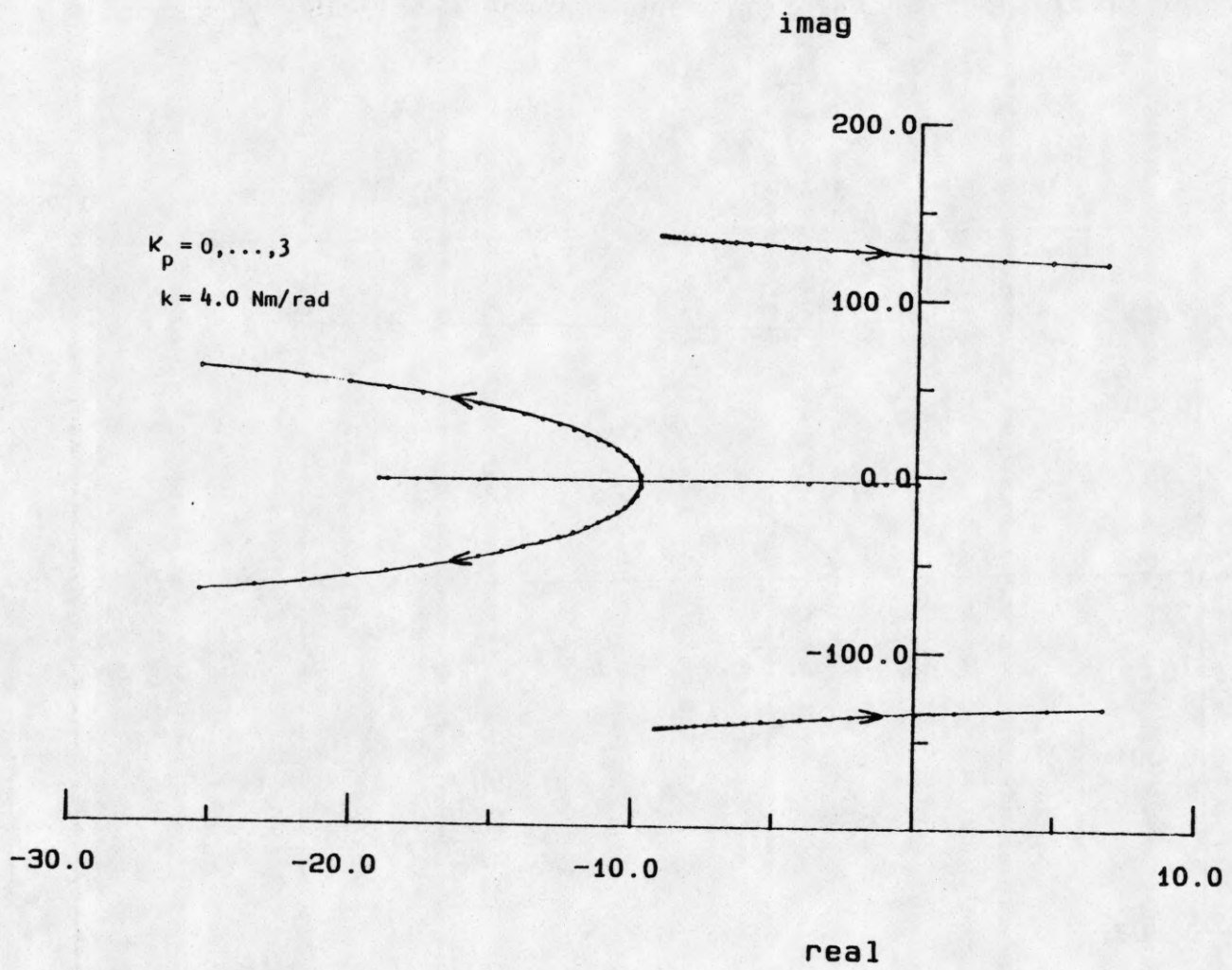

Figure 3.18 Rootlocus for PD-controlled system and variation of controller gain, link position feedback

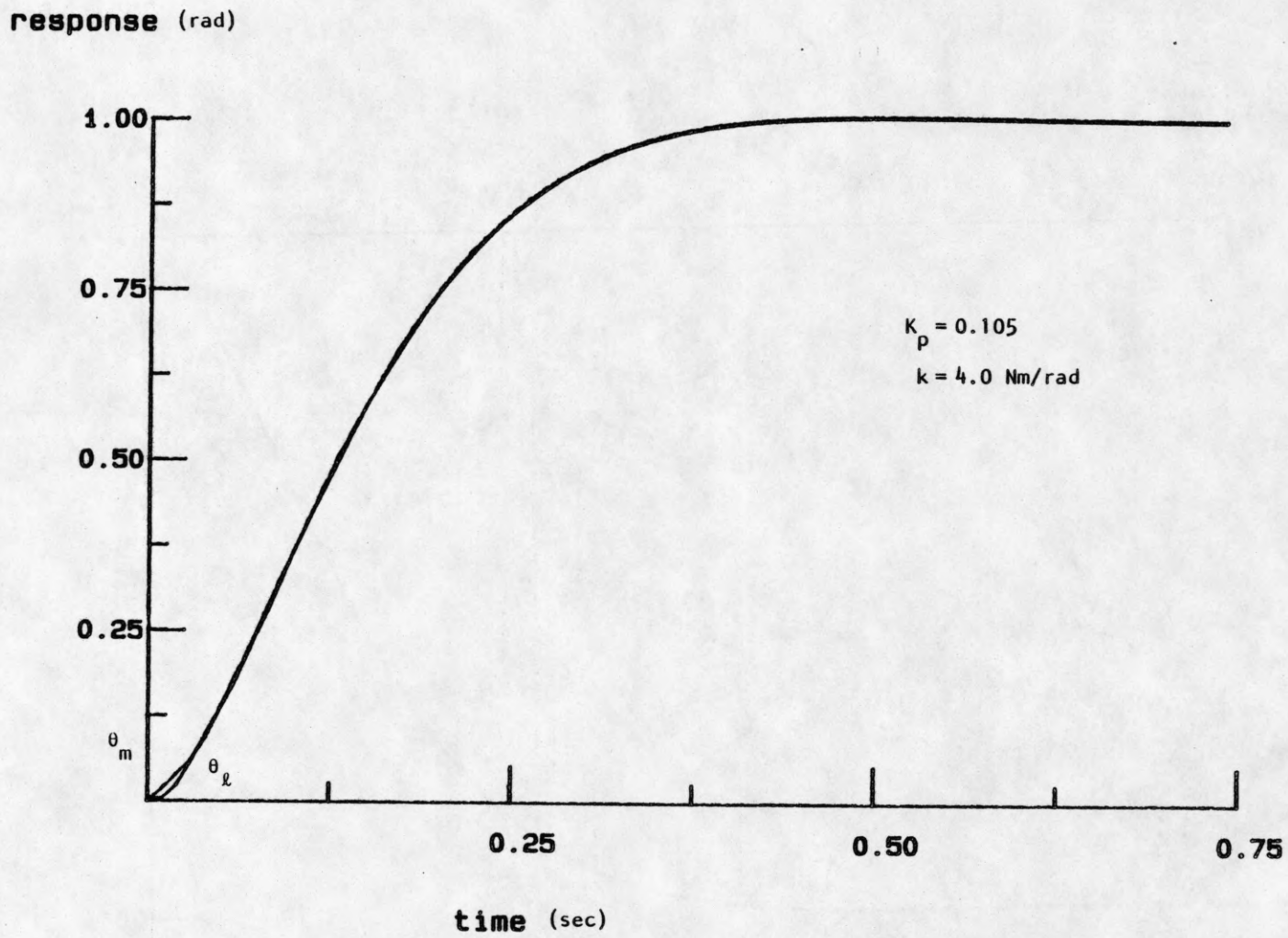

Figure 3.19 Step response for PD-controlled system, motor position feedback

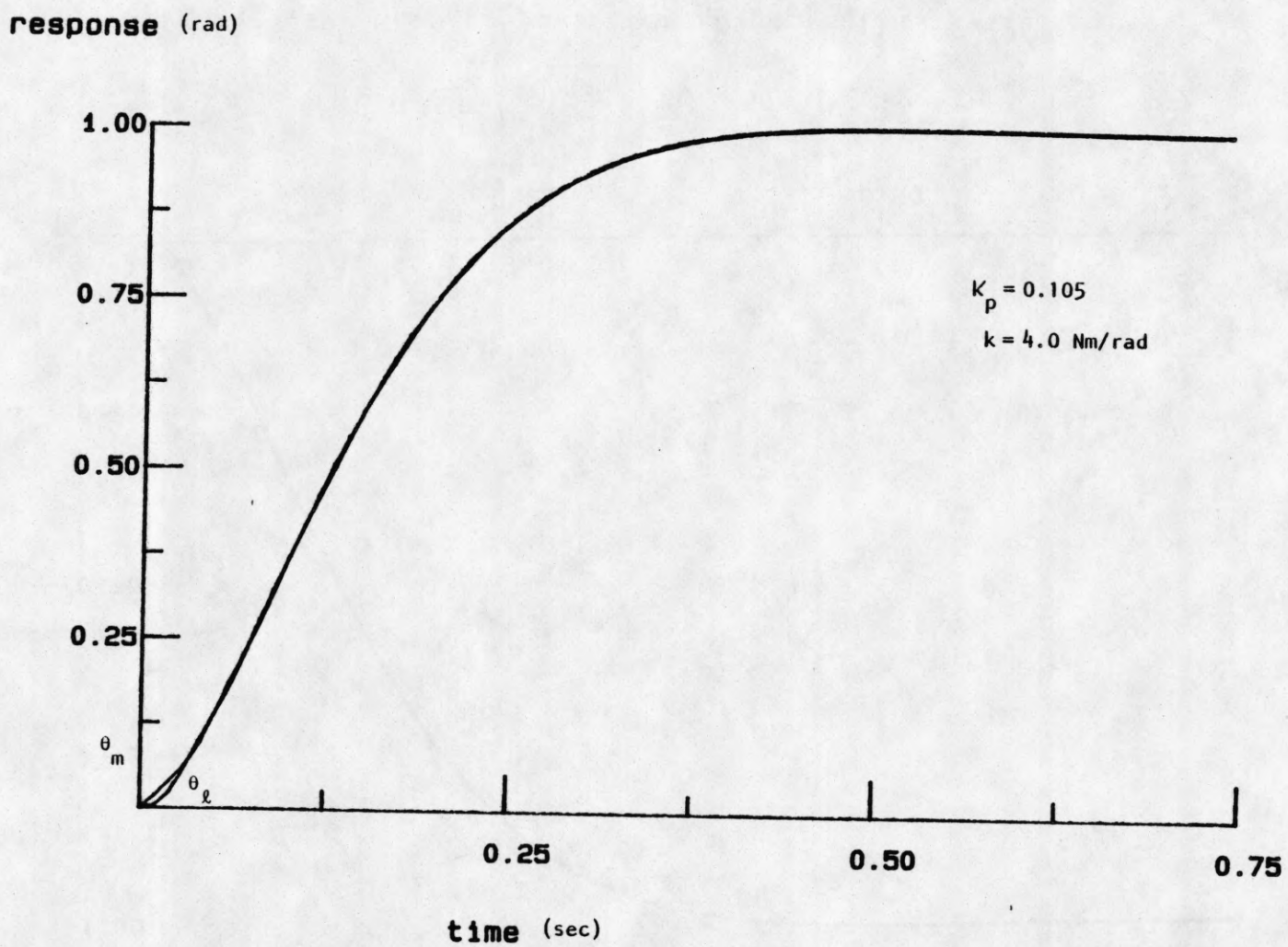

Figure 3.20 Step response for PD-controlled system, link position feedback

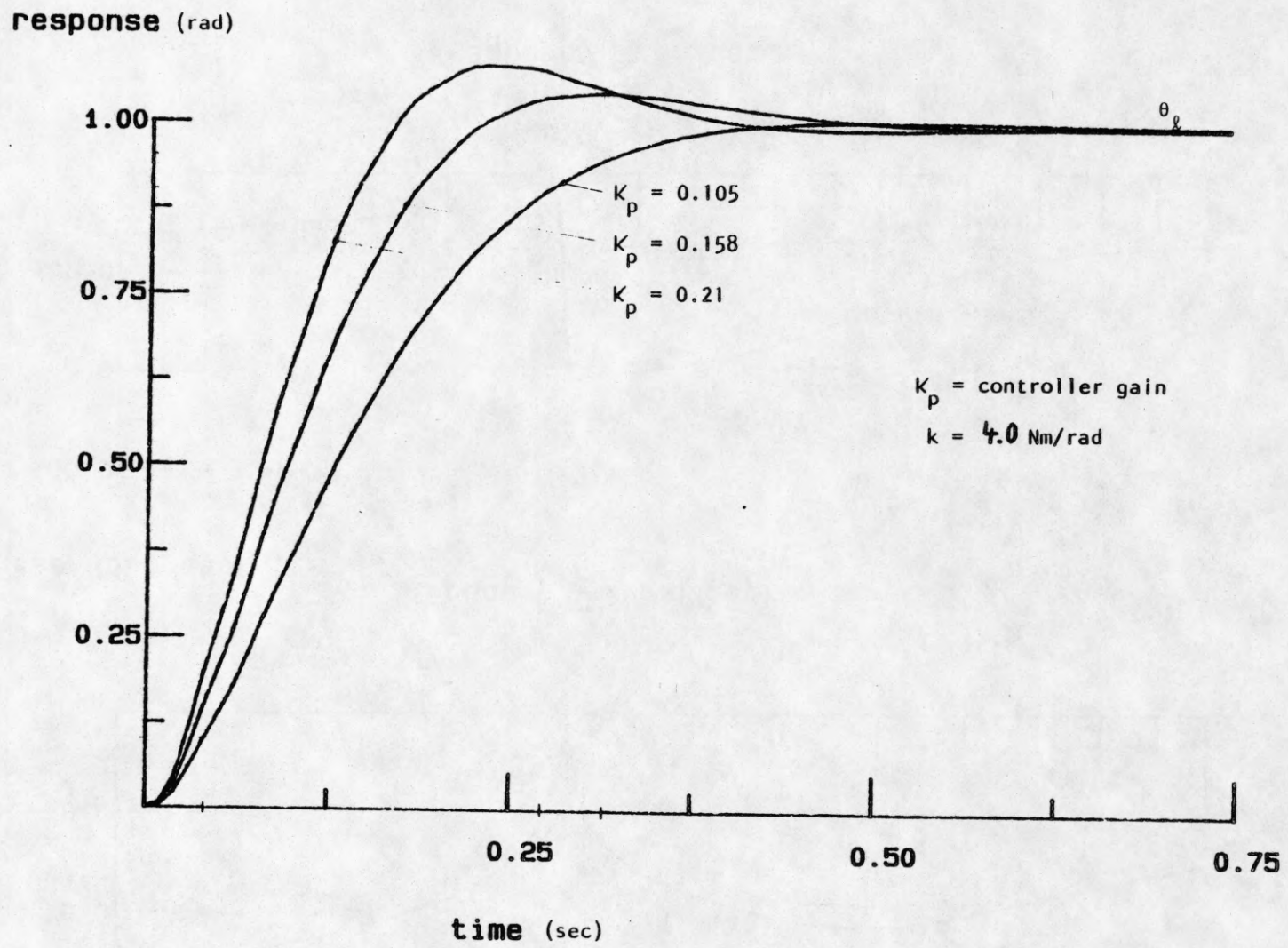

Figure 3.21 Step response for PD-controlled system, link position feedback

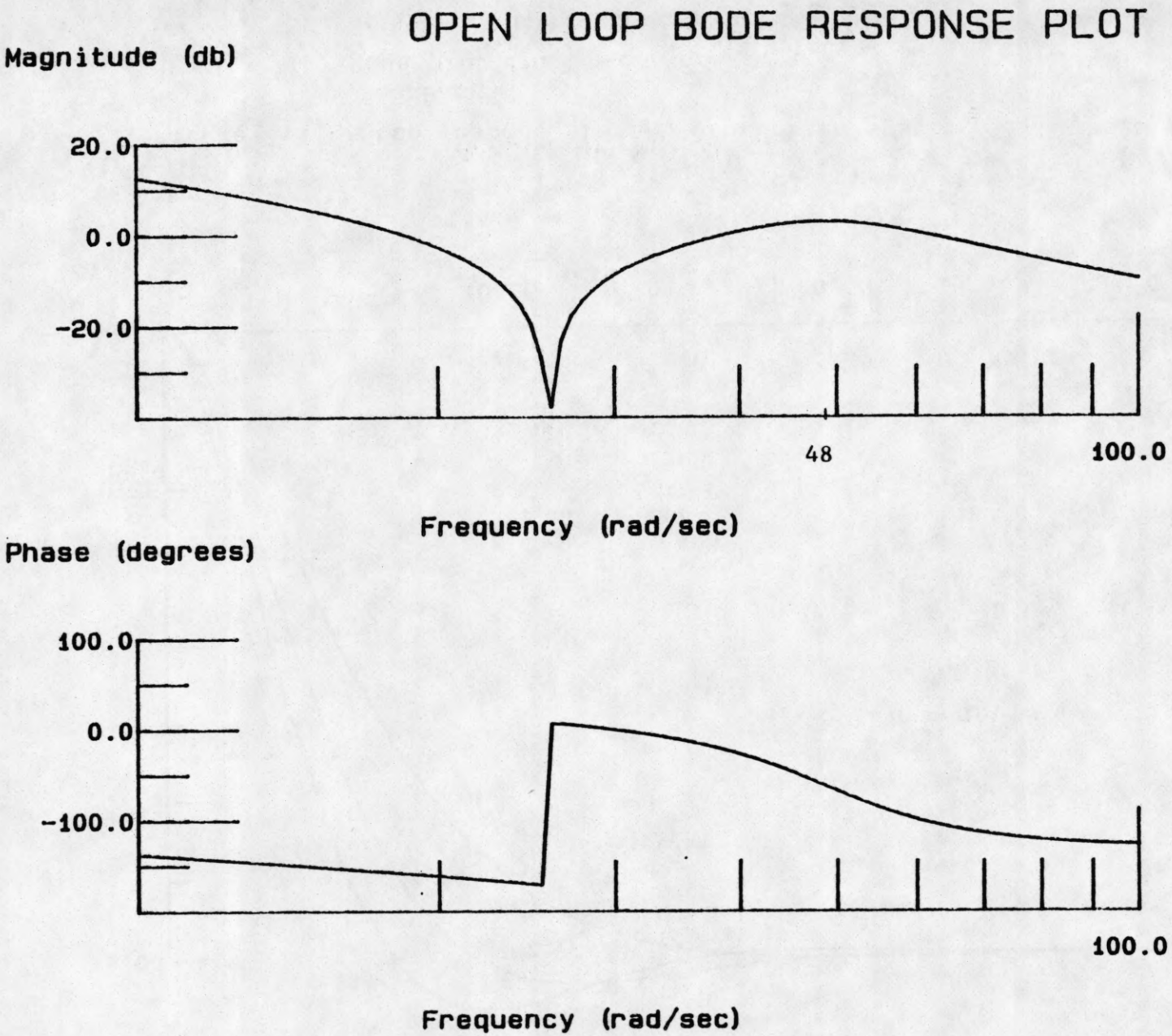

Figure 3.22 Bode plot for PD-controlled system, motor position feedback, J_1=0.0012 Nms^2/rad

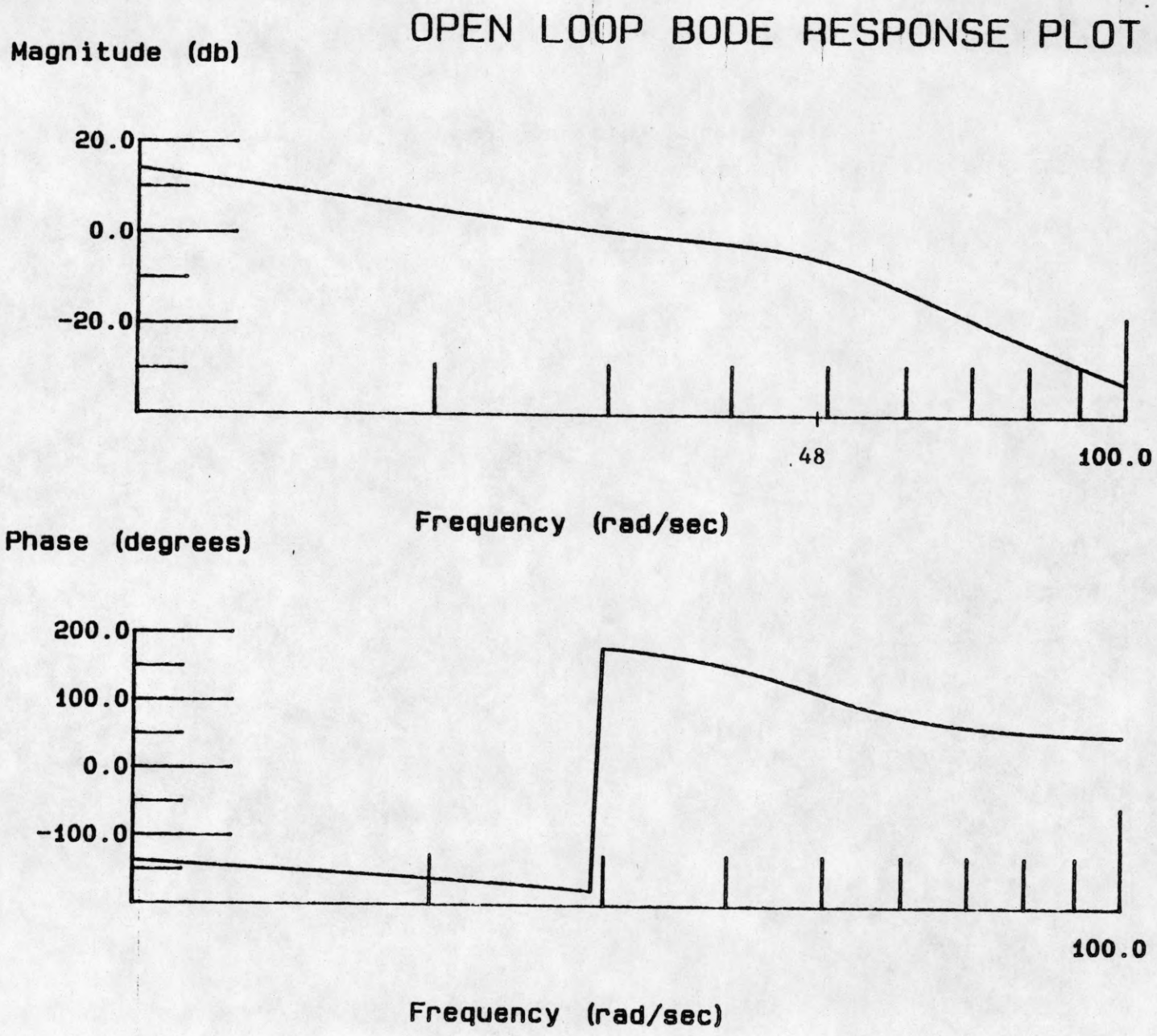

Figure 3.23 Bode plot for PD-controlled system, link position feedback, J_1= 0.0012 Nms^2/rad

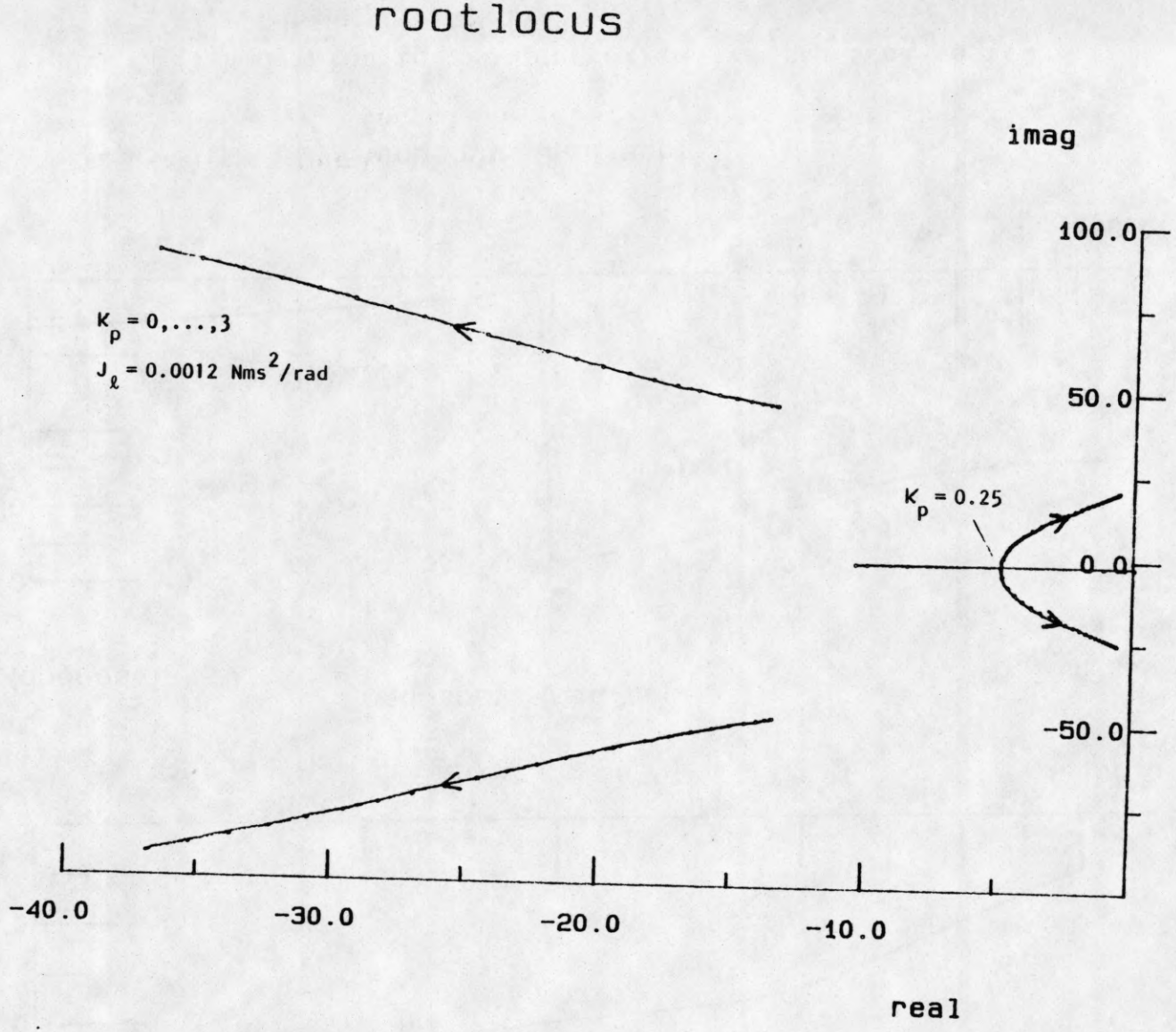

Figure 3.24 Rootlocus for PD-controlled system and variation of controller gain, motor position feedback

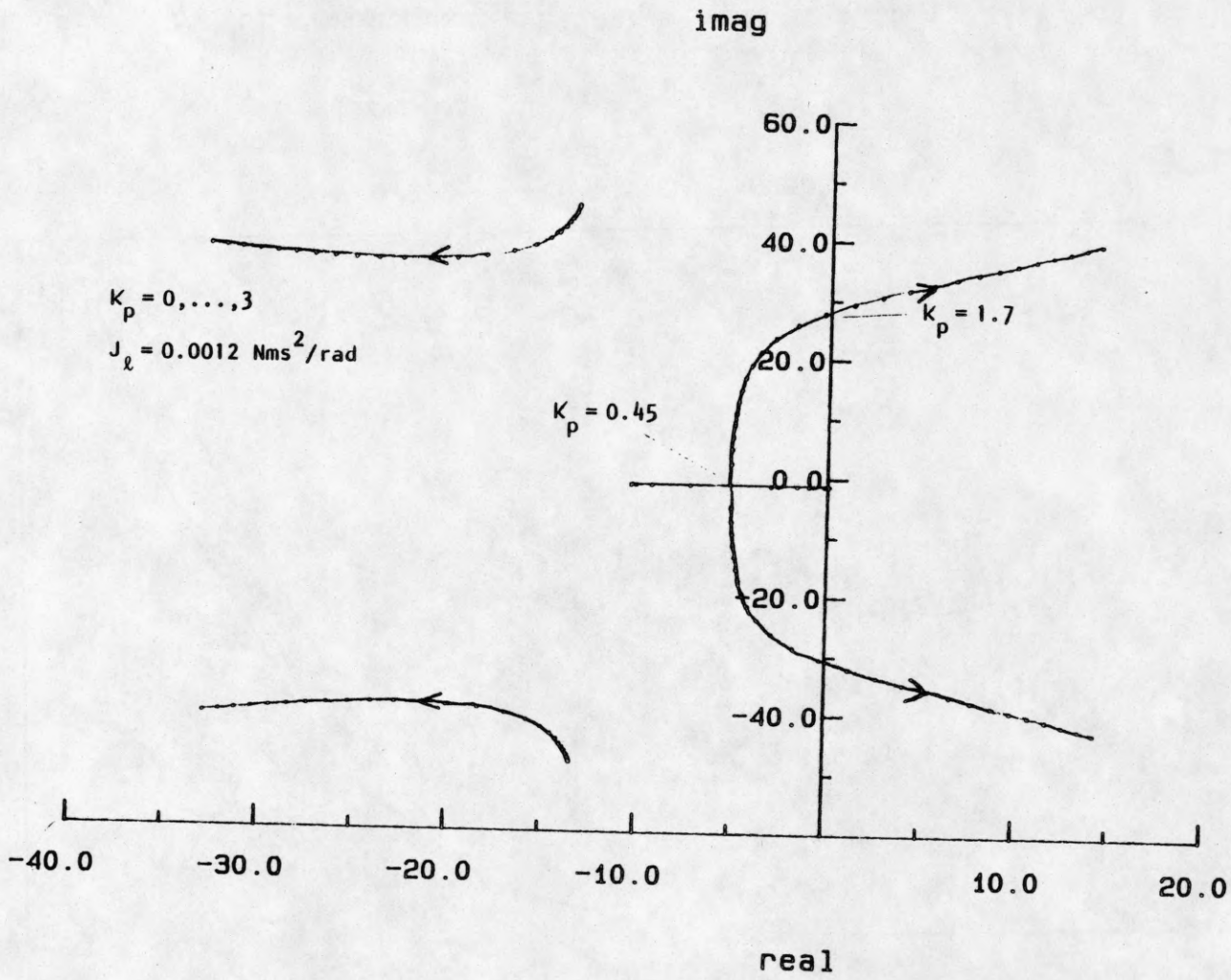

Figure 3.25 Rootlocus for PD-controlled system and variation of controller gain, link position feedback

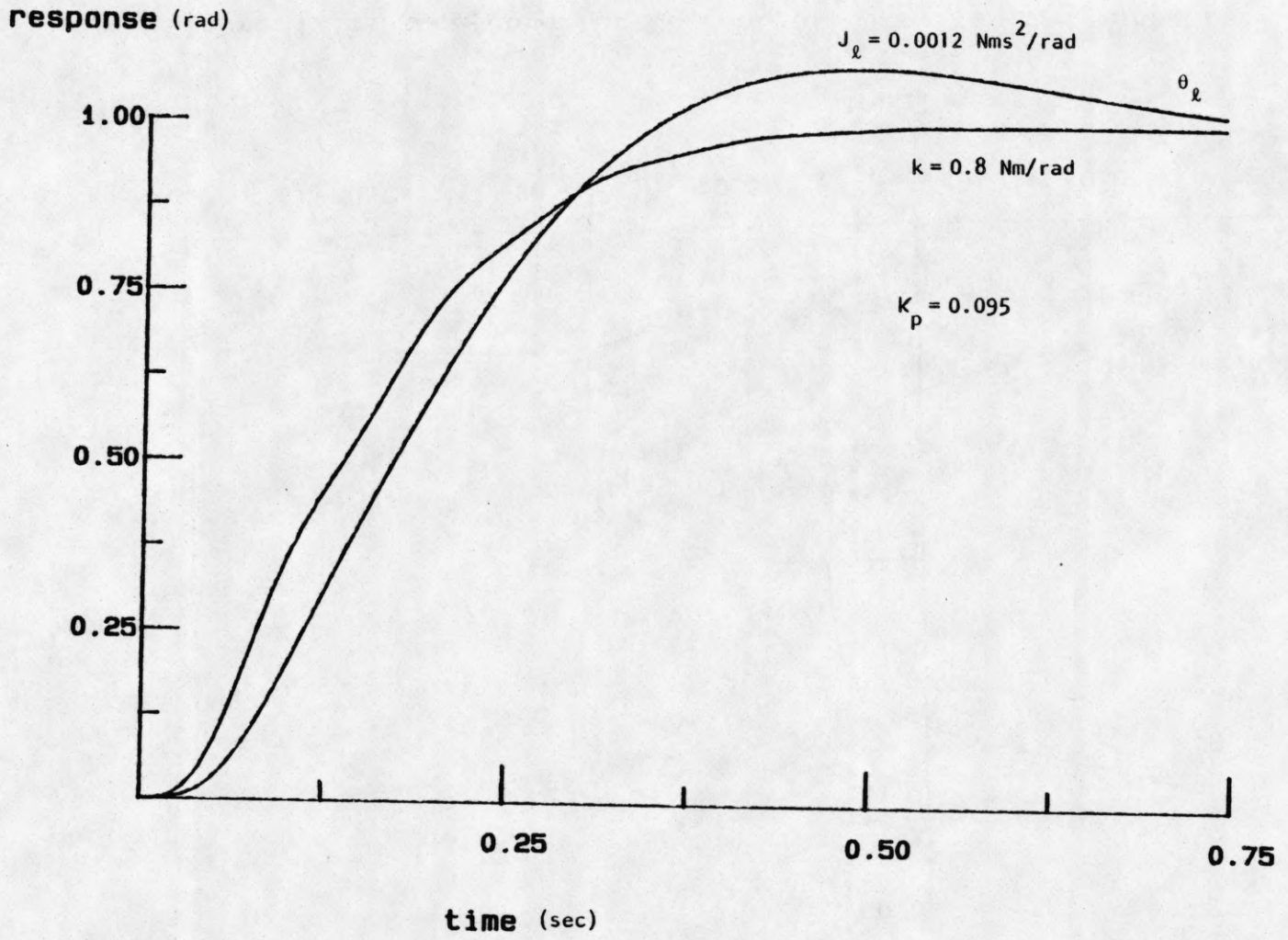

Figure 3.26 Step response for PD-controlled system, link position feedback

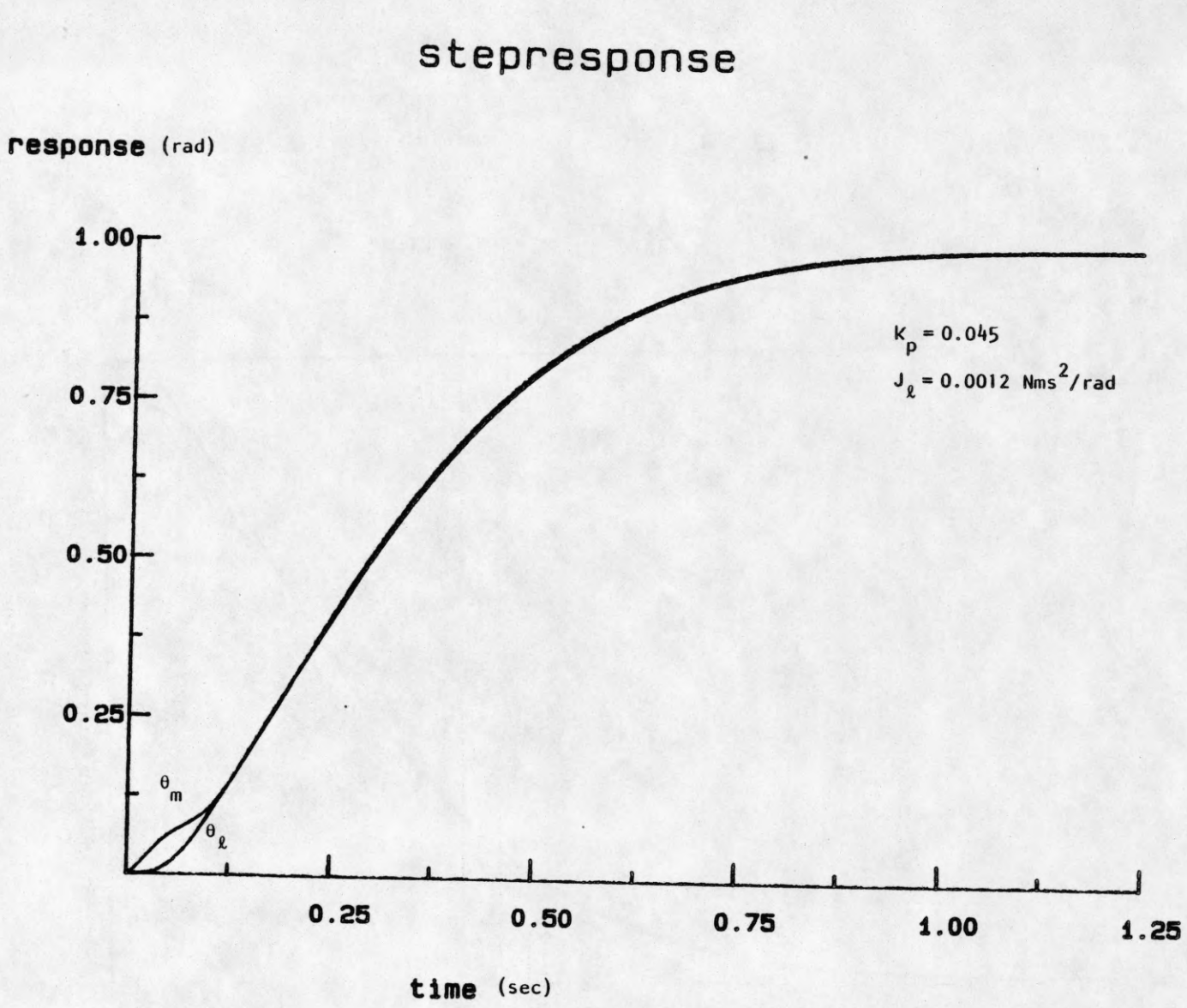

Figure 3.27 Step response for PD-controlled system, motor position feedback

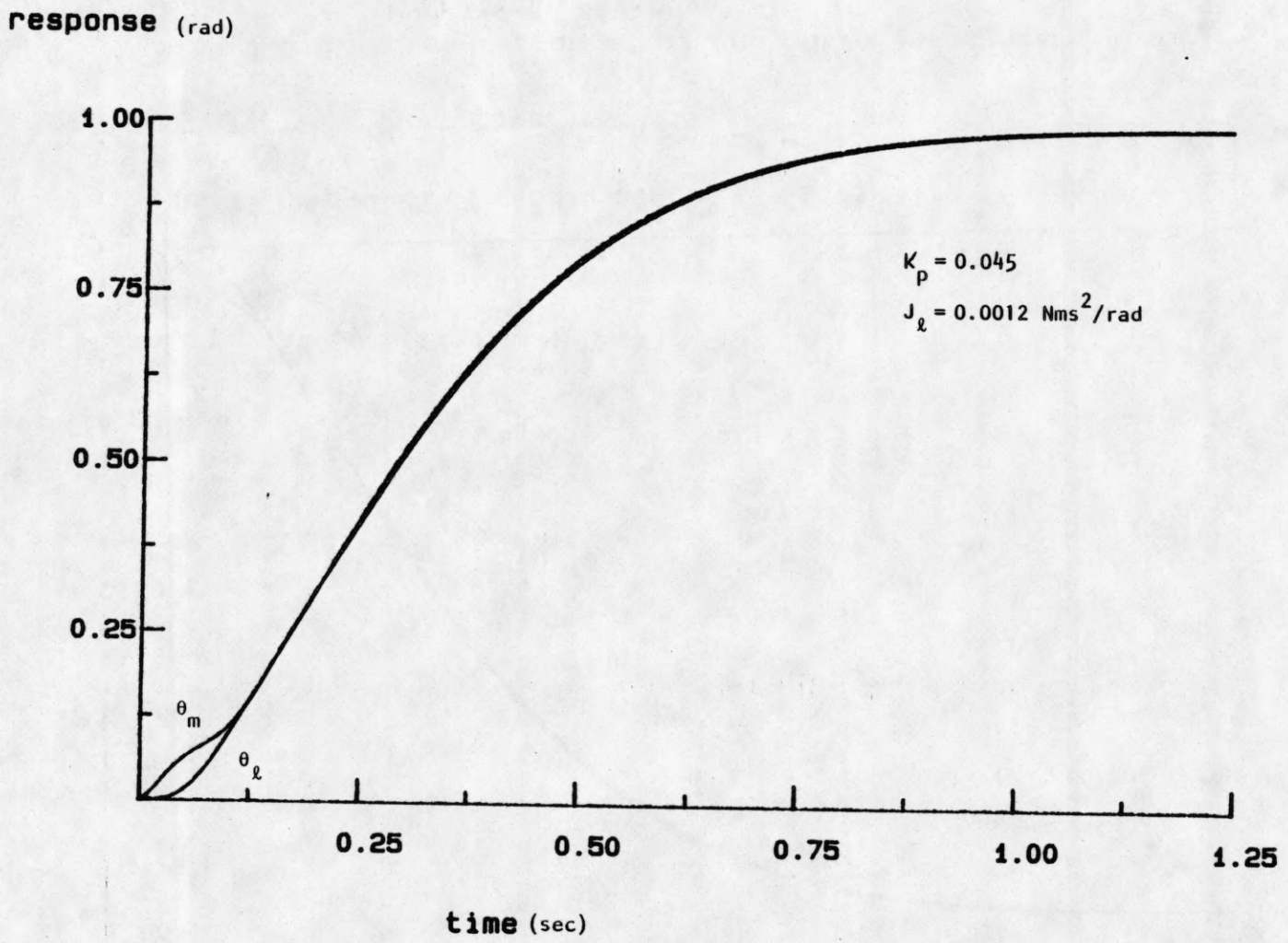

Figure 3.28 Step response for PD-controlled system, link position feedback

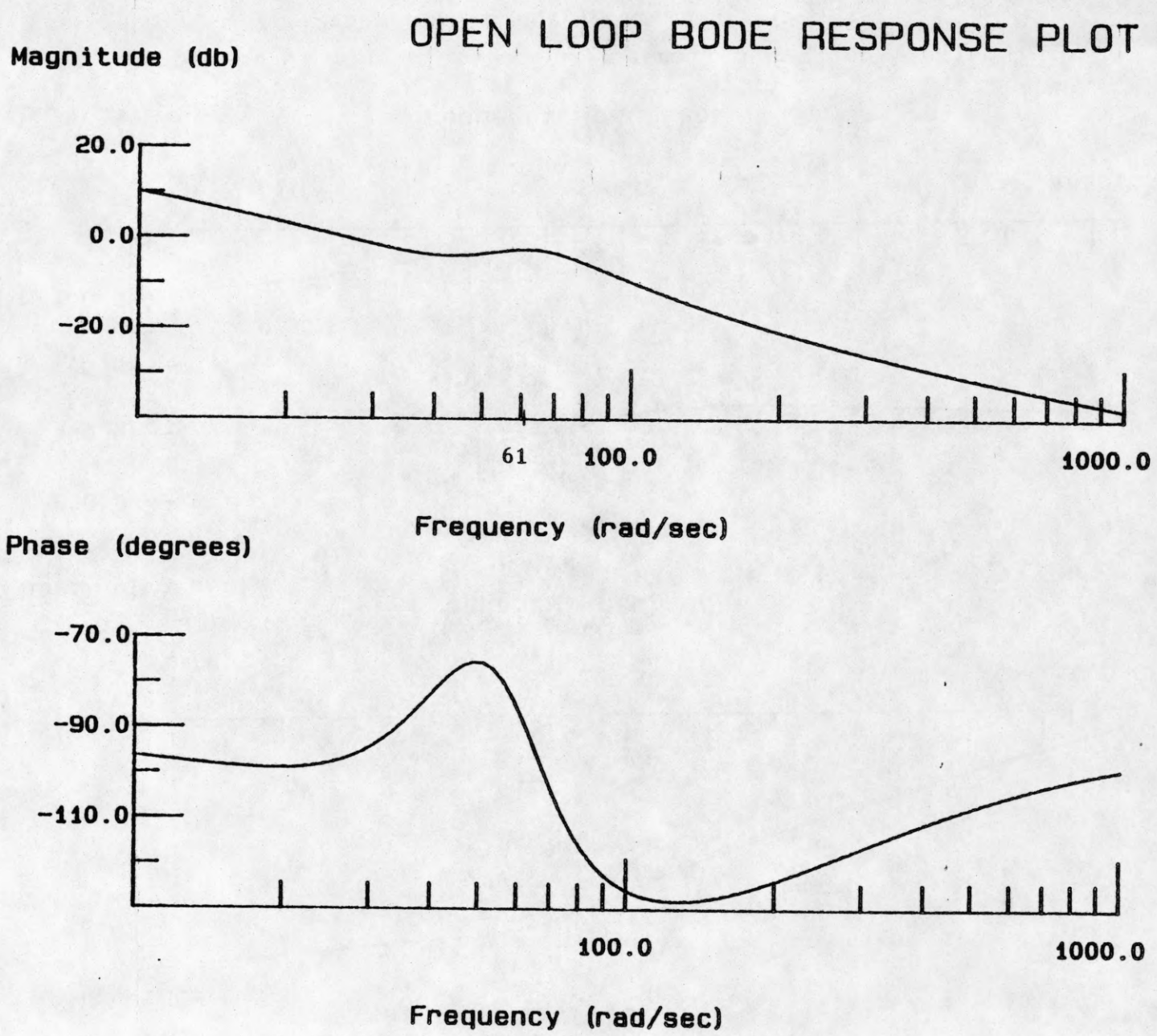

Figure 3.29 Bode plot for PD-controlled sytem, motor position feedback, B_1=0.015 Nms/rad

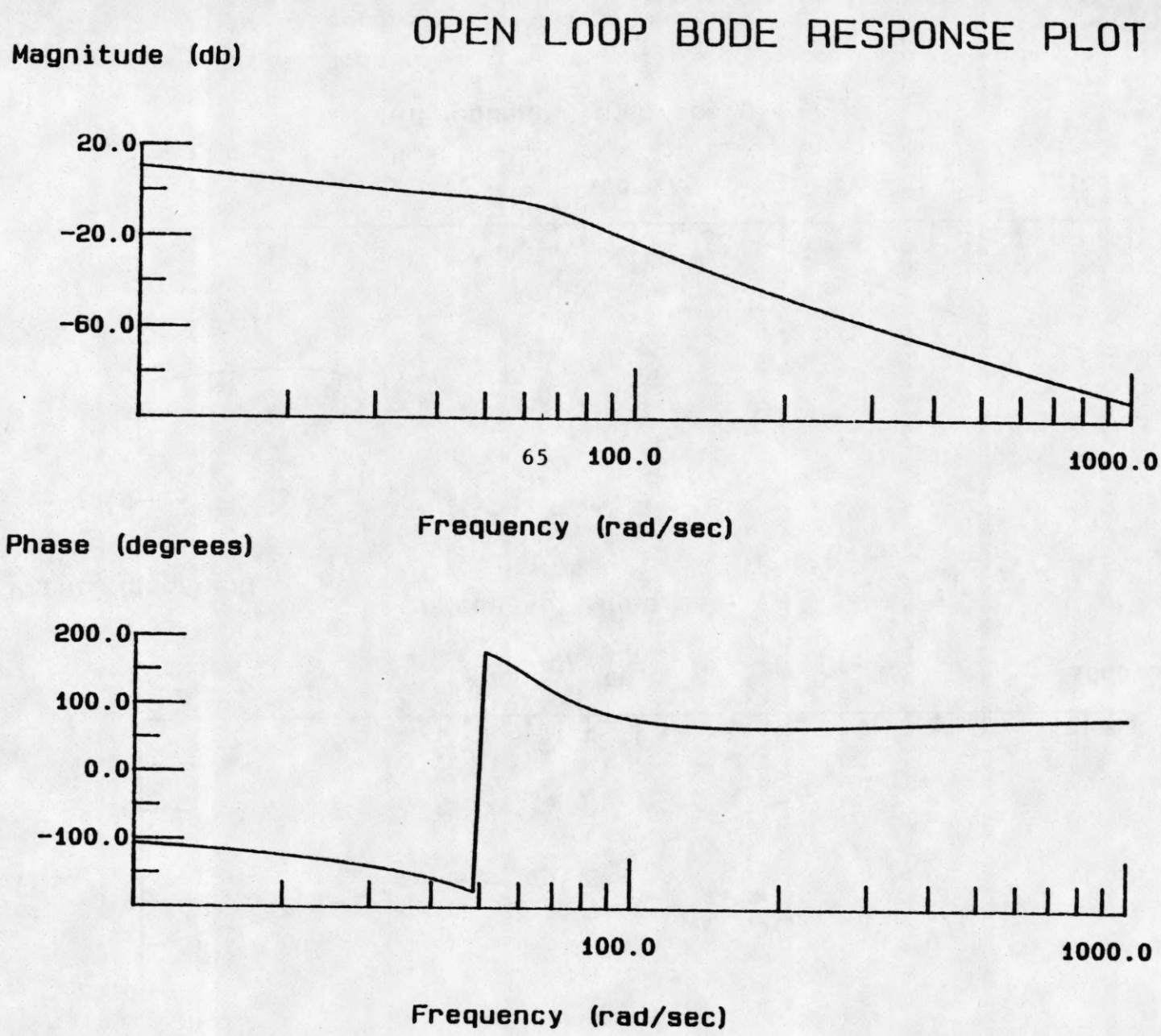

Figure 3.30 Bode plot for PD-controlled system, link position feedback, B_1=0.015 Nms/rad

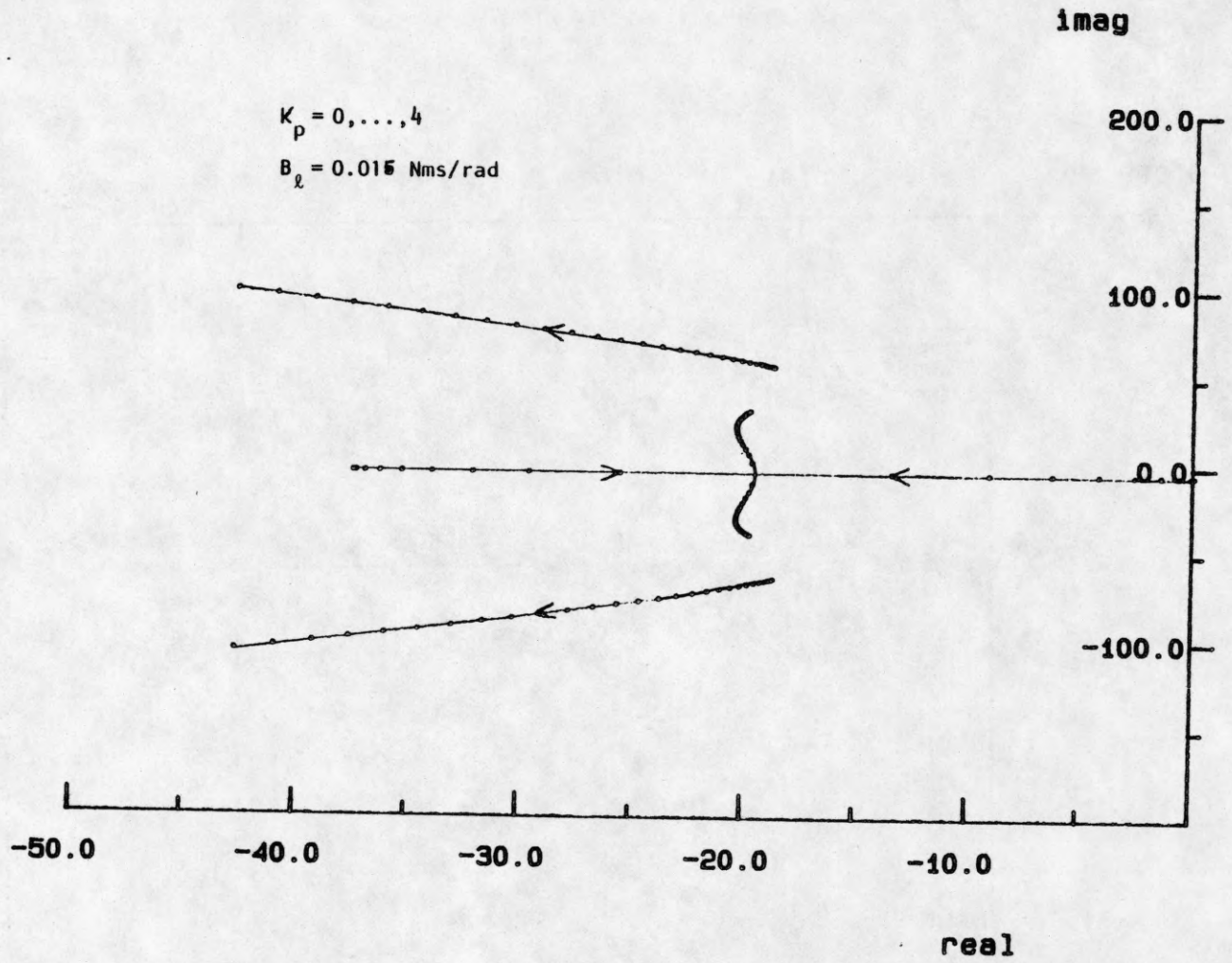

Figure 3.31 Rootlocus for PD-controlled system and variation of controller gain, motor position feedback

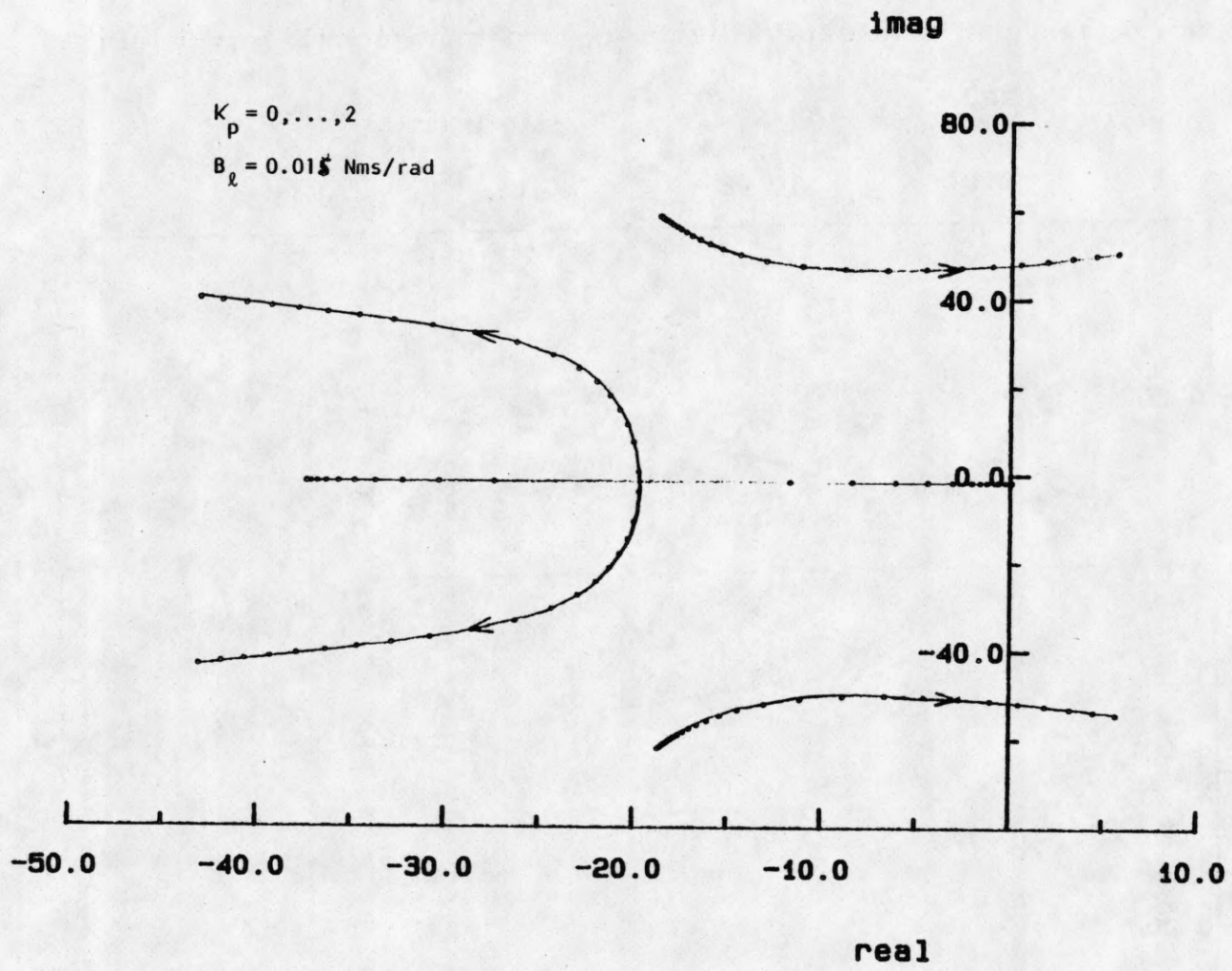

Figure 3.32 Rootlocus for PD-controlled system and variation of controller gain, link position feedback

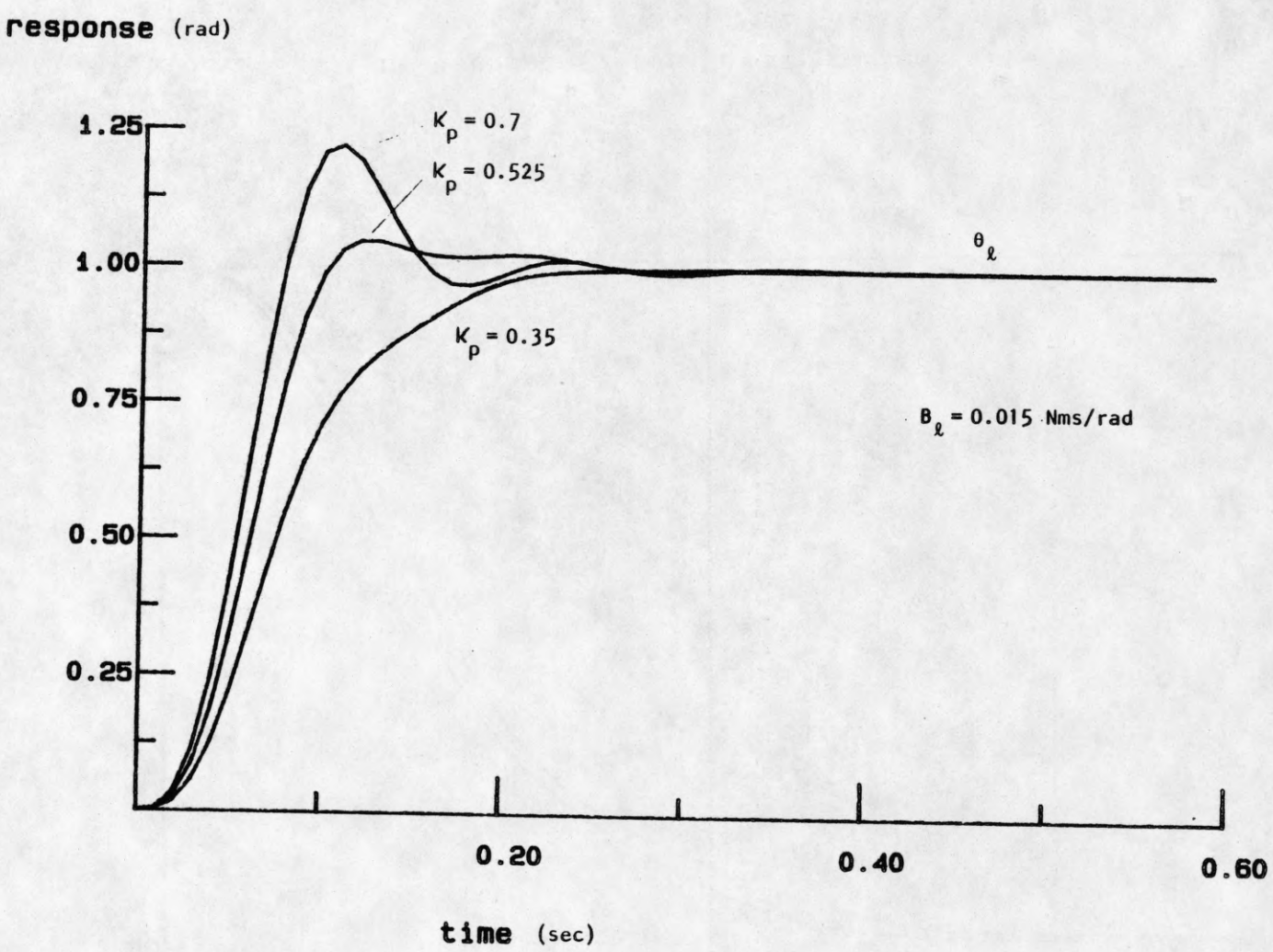

Figure 3.33 Step response for PD-controlled system, link position feedback

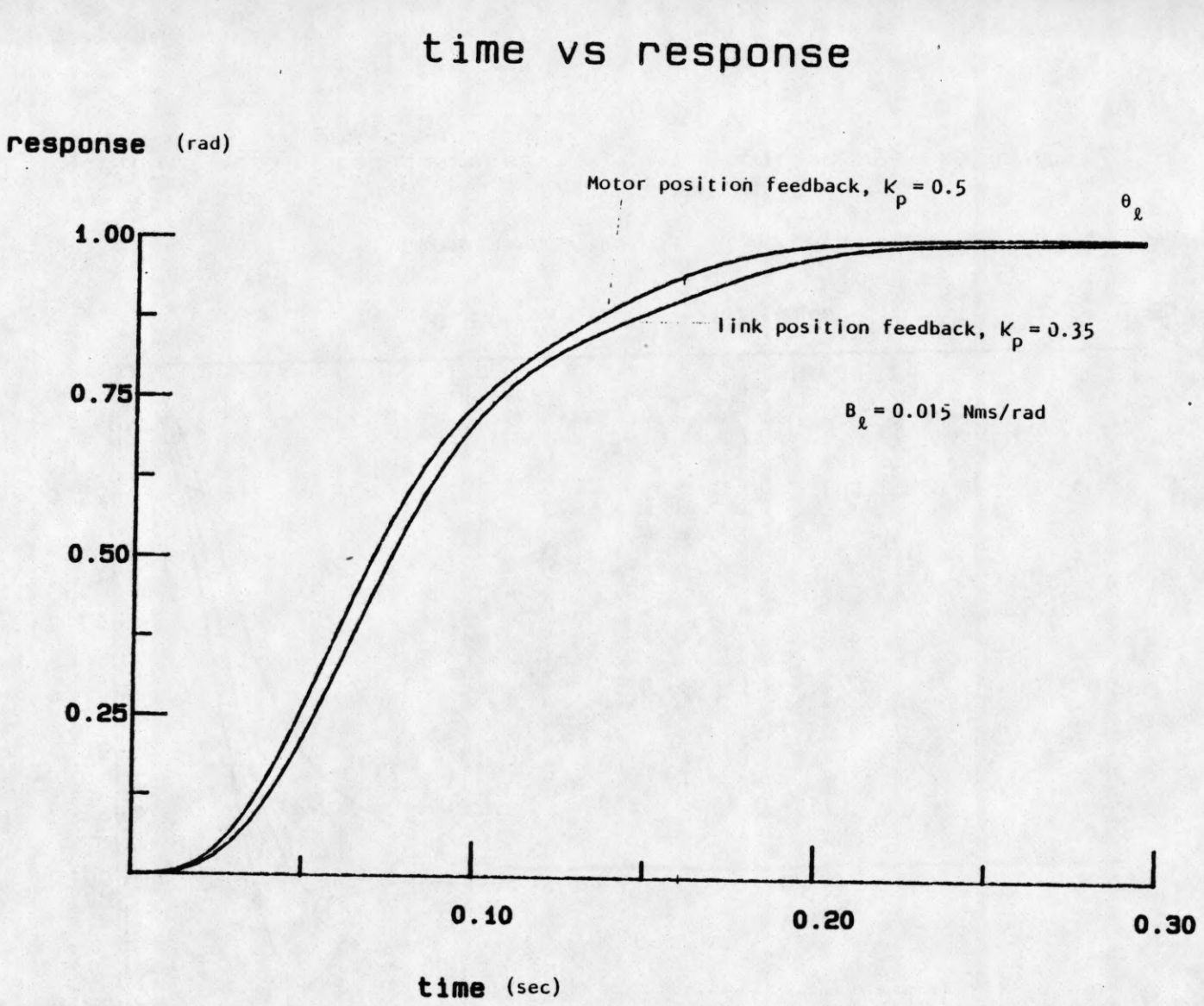

Figure 3.34 Step response for PD-controlled system

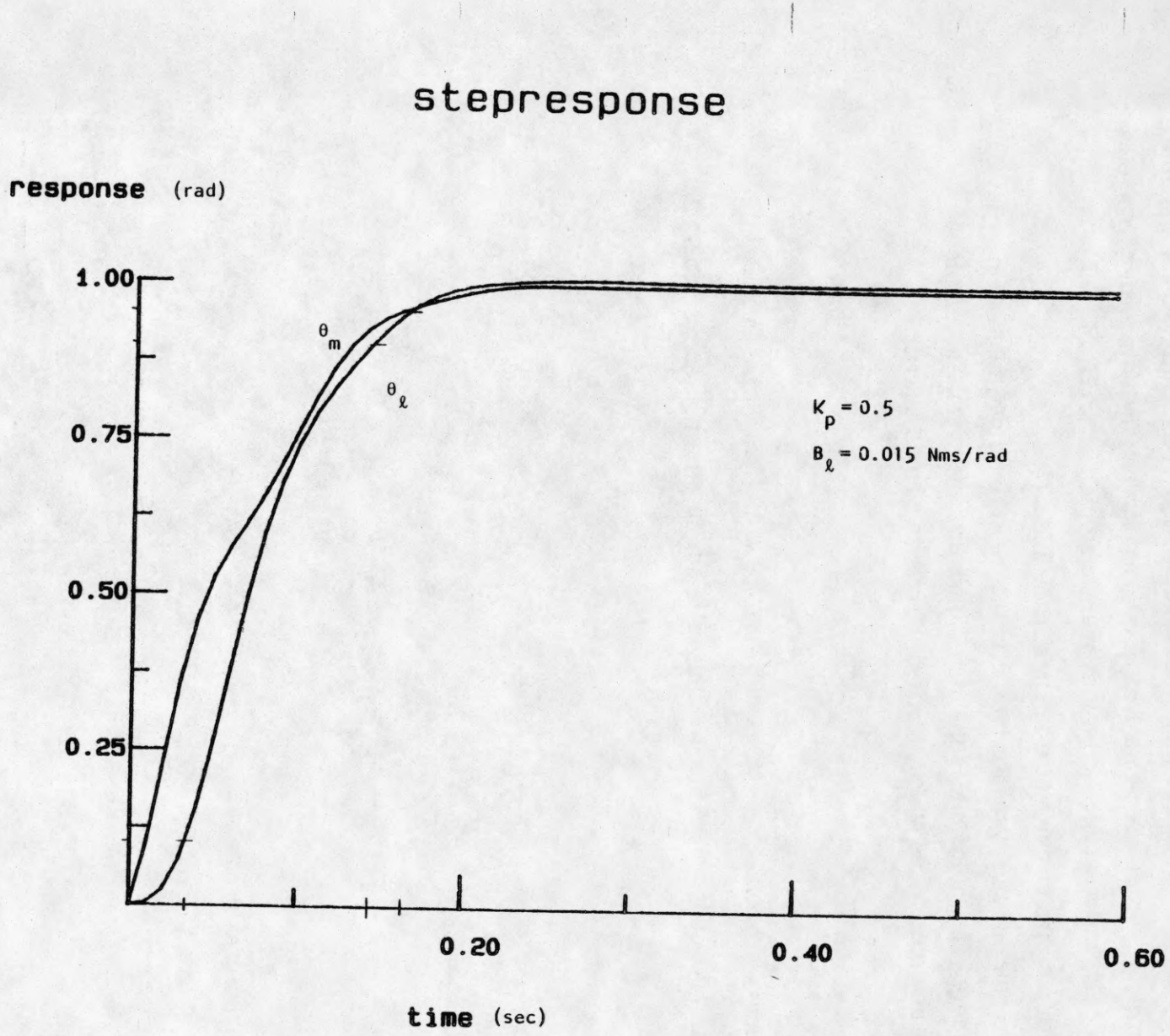

Figure 3.35 Step response for PD-controlled system, motor position feedback

4. STATE SPACE DESIGN

4.1. Formulation of our model in state space

The previous section has shown that the response speed is limited for a simple PD-control. The controller gain has to be kept rather small in order to avoid overshoot and unacceptable oscillations of the manipulator arm.

With a design of our model in state space, and a feedback of all states, we can place the poles of the system arbitrarily and hence improve the system behavior considerably. This holds under the assumption that the system is completely controllable and observable which is indeed the case as we will show.

Let us choose as state variables $x_1,\ldots,x_4$:

$$\begin{aligned} x_1 &= \theta_l \qquad x_3 = \theta_m \\ x_2 &= \dot{\theta}_l \qquad x_4 = \dot{\theta}_m \end{aligned} \tag{4.1}$$

and as an output $y = \theta_l$. Then we can write our linear single joint model (2.3) - (2.4) as

$$\begin{aligned} \dot{x}_1 &= x_2 \\ \dot{x}_2 &= -\frac{k}{J_l} x_1 - \frac{B_l}{J_l} x_2 + \frac{k}{J_l} x_3 \\ \dot{x}_3 &= x_4 \\ \dot{x}_4 &= \frac{k}{J_m} x_1 - \frac{k}{J_m} x_3 - \frac{B_m}{J_m} x_4 + \frac{1}{J_m} u \end{aligned} \tag{4.2}$$

$$y = x_1 \tag{4.3}$$

or in matrix form also as

$$\dot{\mathbf{x}} = \mathbf{A}\mathbf{x} + \mathbf{B}u \tag{4.4}$$

$$y = \mathbf{C}\mathbf{x} \tag{4.5}$$

where

$$A = \begin{bmatrix} 0 & 1 & 0 & 0 \\ -\frac{k}{J_l} & -\frac{B_l}{J_l} & \frac{k}{J_l} & 0 \\ 0 & 0 & 0 & 1 \\ \frac{k}{J_m} & 0 & -\frac{k}{J_m} & -\frac{B_m}{J_m} \end{bmatrix}, \quad B = \begin{bmatrix} 0 \\ 0 \\ 0 \\ \frac{1}{J_m} \end{bmatrix}, \quad \text{and} \quad C = \begin{bmatrix} 1 & 0 & 0 & 0 \end{bmatrix}. \tag{4.6}$$

The system is completely controllable since

$$\det\{Q_C\} = \det\{[B \;\; AB \;\; A^2B \;\; A^3B]\} = \frac{k^2}{J_m^4 J_l^2}, \tag{4.7}$$

which is never zero since $k > 0$.

Also, the system is completely observable, which can be seen from

$$\det\{Q_O\} = \det\{[C \;\; CA \;\; CA^2 \;\; CA^3]^T\} = \frac{k^2}{J_l^2} \tag{4.8}$$

The state space design with state observation and full state feedback is illustrated in Figure 4.1 and explained in the following.

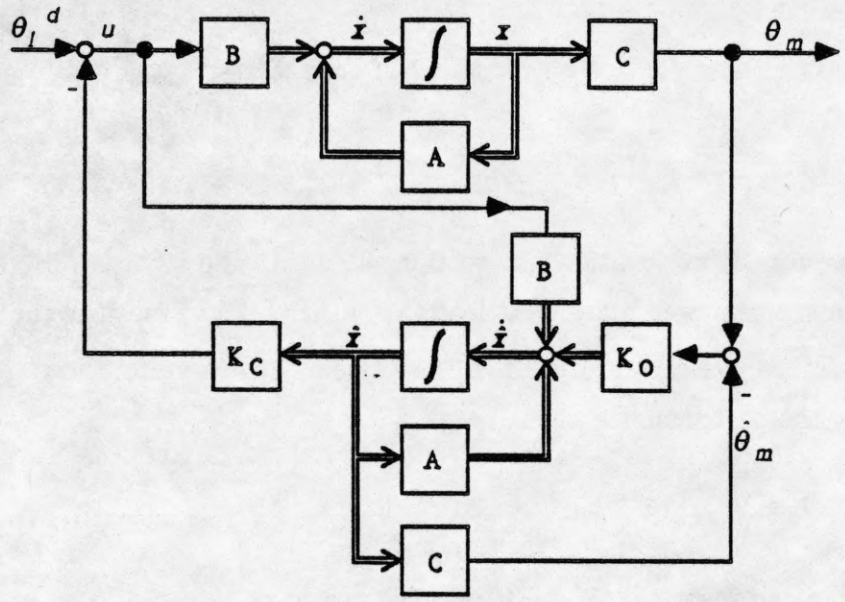

Figure 4.1 Block diagram for state space design and full state observer

Complete controllability of our system means that we can place its poles anywhere we want by applying a feedback of the form

$$u = -\mathbf{K_C}\,\mathbf{x}\,. \tag{4.9}$$

Equation (4.4) then gives the closed loop system dynamics as

$$\dot{\mathbf{x}} = \mathbf{A_C}\,\mathbf{x} \quad \text{with} \quad \mathbf{A_C} = \mathbf{A} - \mathbf{B}\,\mathbf{K_C}\,. \tag{4.10}$$

The feedback vector $\mathbf{K_C}$ can be determined by comparing the coefficients of the equation

$$\alpha_C(s) = \det\{(s\,\mathbf{I} - \mathbf{A_C})\} \tag{4.11}$$

with those of the desired characteristic equation for the system dynamics

$$\alpha_C^d(s) = s^4 + \alpha_{C1}\,s^3 + \alpha_{C2}\,s^2 + \alpha_{C3}\,s + \alpha_{C4}\,. \tag{4.12}$$

Some calculation yields for $\mathbf{K_C} = [K_{C1}\ K_{C2}\ K_{C3}\ K_{C4}]$

$$\begin{aligned}
K_{C4} &= (\alpha_{C1} - \frac{B_l}{J_l})\,J_m - B_m \\
K_{C3} &= (\alpha_{C2} - \frac{k}{J_l})\,J_m - k - \frac{B_l}{J_l}\,(B_m + K_{C4}) \\
K_{C2} &= \frac{1}{k}\,(\alpha_{C3}\,J_m\,J_l - K_{C3}\,B_l) - B_l - B_m - K_{C4} \\
K_{C1} &= \alpha_{C4}\,\frac{J_m\,J_l}{k} - K_{C3}
\end{aligned} \tag{4.13}$$

However, as simulations in section 4.2. will show, obtaining a fast response through arbitrary pole placement leads to rather high values for the input torque.

Therefore, we should optimize the system. Let us state as our goal the minimization of the performance index

$$J = \int_0^\infty (\mathbf{x}^T\,\mathbf{Q}\,\mathbf{x} + u^T\,\mathbf{R}\,u)\,dt\ , \tag{4.14}$$

with weighting matrices Q and R which have to be selected later on. The optimum feedback vector $\mathbf{K_C}$ can then be determined from the matrix Ricatti equation [7]

$$0 = \mathbf{A}^T\mathbf{S} + \mathbf{S}\mathbf{A} + \mathbf{Q} - \mathbf{S}\mathbf{B}\mathbf{R}^{-1}\mathbf{B}^T\mathbf{S} \tag{4.15}$$

as

$$\mathbf{K_C} = \mathbf{R}^{-1}\mathbf{B}^{\mathrm{T}}\mathbf{S}\,. \tag{4.16}$$

Since only the output $y_1 = \theta_l$ is measured we need to construct an observer in order to implement the full state feedback control law (4.9). This observer is designed as

$$\dot{\hat{\mathbf{x}}} = \mathbf{A}\,\hat{\mathbf{x}} + \mathbf{B}u + \mathbf{K_O}(y - \mathbf{C}\,\hat{\mathbf{x}}) \tag{4.17}$$

which leads with equation (4.4) and $\mathbf{e} = \mathbf{x} - \hat{\mathbf{x}}$ to the description of the error dynamics as

$$\dot{\mathbf{e}} = \mathbf{A_O}\,\mathbf{e} \qquad \text{with } \mathbf{A_O} = \mathbf{A} - \mathbf{K_O}\,\mathbf{C}\,. \tag{4.18}$$

The observer feedback $\mathbf{K_O}$ can be determined by comparing the coefficients of $\det\{(s\,\mathbf{I} - \mathbf{A_O})\}$ with those of the desired characteristic equation for the error dynamics.

If the desired error dynamics are given by the equation

$$\alpha_O^d(s) = s^4 + \alpha_{O1}s^3 + \alpha_{O2}s^2 + \alpha_{O3}s + \alpha_{O4}\,. \tag{4.19}$$

the observer feedback $\mathbf{K_O}$ can be determined by equating coefficients of equation (4.19) with the characteristic equation of the observer dynamics

$$\alpha_O(s) = \det\{s\,\mathbf{I} - (\mathbf{A} - \mathbf{K_O}\,\mathbf{C})\}\,. \tag{4.20}$$

After some calculation we obtain for $\mathbf{K_O} = [K_{O1}\ K_{O2}\ K_{O3}\ K_{O4}]^{\mathrm{T}}$

$$\begin{aligned}
K_{O1} &= \alpha_{O1} - \frac{B_m}{J_m} - \frac{B_l}{J_l} \\
K_{O2} &= \alpha_{O2} - K_{O1}\cdot\left(\frac{B_m}{J_m} + \frac{B_l}{J_l}\right) - \frac{B_m B_l}{J_m J_l} + k\left(\frac{1}{J_m} - \frac{1}{J_l}\right) \\
K_{O3} &= \alpha_{O3}\frac{J_l}{k} - K_{O1}\cdot\left(\frac{B_m B_l}{k\,J_m} - \frac{J_l}{J_m}\right) - K_{O2}\frac{J_l B_m}{k\,J_m} - \frac{1}{J_m}(B_m - B_l) \\
K_{O4} &= \alpha_{O4}\frac{J_l}{k} + K_{O1}\frac{B_l}{J_m} + K_{O2}\frac{J_l}{J_m} + K_{O3}\frac{B_m}{J_m}
\end{aligned} \tag{4.21}$$

4.2. State space simulation for different system parameters

For the simulations in this section through section 4.2.3. all initial values for the system variables are zero. The observer design is not relevant for this case since the observed states equal the actual states at all times. Section 4.2.4. treats the observer design separately for initial conditions not equal to zero. Those appear, for example, through measurement errors.

The first simulation in Figures 4.2 and 4.3 shows transient response and input torque for the state model and system parameters as in section 3.2. The input is a step of θ_l^d from 0 rad to 1 rad, and controller poles are all placed at $s_1, s_2, s_3, s_4 = -80$. Corresponding rise and settle times are $T_r = 0.061$ s and $T_s = 0.096$ s, which are about one fourth of the times for the simple PD-control. This result confirms our previous promise that we could obtain a faster response for a full state feedback, but as announced before already, the input torque is rather high compared to the one for the PD-control (Figure 3.14). With an initial value of 7.5 Nm it will not only lead to high energy consumption but also to undesired forces on gears and arm.

In order to keep the input torque within an acceptable limit but still obtain a fast system response without overshoot, an optimized feedback is implemented. Weighting matrices Q and R are chosen with a trial-and-error approach.

Figure 4.4 shows a simulation of the state model with optimized feedback and the system parameters as in section 3.2. The matrices Q and R are chosen as diag {Q} = [100 0.1 100 0.1] and R = [100] which results in the feedback vector K_C = [-0.69037 0.0264752 2.11025 0.0389741]. Corresponding pole locations of the system (4.4) are at $s_1, s_2 = -20.15 \pm j\,54.28$, $s_3 = -35.94$, $s_4 = -58.69$. Measurements of rise and settle times yield $T_r = 0.053$ s and $T_s = 0.087$ s, which are about the same as in the previous non-optimum case, but the input torque now stays below 1.4 Nm (Figure 4.5). The pole placement also leads to a very smooth response, free from the oscillations observed for the PD-control (Figure 3.12).

However, from Figure 4.4 we can also see one disadvantage of the faster response. Motor and link position show in the rising process of the response a displacement of up to 0.3 rad which is equal to a deformation of the gears and the manipulator arm. This means a limit to the speed of the system response because, dependent on the gear ratio, the deformation can get so large that gears and/or

manipulator arm suffer damage.

4.2.1. Simulation for increased stiffness

Figures 4.6 and 4.7 show a simulation of our state space model for an increased stiffness of $k = 4.0$ Nm/rad. The optimum feedback gain $\mathbf{K_C}$ is determined as $\mathbf{K_C}$ = [-0.501667 0.011113 1.50167 0.02889] according to weighting matrices diag {Q} = [100 0.1 100 0.1] and R = [200]. This results in system poles at $s_1, s_2 = -21.21 \pm j\,138.48$, $s_3, s_4 = -33.66 \pm j\,11.88$. Again we are able to decrease the response time for a unit step input to almost one fourth of the time for the simple PD-control. The measurements for the rise and settle times are $T_r = 0.08$ s and $T_s = 0.122$ s. A comparison of Figure 4.6 with Figure 3.20 shows that we now obtain slight oscillations in the link position. The reason for that is the increased response speed in combination with the optimization of the feedback vector. However, these oscillations do not cause a problem here. By choosing other pole locations while forgoing an optimum feedback, we could receive a response free from oscillations.

A second effect of an increase in stiffness is a smaller displacement between link and motor position compared to the case for $k = 0.8$ Nm/rad. The maximum here is about 0.1 rad over the rise of the unit step response. However, that does not imply a smaller torque in the gears and manipulator arm since torque is the product of displacement and stiffness. Overall, the torque is then about the same as in the previous state space simulations and the same problems with the mechanical stability of the robot structure arise.

4.2.2. Simulation for increased load inertia

For the simple PD-controller and an increased manipulator load, the gain had to be kept smaller in order to prevent an overshoot. The consequence was a slower response (Figure 3.28). For full state feedback the same can be observed as a simulation for a load $J_l = 0.0012$ Nms^2/rad shown in Figures 4.8 and 4.9 indicates.

The optimized feedback vector $\mathbf{K_C}$ here has been derived as $\mathbf{K_C}$ = [-0.09479 0.0354828 0.911287 0.0252579] with weighting matrices diag {Q} = [100 0.3 100 0.2] and R = [300] for equation (4.14). Although the

step response is slower than for the smaller load inertia (Figure 4.4), we still get about five times as fast as for the PD-control with $T_r = 0.096$ s and $T_s = 0.158$ s. The price for that increase in response speed is again a large displacement between link and motor position (maximum of 0.33 rad for a step input of $\theta_l^d = 1$ rad) which can mean a limit to further speed increases if we want to avoid damage in gears or on the arm. The system poles are for this case at $s_1, s_2 = -22.65 \pm j\,32.55$, $s_3, s_4 = -27.68 \pm j\,9.97$.

4.2.3. Simulation for increased damping

The simulations for a damping of $B_l = 0.015$ Nm shown in Figures 4.10 and 4.11 indicate that a state space design brings here little advantages over the PD-control. In order to get the response of $T_r = 0.079$ s and $T_s = 0.140$ s which is not even twice as fast as the response for the PD-control (Figure 3.33), we have to accept a maximum displacement between link and motor position of 0.42 rad. The reason for the larger displacement is the mechanical resistance on the load side due to the damping which can only be overcome with a high torque on the motor side. While we probably will not find a damping as high as in this case in reality (normally we can even neglect it), we still see that the advantages of a full state feedback diminish when the damping increases.

The weighting matrices for the derivation of the optimum feedback vector K_C were chosen as diag {Q} = [100 0.3 200 0.1] and R = [150]. K_C itself is [-0.0725941 0.0115011 1.34162 0.0293279], and the resulting pole locations are at $s_1, s_2 = -32.42 \pm j\,59.06$, $s_3 = -28.16$, $s_4 = -55.31$.

4.2.4. Observer design

In order to force the observed states to approach the actual states as quickly as possible, the observer poles should be placed far left of the controller poles. In the following simulation shown in Figure 4.12 the observer poles are placed at $s = -200$ and system parameters are as in section 3.2. An optimized controller design is applied with weighting matrices of diag {Q} = [100 0.1 100 0.1] and R = [100] as under 4.2. The corresponding controller pole locations are at $s_1, s_2 = -20.15 \pm j\,54.28$, $s_3 = -35.94$, $s_4 = -58.69$.

We assume an error of 0.05 rad (or 0.03° for a gear ratio of 100) for the link angle measurement which results in the same error for the motor angle because the system is in equilibrium for $t = 0$.

From the system response we can see that the response for a feedback of the estimated states is almost equivalent to the response for a feedback of the actual states. For the rise and settle times we measure for a feedback of the estimated states $T_r = 0.048$ s and $T_s = 0.088$ s, and for a feedback of the actual states $T_r = 0.052$ s and $T_s = 0.088$ s.

The difference is minor and could be reduced even further by placing the poles farther to the left. Since the estimated states are only numerical values, there are no physical limits in the observer pole placement such as for the controller pole placement. In reality, however, we have to reckon upon noise in the measurements of output state and input torque. If the observer poles are then placed too far to the left this noise will be amplified so much that unsatisfactory system responses result. This problem can be reduced through the application of a Kalmann-filter, which is not analyzed in detail here.

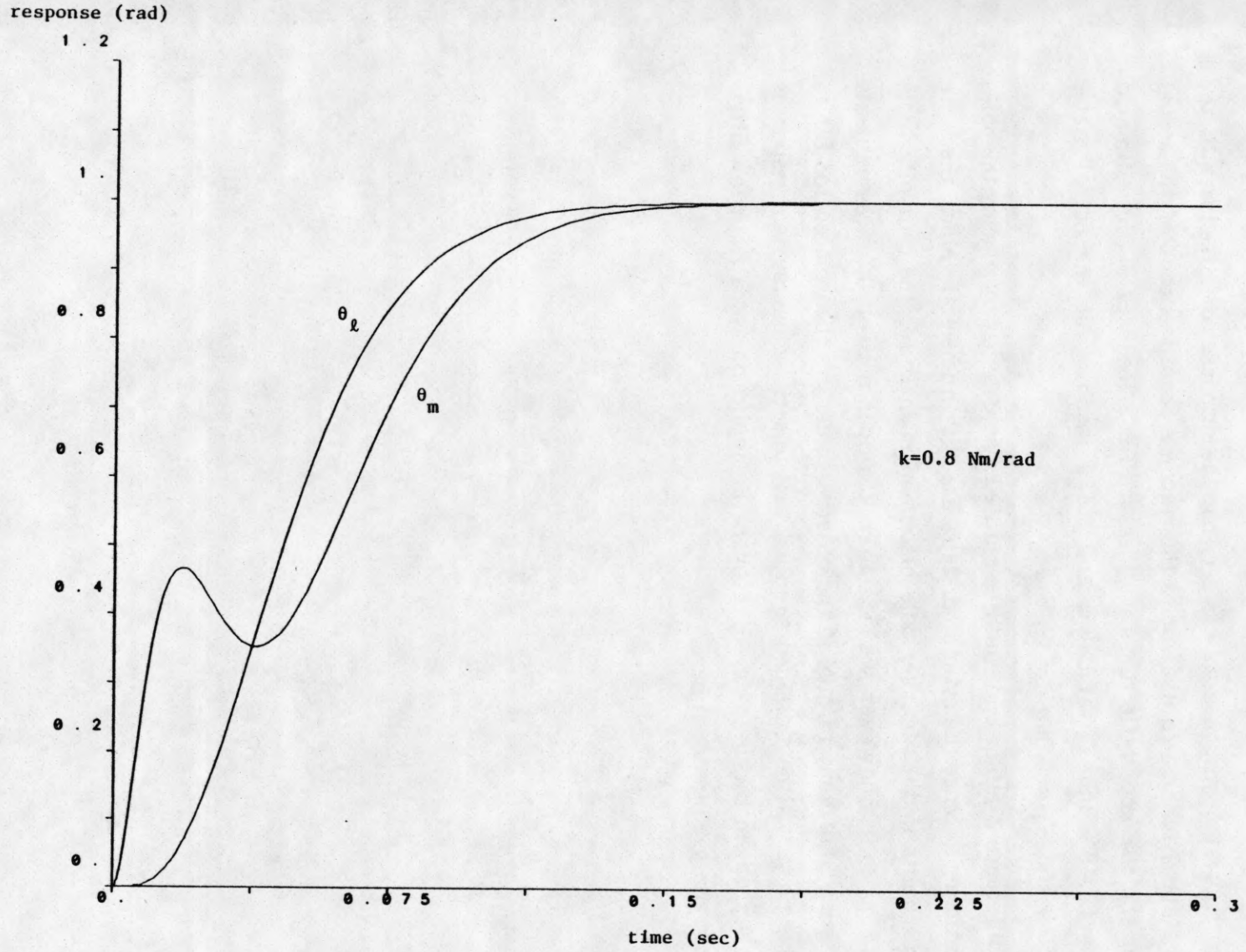

Figure 4.2 Step response for system in state space and pole placement

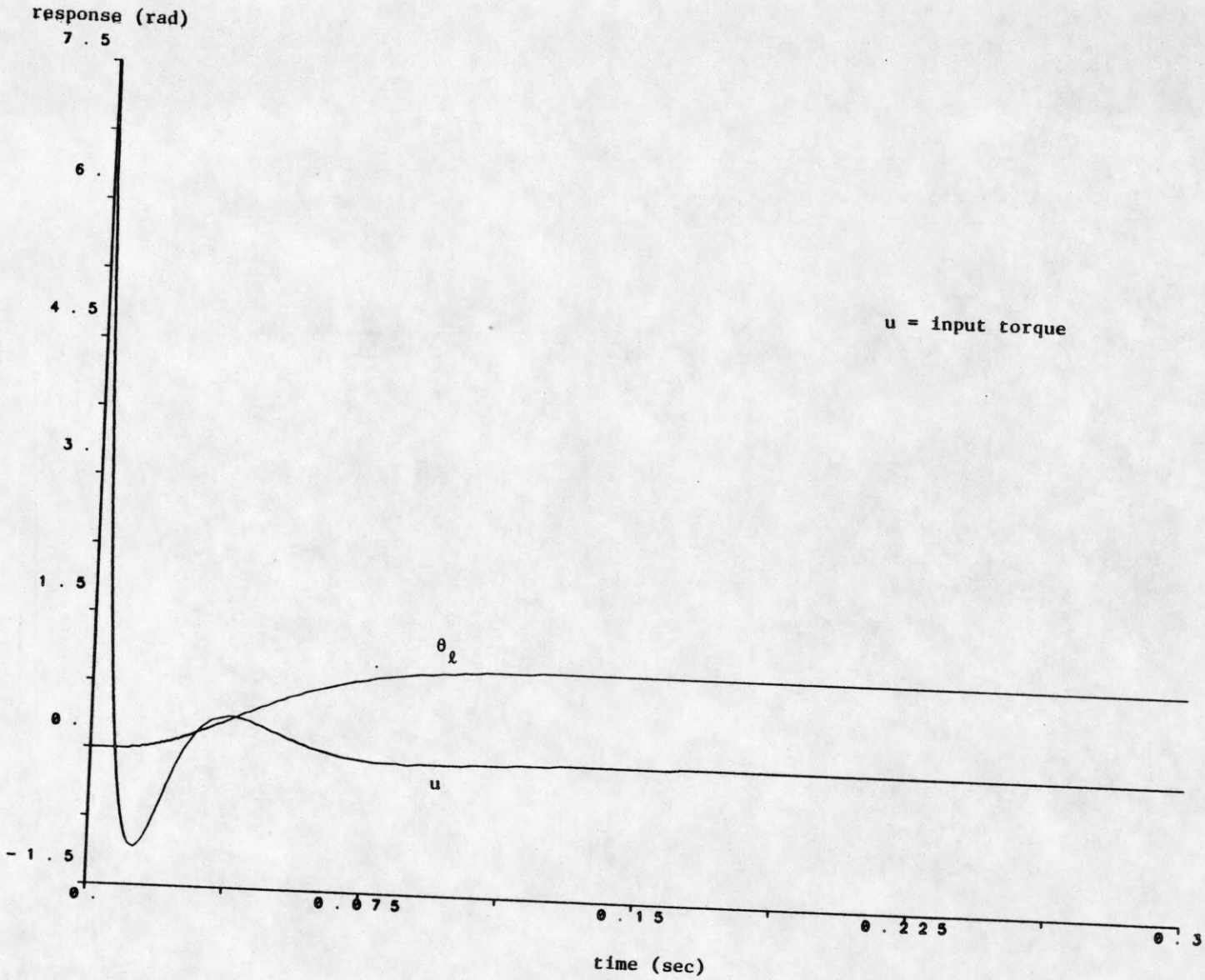

Figure 4.3 Input torque for system in state space and pole placement

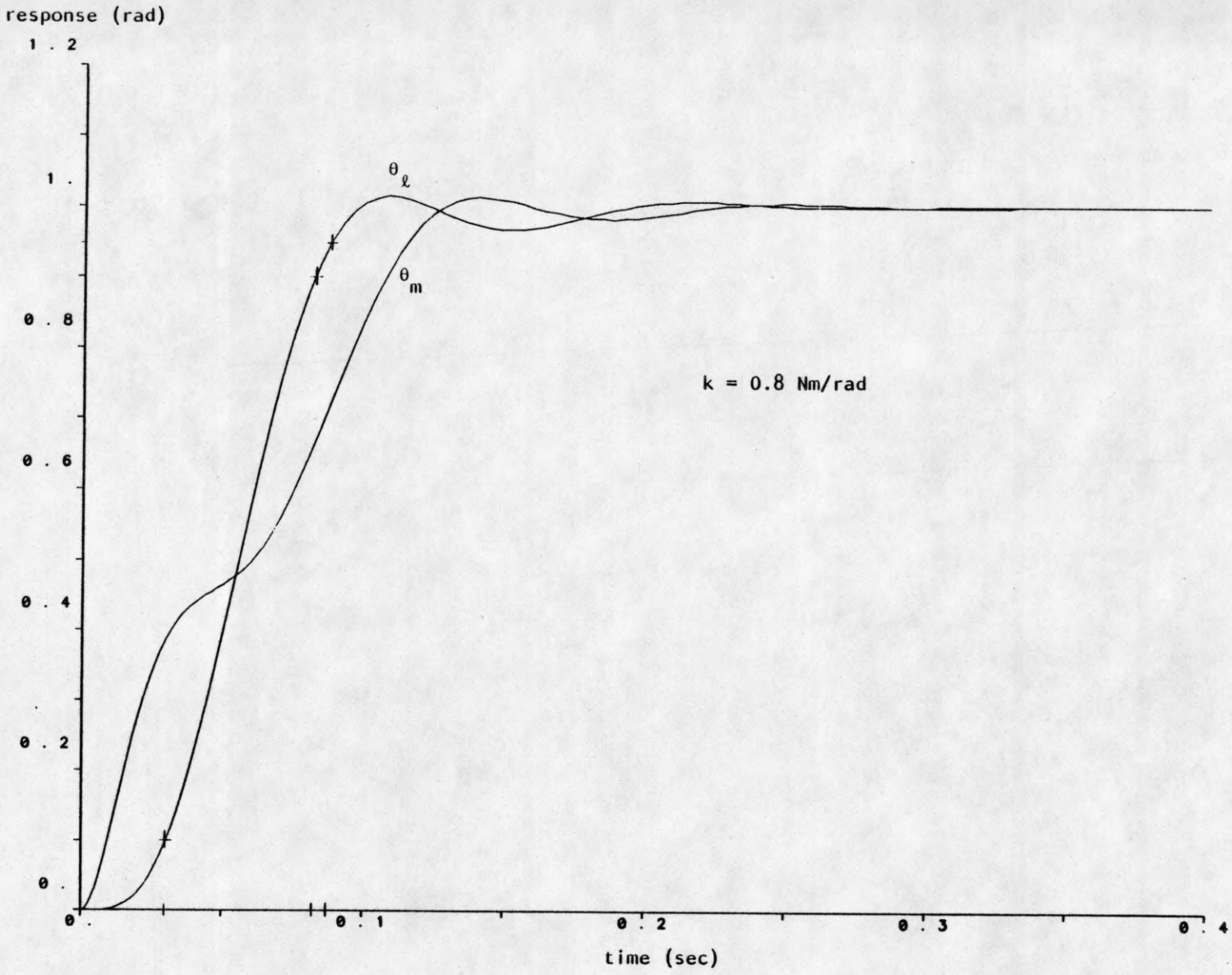

Figure 4.4 Step response for system in state space and optimized pole placement

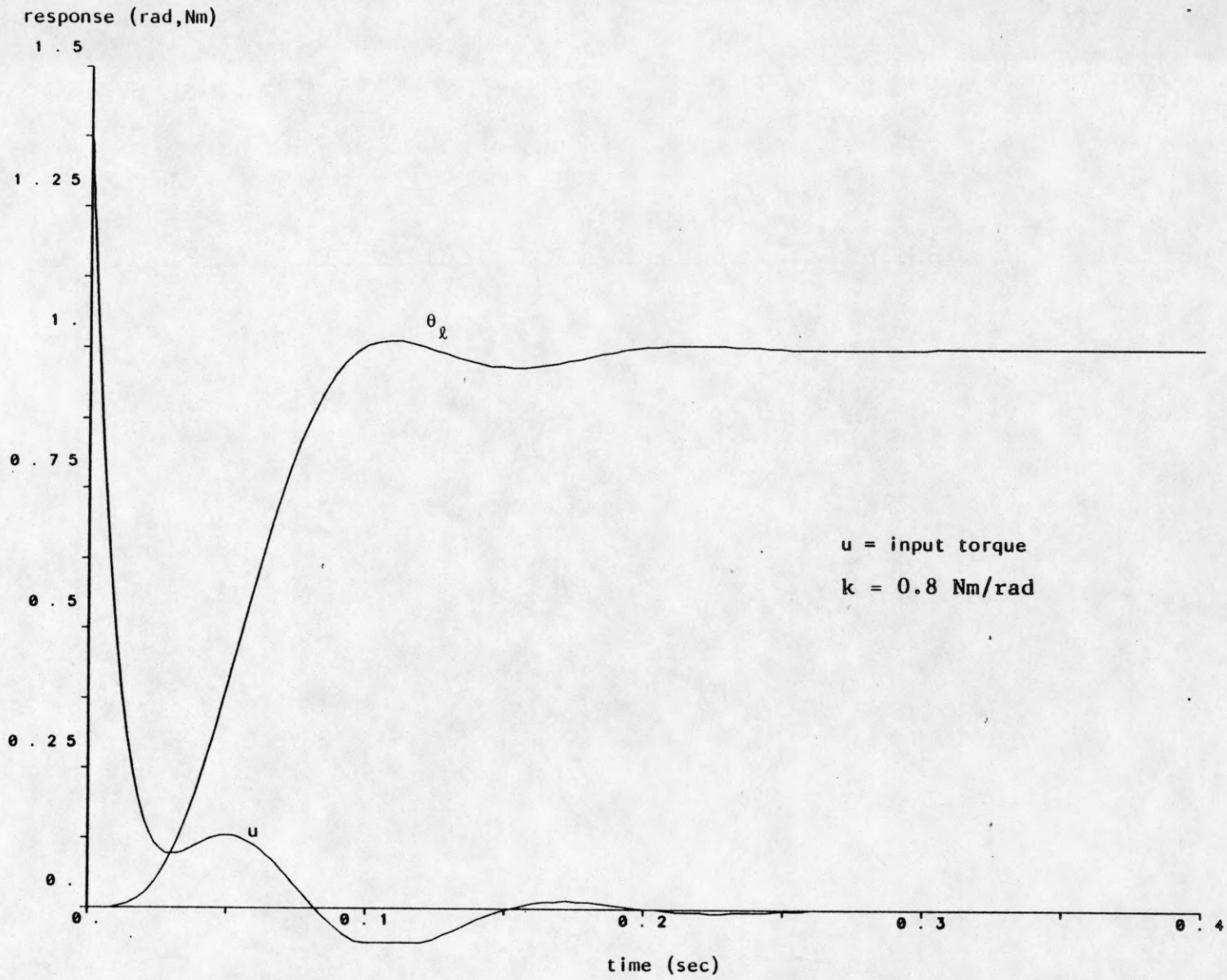

Figure 4.5 Input torque for system in state space and optimized pole placement

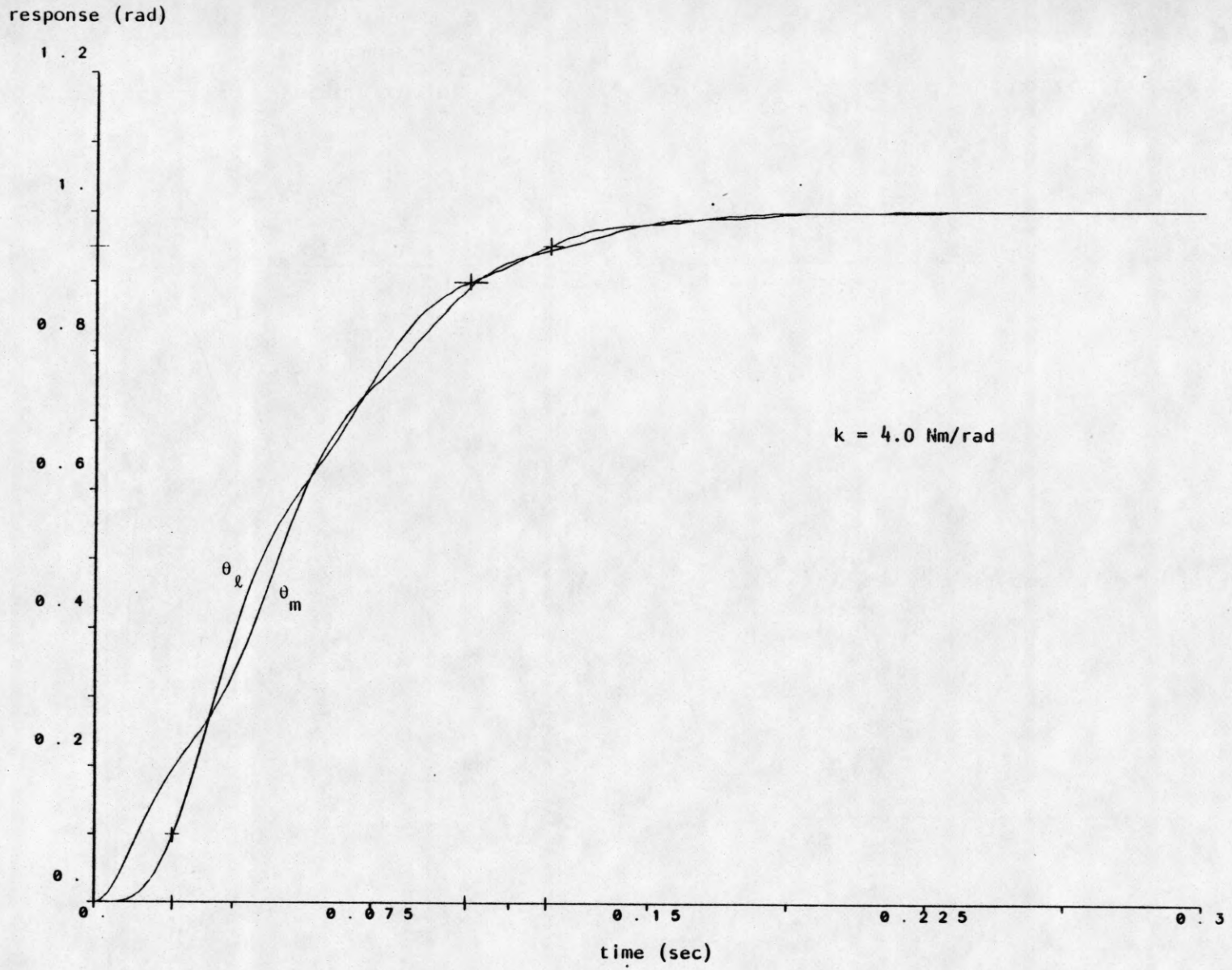

Figure 4.6 Step response for system in state space and optimized pole placement

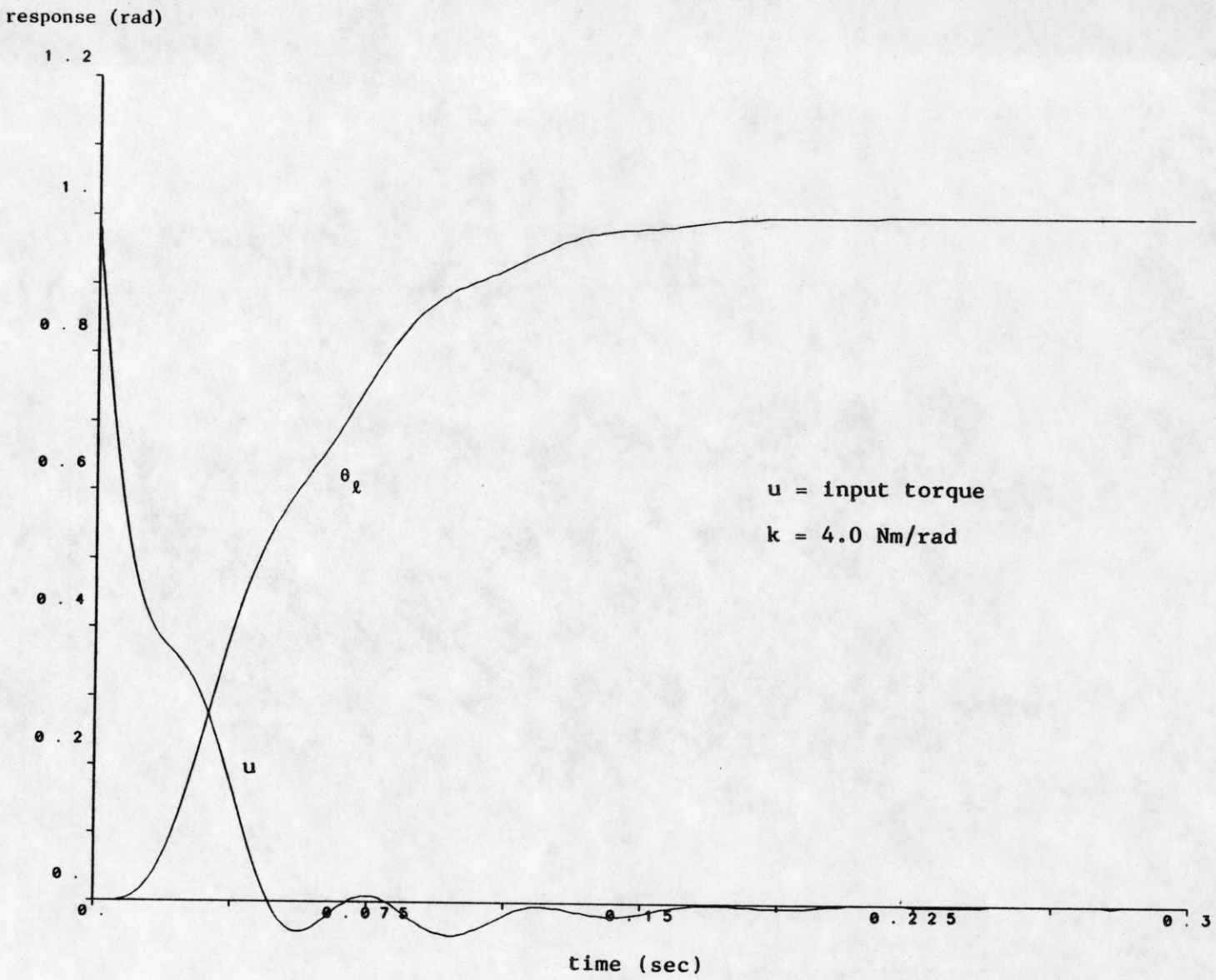

Figure 4.7 Input torque for system in state space and optimized pole placement

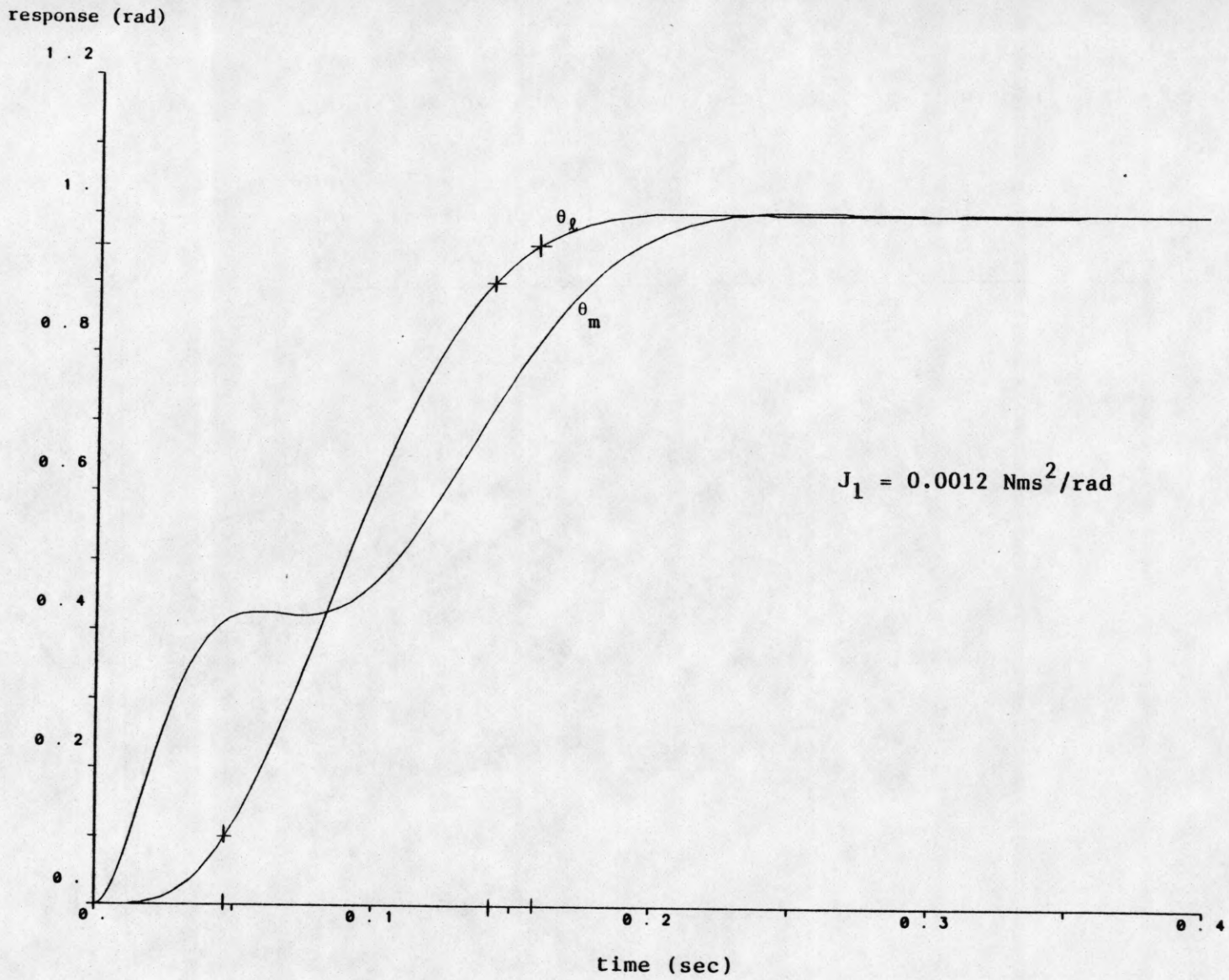

Figure 4.8 Step response for system in state space and optimized pole placement

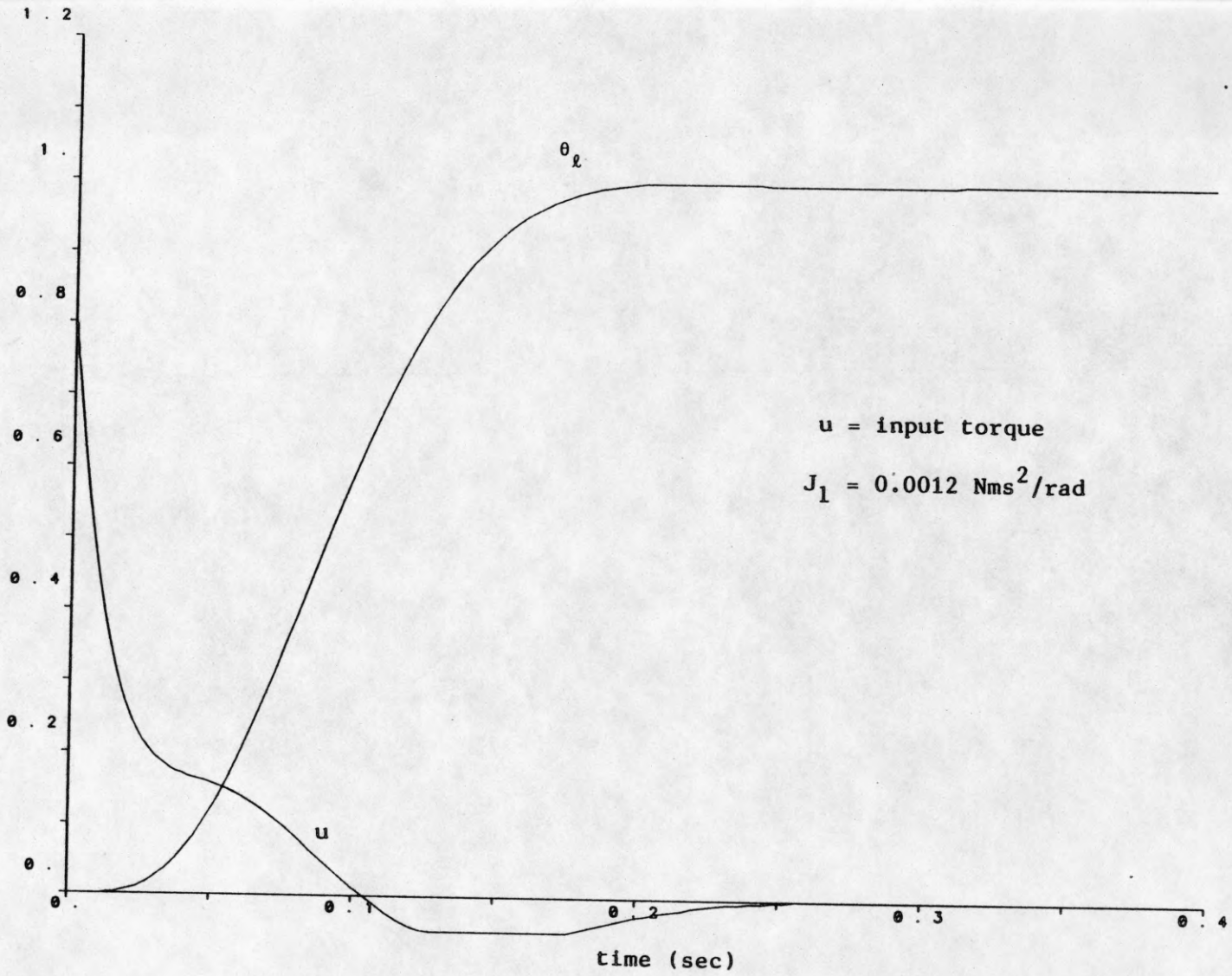

Figure 4.9 Input torque for system in state space and optimized pole placement

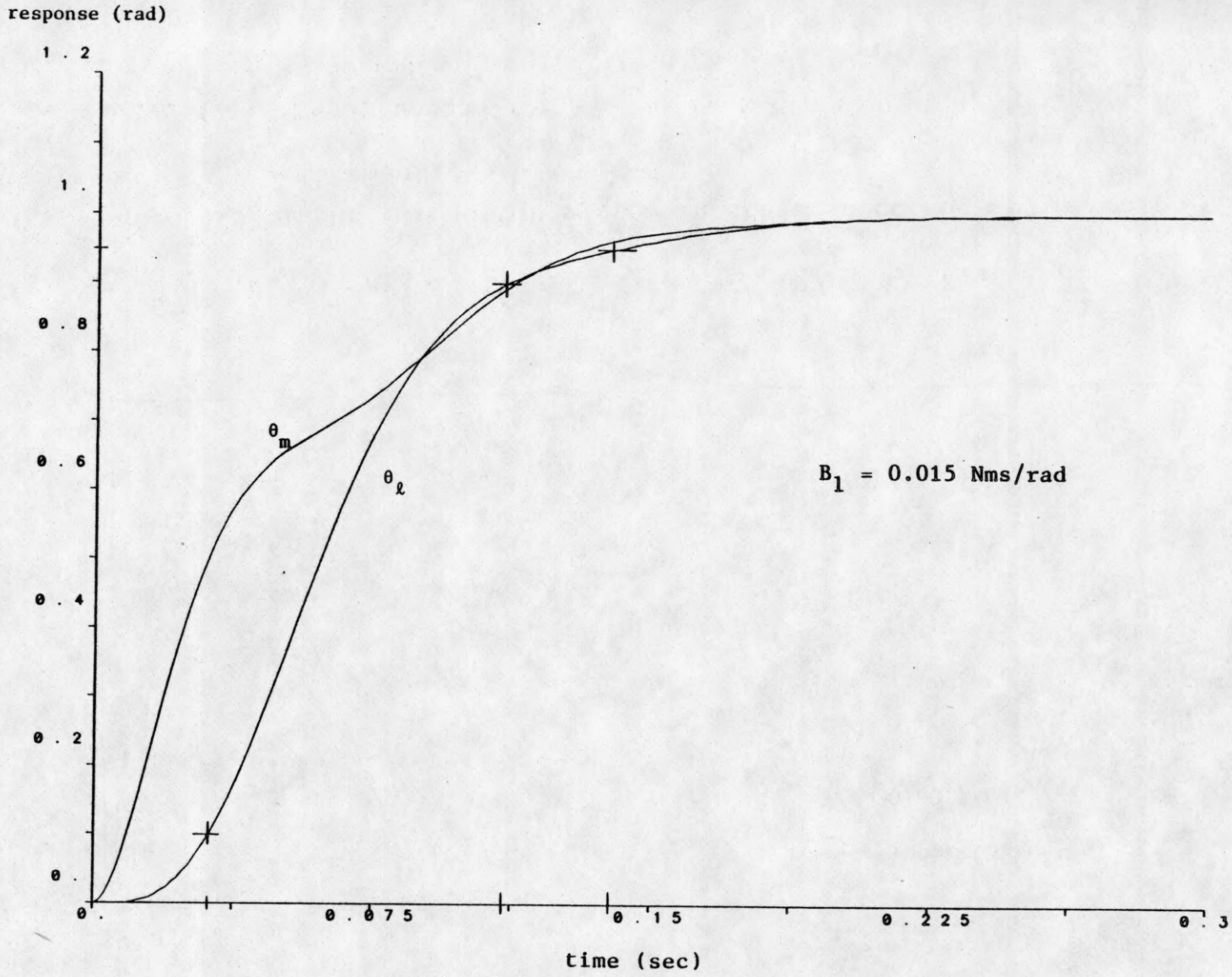

Figure 4.10 Step response for system in state space and optimized pole placement

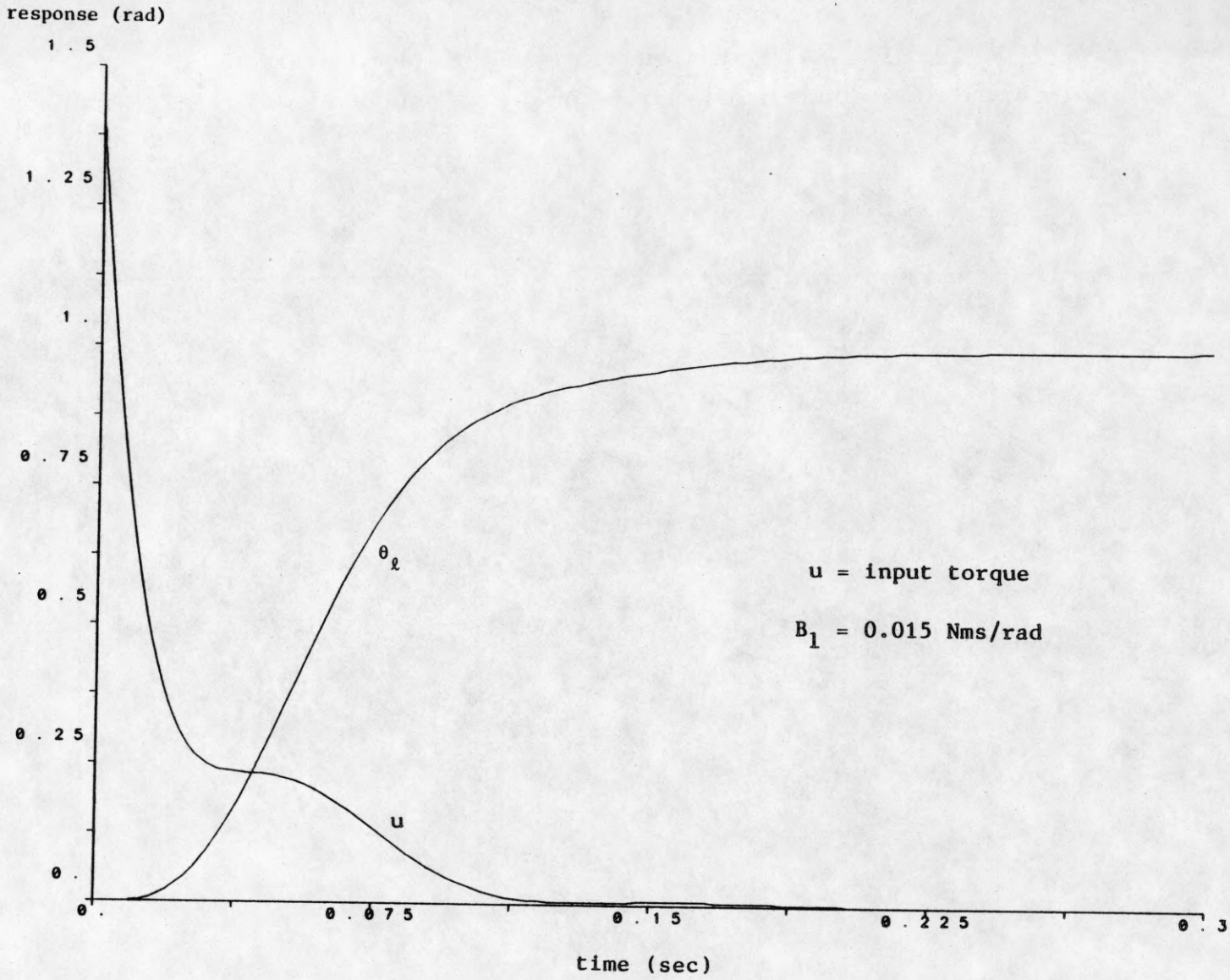

Figure 4.11 Input torque for system in state space and optimized pole placement

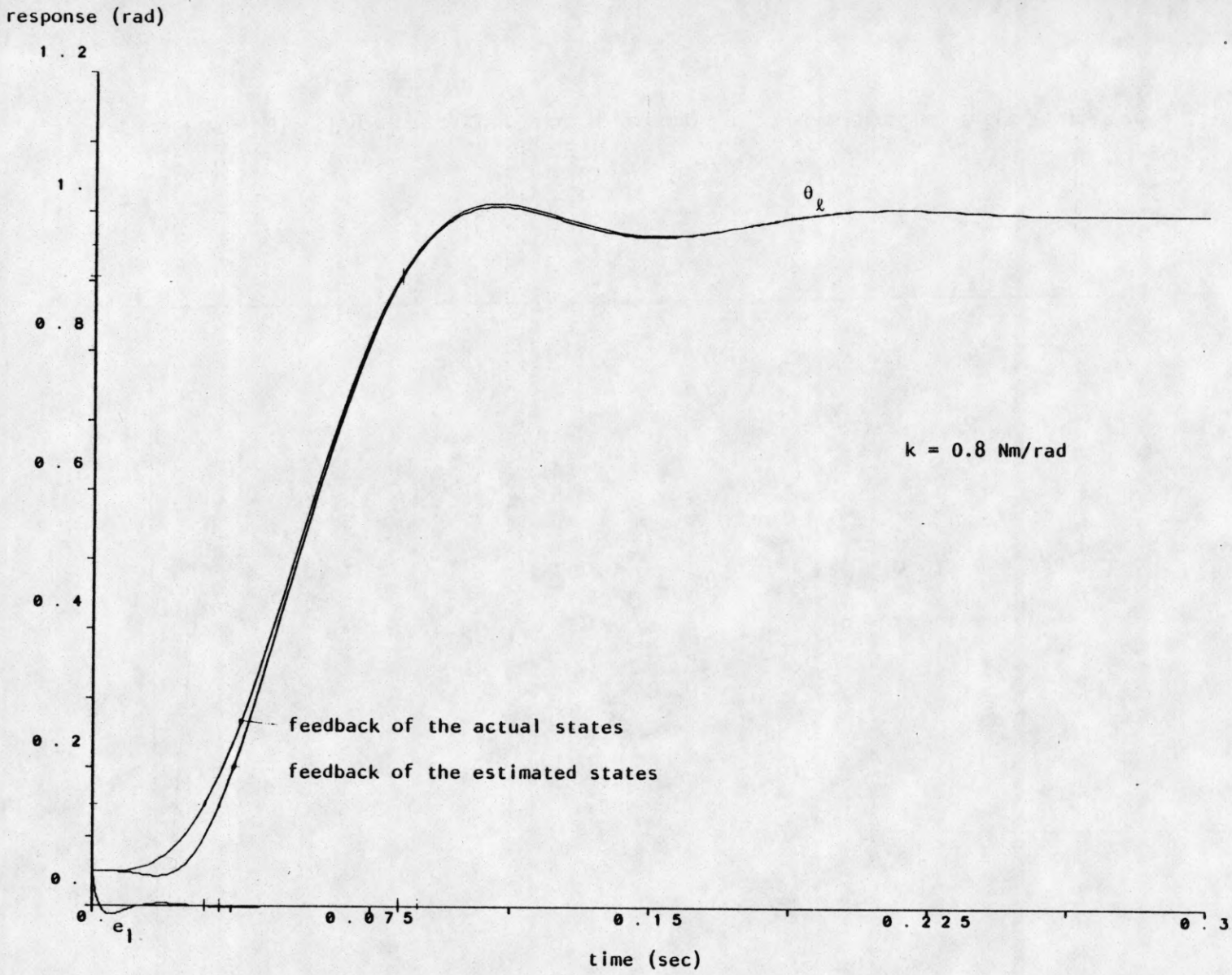

Figure 4.12 Step response for system in state space, optimized pole placement and a measurement error

5. NONLINEAR DESIGN

The linear design in the preceeding sections ignores the nonlinearity due to gravitational loading on the robot arm. In this section we consider the control problem for the nonlinear system (2.1) - (2.2). At this point a traditional gain scheduling approach could be used. The nonlinear equations of motion could be linearized around several operating points and an observer/state feedback compensator designed for each of the approximating linear systems. The resulting gain matrices could then be "scheduled" or switched appropriately in order to cover the full range of the manipulator motion.

We take a different approach here. Using some fairly recent results in differential geometric control theory we will instead design a nonlinear state feedback control law which, after a suitable state space change of coordinates, results in a globally linear system. We then design a nonlinear observer based on measurement of only the link angle which results in globally linear and asymptotically stable error dynamics between the observed and actual states. Our approach effectively compensates the nonlinearity in the system so that the preceeding linear design can be utilized. Hence, the linear behavior of the system is recovered. The advantage of this over the gain scheduling approach is that the control design is based on a single linear model which is globally exact rather than on a sequence of approximate linear models. Our approach can actually be viewed then as a kind of continuous gain scheduling in that the nonlinear observer/nonlinear state feedback compensator has the effect of continuously updating the gains at each point in order to achieve an exact linear response in the ideal case.

In the case of a rigid joint manipulator the gravitational term can be included directly in the control law (inverse dynamics) in order to cancel its effect on the arm. In the flexible joint case the nonlinearity is not in the range of the input and hence cannot be cancelled so simply. A generalization of this idea known as external or feedback linearization[4] can be used in the flexible joint case as shown in [3] for the single input system here considered and in [8] for the general n -link case.

We begin by choosing state variables $x_1, \ldots, x_4$ as before by setting

$$\begin{aligned} x_1 &= \theta_l & x_3 &= \theta_m \\ x_2 &= \dot{\theta}_l & x_4 &= \dot{\theta}_m \end{aligned} \tag{5.1}$$

Then from equation (2.1) - (2.2) we obtain

$$\begin{aligned}
\dot{x}_1 &= x_2 \\
\dot{x}_2 &= \frac{-Mgl}{J_l}\sin(x_1) - \frac{B_l}{J_l}x_2 - \frac{k}{J_l}(x_1 - x_3) \\
\dot{x}_3 &= x_4 \\
\dot{x}_4 &= -\frac{B_m}{J_m}x_4 + \frac{k}{J_m}(x_1 - x_3) + \frac{1}{J_m}u.
\end{aligned} \tag{5.2}$$

The system (5.2) is thus of the form

$$\dot{\mathbf{x}} = \mathbf{f}(\mathbf{x}) + \mathbf{g}(\mathbf{x})\,u \tag{5.3}$$

where

$$\mathbf{f}(\mathbf{x}) = \begin{pmatrix} x_2 \\ \frac{-Mgl}{J_l}\sin(x_1) - \frac{B_l}{J_l}x_2 - \frac{k}{J_l}(x_1 - x_3) \\ x_4 \\ -\frac{B_m}{J_m}x_4 + \frac{k}{J_m}(x_1 - x_3) \end{pmatrix}; \quad \mathbf{g}(\mathbf{x}) = \begin{pmatrix} 0 \\ 0 \\ 0 \\ \frac{1}{J_m} \end{pmatrix}. \tag{5.4}$$

Taking as our output y the measured link angle x_1, we have the output equation

$$y = \mathbf{C}\mathbf{x} \qquad \text{where} \qquad \mathbf{C} = \begin{bmatrix} 1 & 0 & 0 & 0 \end{bmatrix}. \tag{5.5}$$

5.1. Feedback Linearization

We first consider the control design problem for system (5.2) using full state feedback. The design and optimization of nonlinear systems is in general a rather difficult issue. Therefore we introduce the concept of feedback linearization which will enable us to apply the linear state space design of section 4. to the nonlinear system (5.2).

Definition: A nonlinear system

$$\dot{\mathbf{x}} = \mathbf{f}(\mathbf{x}) + \mathbf{g}(\mathbf{x})\,u \tag{5.7}$$

where $\mathbf{f}(\mathbf{x})$ and $\mathbf{g}(\mathbf{x})$ are C^∞ vector fields on R^n, with $\mathbf{f}(0) = 0$, and $u \in R$, is said

to be **feedback linearizable** in a neighborhood U of the origin if there is a C^∞ diffeomorphism $T : U \to R^n$ and nonlinear feedback

$$u = \alpha(x) + \beta(x)\, v \tag{5.8}$$

with $\beta(x) \neq 0$ on U such that

$$z = T(x) \tag{5.9}$$

satisfies the linear system

$$\dot{z} = A z + b v \tag{5.10}$$

where

$$A = \begin{bmatrix} 0 & 1 & 0 & & 0 \\ 0 & 0 & 1 & & . \\ . & . & . & . & . \\ . & . & . & . & . \\ . & . & . & & 1 \\ 0 & 0 & . & . 0 & 0 \end{bmatrix} ; \qquad b = \begin{bmatrix} 0 \\ 0 \\ . \\ . \\ . \\ 1 \end{bmatrix} \tag{5.11}$$

Remark

1) The nonlinear transformation (5.9) and the nonlinear control law (5.8) result in a linear controllable system (5.10), which we assume to be in Brunovsky canonical form without loss of generality. The diffeomorphism $T(x)$ can be thought of as a nonlinear state space change of coordinates. The idea of feedback linearization is that if one first changes to the coordinate system $z = T(x)$, then there exists a nonlinear control law to cancel the nonlinearities in the system.

Necessary and sufficient conditions on the vector fields f and g defining (5.7) are given in [4] as the following.

1. The vector fields $\{g, ad_f(g), \ldots, ad_f^{n-1}(g)\}$ are linearily independent in U;
2. The set $\{g, ad_f(g), \ldots, ad_f^{n-2}(g)\}$ is an involutive distribution of rank $n-1$ in U.

Here notations and terminology are as follows:

$$ad_f(g) = \left[\frac{\partial g}{\partial x}\right] f - \left[\frac{\partial f}{\partial x}\right] g \tag{5.12}$$

$$\mathrm{ad}_f^i g = \mathrm{ad}_f\,(\mathrm{ad}_f^{i-1}\, g) \tag{5.13}$$

A distribution D is said to be involutive if for any two vector fields X, Y belonging to D, $\mathrm{ad}_X Y$ belongs to D as well.

By performing the indicated calculations for system (5.3) we obtain

$$\left[g,\ \mathrm{ad}_f(g),\ \mathrm{ad}_f^2(g),\ \mathrm{ad}_f^3(g)\right] = \begin{bmatrix} 0 & 0 & 0 & \dfrac{k}{J_m J_l} \\ 0 & 0 & \dfrac{k}{J_m J_l} & \dfrac{k}{J_m J_l}\left[\dfrac{B_l}{J_l} - \dfrac{B_m}{J_m}\right] \\ 0 & -\dfrac{1}{J_m} & \dfrac{B_m}{J_m^2} & -\dfrac{k}{J_m^2} + \dfrac{B_m^2}{J_m^3} \\ \dfrac{1}{J_m} & -\dfrac{B_m}{J_m^2} & -\dfrac{k}{J_m^2} + \dfrac{B_m^2}{J_m^3} & \dfrac{B_m^3}{J_m^4} \end{bmatrix} \tag{5.14}$$

from which we can see that our system fulfills conditions 1. and 2. for feedback linearizability.

Let us now derive the appropriate coordinate system T(x) in which the system is linearizable by nonlinear feedback. For that purpose we rewrite equation (5.9)

$$z = T(x). \tag{5.15}$$

and see what conditions the transformation T(x) must satisfy. Differentiating both sides of (5.15) with respect to time yields,

$$\dot{z} = J_T(x)\,\dot{x} \tag{5.16}$$

where J_T is the Jacobian of the transformation T(x).

Using equations (5.10) and (5.3) equation (5.16) can be written

$$Az + b\nu = J_T\,(f(x) + g(x)\,u). \tag{5.17}$$

In component form with

$$T = \begin{bmatrix} T_1 \\ T_2 \\ T_3 \\ T_4 \end{bmatrix};\quad A = \begin{bmatrix} 0 & 1 & 0 & 0 \\ 0 & 0 & 1 & 0 \\ 0 & 0 & 0 & 1 \\ 0 & 0 & 0 & 0 \end{bmatrix};\quad b = \begin{bmatrix} 0 \\ 0 \\ 0 \\ 1 \end{bmatrix} \tag{5.18}$$

we see that the first equation in (5.17) is

$$\frac{\partial T_1}{\partial x_1}\dot{x}_1 + \frac{\partial T_1}{\partial x_2}\dot{x}_2 + \frac{\partial T_1}{\partial x_3}\dot{x}_3 + \frac{\partial T_1}{\partial x_4}\dot{x}_4 = T_2 \tag{5.19}$$

which can be written compactly as

$$<dT_1, \dot{x}> = <dT_1, f(x) + g(x)u> = T_2. \tag{5.20}$$

where we use the notation

$$<dT_n, g> = \frac{\delta T_n}{\delta x_1} g_1 + \frac{\delta T_n}{\delta x_2} g_2 + \frac{\delta T_n}{\delta x_3} g_3 + \frac{\delta T_4}{\delta x_4} g_4. \tag{5.21}$$

Similarly, the other components of T satisfy

$$<dT_2, f(x) + g(x)u> = T_3 \tag{5.22}$$

$$<dT_3, f(x) + g(x)u> = T_4 \tag{5.23}$$

$$<dT_4, f(x) + g(x)u> = v \tag{5.24}$$

This leads to the system of partial differential equations

$$\begin{aligned} <dT_1, f> + <dT_1, g>u &= T_2 \\ <dT_2, f> + <dT_2, g>u &= T_3 \\ <dT_3, f> + <dT_3, g>u &= v \end{aligned} \tag{5.25}$$

Since $T_1, \ldots, T_4$ are independent of u while v is not independent of u we conclude that

$$<dT_1, g> = 0,\ <dT_2, g> = 0,\ <dT_3, g> = 0,\ <dT_4, g> \neq 0 \tag{5.26}$$

$$<dT_i, f> = T_{i+1}; \quad i = 1,\ldots,3 \tag{5.27}$$

For system (5.3) one explicit solution of (5.26) can be found as

$$T_1 = x_1. \tag{5.28}$$

With this T_1 the components $T_2, \ldots, T_4$ can be computed inductively from (5.27). We obtain for T(x)

$$z_1 = T_1 = x_1$$

$$z_2 = T_2 = x_2$$

$$z_3 = T_3 = \dot{z}_2 = \frac{-Mgl}{J_l}\sin(x_1) - \frac{B_l}{J_l}x_2 - \frac{k}{J_l}(x_1 - x_3) \tag{5.29}$$

$$z_4 = T_4 = \dot{z}_3 = \frac{-Mgl}{J_l}\cos(x_1)\cdot x_2$$

$$- \frac{B_l}{J_l}\left[\frac{-Mgl}{J_l}\sin(x_1) - \frac{B_l}{J_l}x_2 - \frac{k}{J_l}(x_1 - x_3)\right] - \frac{k}{J_l}(x_2 - x_4).$$

The feedback linearizing control input u is found from the condition $\dot{z}_4 = v$ (from (5.10)) as

$$u = \frac{J_m J_l}{k}\left[v - a(x)\right] = \beta(x)\, v + \alpha(x) \tag{5.30}$$

where

$$a(x) := \left[\frac{-Mgl}{J_l}\sin(x_1) - \frac{B_l}{J_l}x_2 - \frac{k}{J_l}(x_1 - x_3)\right]\left[\frac{-Mgl}{J_l}\cos(x_1) + \frac{B_l^2}{J_l^2} - \frac{k}{J_l}\right]$$

$$+ \frac{Mgl}{J_l}\sin(x_1)\cdot x_2^2 + \frac{B_l Mgl}{J_l^2}\cos(x_1)\cdot x_2 + \frac{B_l k}{J_l^2}(x_2 - x_4) \tag{5.31}$$

$$- \frac{kB_m}{J_m J_l}x_4 + \frac{k^2}{J_m J_l}(x_1 - x_3)$$

Therefore in the coordinates $z_1, \ldots, z_4$ with the above control law u the system becomes

$$\dot{z}_1 = z_2\ , \qquad \dot{z}_3 = z_4$$
$$\dot{z}_2 = z_3\ , \qquad \dot{z}_4 = v \tag{5.32}$$

or, in matrix form,

$$\dot{z} = A z + b v \tag{5.33}$$

where

$$A = \begin{bmatrix} 0 & 1 & 0 & 0 \\ 0 & 0 & 1 & 0 \\ 0 & 0 & 0 & 1 \\ 0 & 0 & 0 & 0 \end{bmatrix} \quad ; \quad b = \begin{bmatrix} 0 \\ 0 \\ 0 \\ 1 \end{bmatrix}. \tag{5.34}$$

Remarks

2) The state space change of coordinates $z = T(x)$ given by (5.29) is actually a global diffeomorphism. In order to see this we need only compute the inverse transformation. By inspection we see that

$$\begin{aligned} x_1 &= z_1 \\ x_2 &= z_2 \\ x_3 &= z_1 + \frac{J_l}{k}\left[z_3 + \frac{Mgl}{J_l}\sin(z_1) + \frac{B_l}{J_l}z_2\right] \\ x_4 &= z_2 + \frac{J_l}{k}\left[z_4 + \frac{B_l}{J_l}z_3 + \frac{Mgl}{J_l}\cos(z_1)\cdot z_2\right]. \end{aligned} \tag{5.35}$$

The inverse transformation is well defined and C^∞ everywhere and hence the feedback linearization for the system (5.2) holds globally.

3) The transformed variables $z_1, \ldots, z_4$ are themselves physically meaningful. We see that

$$\begin{aligned} z_1 &= x_1 = \text{ link position }, & z_3 &= \dot{z}_2 = \text{ link acceleration} \\ z_2 &= x_2 = \text{ link velocity }, & z_4 &= \dot{z}_3 = \text{ link jerk} \end{aligned} \tag{5.36}$$

Since the motion trajectory of the link is typically specified in terms of these quantities they are natural variables to use for feedback.

The linear system (5.33) in fact is the Brunovsky canonical form of the linear system (4.2) for which we have already designed a linear state feedback controller in the previous section. We can then choose the input v to be a linear state feedback control

$$\begin{aligned} v &= -\alpha_4 z_1 - \alpha_3 z_2 - \alpha_2 z_3 - \alpha_1 z_4 + r \\ &= -\alpha_4 T_1(x) - \alpha_3 T_2(x) - \alpha_2 T_3(x) - \alpha_1 T_4(x) + r \ . \end{aligned} \tag{5.37}$$

in order to place the closed loop poles. The characteristic equation of the linear

system is then given by

$$\alpha(s) = \det\{s\,\mathbf{I} - \mathbf{A}_c\} \quad \text{with} \quad \mathbf{A}_c = \begin{bmatrix} 0 & 1 & 0 & 0 \\ 0 & 0 & 1 & 0 \\ 0 & 0 & 0 & 1 \\ -\alpha_4 & -\alpha_3 & -\alpha_2 & -\alpha_1 \end{bmatrix} \tag{5.38}$$

which leads to

$$\alpha(s) = s^4 + \alpha_1 s^3 + \alpha_2 s^2 + \alpha_3 s + \alpha_4 . \tag{5.39}$$

By choosing the parameters $\alpha_1, \ldots, \alpha_4$ identical to the parameters of the equation $\det\{s\,\mathbf{I} - \mathbf{A}_C\}$ with $\mathbf{A}_C$ from equation (4.10) we obtain for the characteristic behavior of the linearized system the same as for the system (4.2). Hence, we can directly apply the design of our linear model to the linearized model.

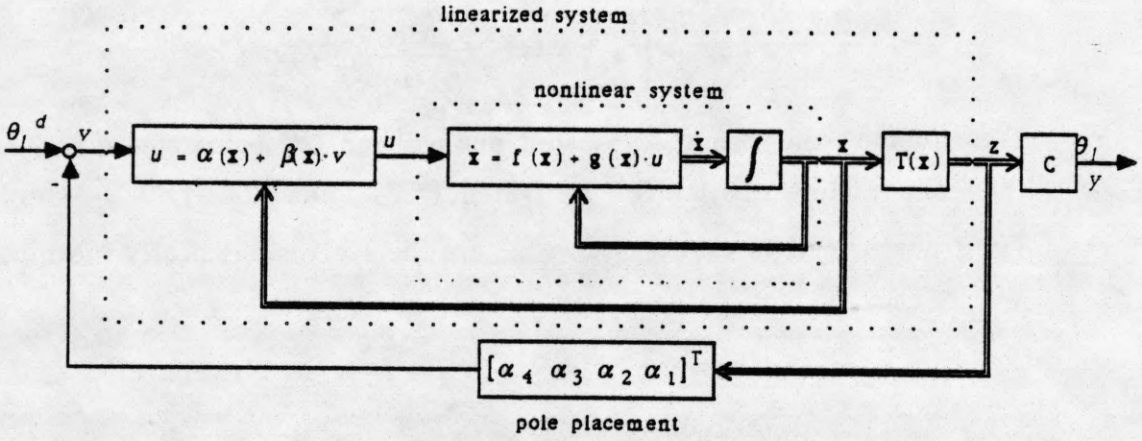

Figure 5.1 The nonlinear system with a linear design

Figure 5.1 shows the structure of our new nonlinear system with linearizing feedback and pole assignment.

5.2. Nonlinear observer design

We now turn to the design of an observer to estimate the state of the system (5.2) using the measured output y in order to apply the state feedback control law (5.8), (5.37). Note, since the system is nonlinear, the linear observer design of the previous section is inadequate as it does not necessarily lead to stable error

dynamics. Using the results of Krener and Isidori [5] we can, however, design a nonlinear observer such that globally the error between the estimated state and actual state satisfies a stable linear system.

To see this it suffices to note that the nonlinear system (5.2) can be rewritten in terms of the output y as

$$\dot{\mathbf{x}} = \mathbf{A}\mathbf{x} + \mathbf{b}u + \boldsymbol{\phi}(y) \tag{5.40}$$

$$y = \mathbf{C}\mathbf{x} \tag{5.41}$$

where

$$\mathbf{A} = \begin{bmatrix} 0 & 1 & 0 & 0 \\ -\frac{k}{J_l} & -\frac{B_l}{J_l} & \frac{k}{J_l} & 0 \\ 0 & 0 & 0 & 1 \\ \frac{k}{J_m} & 0 & -\frac{k}{J_m} & -\frac{B_m}{J_m} \end{bmatrix}; \quad \mathbf{b} = \begin{bmatrix} 0 \\ 0 \\ 0 \\ \frac{1}{J_m} \end{bmatrix}; \quad \mathbf{C} = \begin{bmatrix} 1 & 0 & 0 & 0 \end{bmatrix} \tag{5.42}$$

and

$$\boldsymbol{\phi}(y) = \begin{bmatrix} 0 \\ -Mgl \sin y \\ 0 \\ 0 \end{bmatrix} \tag{5.43}$$

Since the nonlinear term $\boldsymbol{\phi}$ in (5.40) is a function of the measured output we can construct a nonlinear observer of the form

$$\dot{\hat{\mathbf{x}}} = \mathbf{A}\hat{\mathbf{x}} + \mathbf{b}u + \boldsymbol{\phi}(y) + \mathbf{G}(y - \mathbf{C}\hat{\mathbf{x}}). \tag{5.44}$$

Combining (5.40) and (5.44) we see that the error $\mathbf{e} = \mathbf{x} - \hat{\mathbf{x}}$ satisfies the linear system

$$\dot{\mathbf{e}} = (\mathbf{A} - \mathbf{G}\mathbf{C})\mathbf{e}. \tag{5.45}$$

and we have recovered the earlier linear dynamics (4.18). The block diagram in Figure 5.2 demonstrates how the observer is designed.

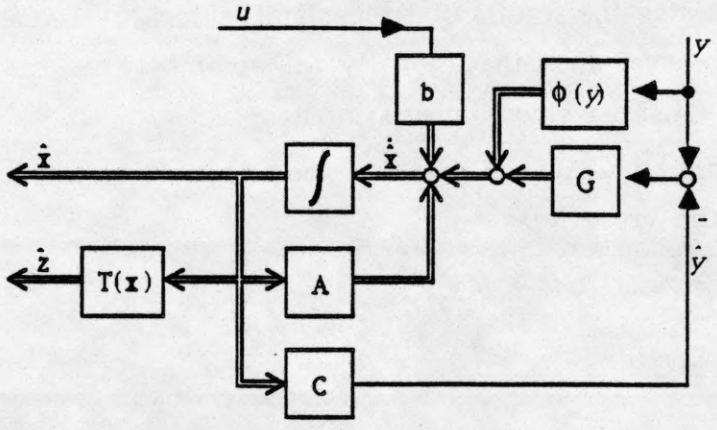

Figure 5.2 Nonlinear observer design

The observer feedback matrix $\mathbf{G} = [G_1\ G_2\ G_3\ G_4]^T$ is then found by comparing the coefficients of the characteristic equation of the observer

$$\alpha_O(s) = \det\{s\,\mathrm{I} - (\mathrm{A} - \mathbf{G}\,\mathrm{C})\} \tag{5.46}$$

with the desired characteristic equation

$$\alpha_O^d(s) = s^4 + \alpha_1 s^3 + \alpha_2 s^2 + \alpha_3 s + \alpha_4 \tag{5.47}$$

This is equivalent to the derivation of $\mathbf{K_O}$ in section 4. (equation (4.20)).

5.3. Simulation Results

Figure 5.3 shows the step response of the nonlinear system using the above nonlinear observer/feedback linearizing control law. As in the linear case in section 4.2.4. we assume an error of 0.05 rad for the link measurement in order to obtain insight not only into the system behavior but also into the observer behavior. The parameters of the system are identical to the parameters used earlier for the linear model (section 3.2.). In addition M is chosen as 2 kg which after reflection through a 100:1 gear ratio is equivalent to 0.02 kg at the motor side. The distance l to the center of mass of the link is 0.5 m. The observer gains and outer loop control gains are also chosen identical to those used in the linear case under section 4.2. We see from Figure 5.3 that the response of the linearized nonlinear system is nearly identical to the response of the linear system shown in Figure 4.12.

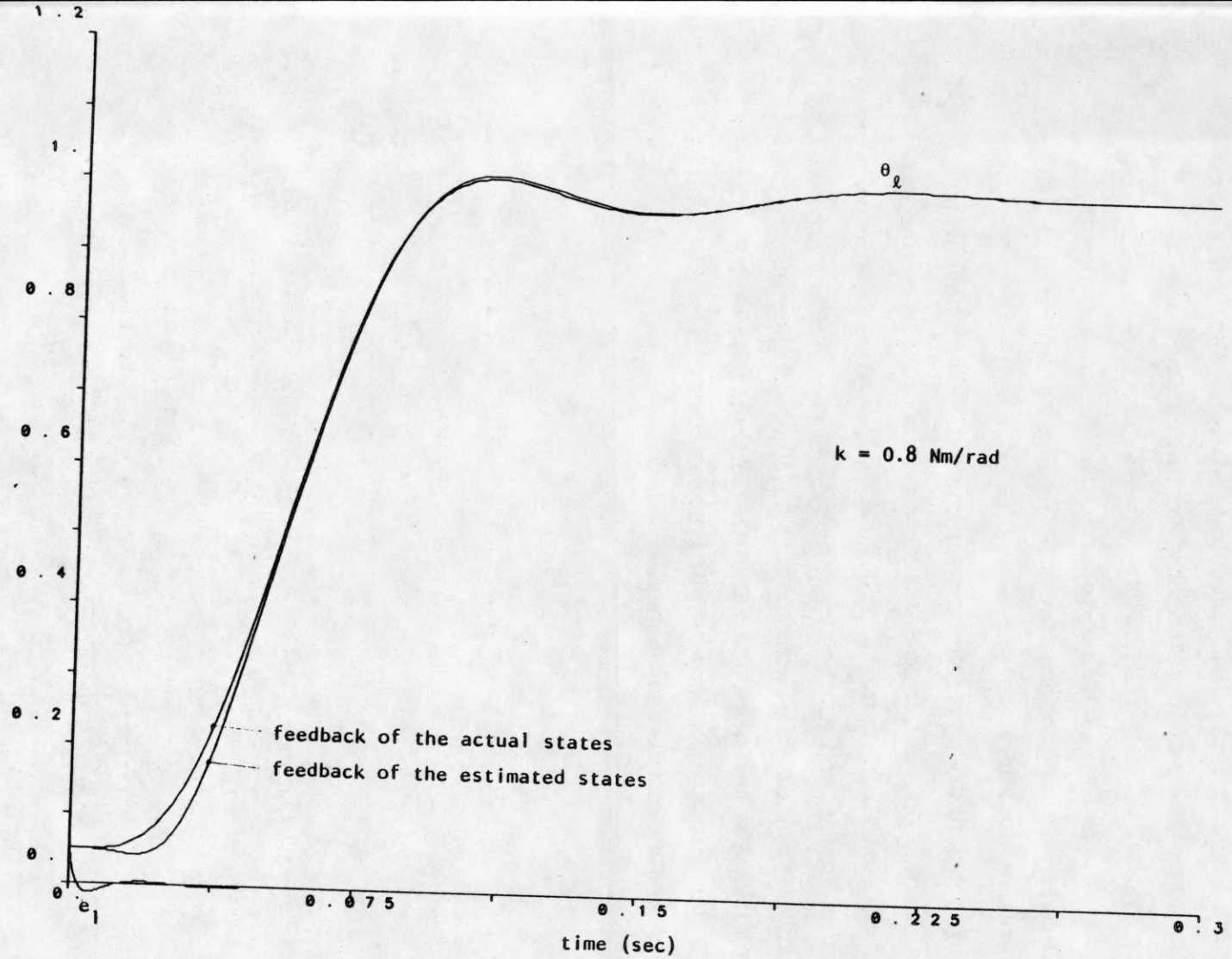

Figure 5.3 Step response for nonlinear system with linearizing feedback and a measurement error

6. SINGULAR PERTURBATION DESIGN

In the preceeding linear and nonlinear control design for our single link model we had to operate on a fourth order system. It would be advantageous, however, to reduce the single link model to second order. This would ease the design because for a second order system, a direct relationship between the characteristic frequency and damping ratio of its unit step response exists. The singular perturbation approach undertaken in this section allows the accomplishment of this goal through a parameter transformation.

The underlying idea is to divide a given system into a dominant slow system and into a fast boundary layer. In our case, the slow system would describe the dynamics of mass and inertia of motor and link, and the fast system would describe the dynamics arising from the joint stiffness. The second order system obtained for the slow dynamics will then represent an approximation of a rigid link, provided the stiffness is sufficiently large. In the following we describe the derivation of a singular perturbation form of our linear system (2.3) - (2.4) and the design procedure for slow and fast subsystem.

The linear transformation

$$\begin{aligned} x_1 &= \theta_l \quad , \qquad z_1 = k_1 \cdot k_2 (\theta_l - \theta_m) \\ x_2 &= \dot{x}_1 \quad , \qquad z_2 = \epsilon \dot{z}_1 \end{aligned} \tag{6.1}$$

where

$$k_1 \cdot k_2 = k \quad , \quad \epsilon = \frac{1}{\sqrt{k_1}}$$

transforms system (2.3) - (2.4) into

$$J_l \dot{x}_2 + B_l x_2 + z_1 = 0 \tag{6.2}$$

and

$$J_m \left(-\frac{1}{k_1 k_2} \ddot{z}_1 + \ddot{x}_1 \right) + B_m \left(-\frac{1}{k_1 k_2} \dot{z}_1 + \dot{x}_1 \right) - z_1 = u$$

which is after some rearrangement

$$-\epsilon \frac{J_m}{k_2} \dot{z}_2 + J_m \dot{x}_2 - \epsilon \frac{B_m}{k_2} z_2 + B_m \dot{x}_1 - z_1 = u \; . \tag{6.3}$$

The state space representation of system (6.2) - (6.3) is

$$\begin{bmatrix} \dot{x}_1 \\ \dot{x}_2 \\ \epsilon\dot{z}_1 \\ \epsilon\dot{z}_2 \end{bmatrix} = \begin{bmatrix} 0 & 1 & 0 & 0 \\ 0 & -\frac{B_l}{J_l} & -\frac{1}{J_l} & 0 \\ 0 & 0 & 0 & 1 \\ 0 & k_2\left(\frac{B_m}{J_m} - \frac{B_l}{J_l}\right) & -k_2\left(\frac{1}{J_m} + \frac{1}{J_l}\right) & -\epsilon\frac{B_m}{J_m} \end{bmatrix} \cdot \begin{bmatrix} x_1 \\ x_2 \\ z_1 \\ z_2 \end{bmatrix} + \begin{bmatrix} 0 \\ 0 \\ 0 \\ -\frac{k_2}{J_m} \end{bmatrix} \tag{6.4}$$

or also

$$\begin{bmatrix} \dot{\mathbf{x}} \\ \epsilon\dot{\mathbf{z}} \end{bmatrix} = \begin{bmatrix} \mathbf{A}_{11} & \mathbf{A}_{12} \\ \mathbf{A}_{21} & \mathbf{A}_{22} \end{bmatrix} \cdot \begin{bmatrix} \mathbf{x} \\ \mathbf{z} \end{bmatrix} + \begin{bmatrix} \mathbf{B}_1 \\ \mathbf{B}_2 \end{bmatrix} \cdot u \tag{6.5}$$

with

$$\mathbf{x} = \begin{bmatrix} x_1 \\ x_2 \end{bmatrix}, \qquad \mathbf{z} = \begin{bmatrix} z_1 \\ z_2 \end{bmatrix} \tag{6.6}$$

and

$$\mathbf{A}_{11} = \begin{bmatrix} 0 & 1 \\ 0 & -\frac{B_l}{J_l} \end{bmatrix}, \qquad \mathbf{A}_{12} = \begin{bmatrix} 0 & 0 \\ -\frac{1}{J_l} & 0 \end{bmatrix},$$

$$\mathbf{A}_{21} = \begin{bmatrix} 0 & 0 \\ 0 & k_2\left(\frac{B_m}{J_m} - \frac{B_l}{J_l}\right) \end{bmatrix}, \quad \mathbf{A}_{22} = \begin{bmatrix} 0 & 1 \\ -k_2\left(\frac{1}{J_m} + \frac{1}{J_l}\right) & -\epsilon\frac{B_m}{J_m} \end{bmatrix}, \tag{6.7}$$

$$\mathbf{B}_1 = \begin{bmatrix} 0 \\ 0 \end{bmatrix}, \qquad \mathbf{B}_2 = \begin{bmatrix} 0 \\ -\frac{k_2}{J_m} \end{bmatrix}.$$

It is obvious from (6.4) that for small parameters ϵ, that is for large stiffnesses k, the vector $\dot{\mathbf{z}}$ is relatively large compared to $\dot{\mathbf{x}}$. This results in a rapid decline of the vector z. Consequently, variables z_1 and z_2 can be referred to as fast variables and variables x_1 and x_2 as slow variables.

From our original linear model in the form (6.4) we can show, as an example, how to obtain the system equation for a rigid link. For constant parameters k_2, (6.4) becomes for $\epsilon \rightarrow 0$, that is $k \rightarrow \infty$

$$\dot{x}_2 = -\frac{B_l}{J_l} x_2 - \frac{1}{J_l} z_1 \tag{6.8}$$

$$0 = k_2 \left(\frac{B_m}{J_m} - \frac{B_l}{J_l} \right) x_2 - k_2 \left(\frac{1}{J_m} + \frac{1}{J_l} \right) z_1 - \frac{k_2}{J_m} u \tag{6.9}$$

Equation (6.9) in (6.8) yields

$$\dot{x}_2 = -\frac{B_l}{J_l} x_2 - \frac{1}{J_l} \frac{B_m J_l - B_l J_m}{J_m + J_l} x_2 + \frac{1}{J_l} \frac{J_l}{J_m + J_l} u ,$$

$$= -\frac{B_m + B_l}{J_m + J_l} x_2 + \frac{1}{J_m + J_l} u , \tag{6.10}$$

and with $x_2 = \dot{\theta}_l$

$$(J_m + J_l) \ddot{\theta}_l + (B_m + B_l) \theta_l = u . \tag{6.11}$$

Equation (6.11) represents an approximation of the fourth order system (2.3) - (2.4) through its slow dynamics which is valid for large stiffnesses. Furthermore, (6.11) shows that a rigid link can be modelled by taking motor and link inertia together as one inertia and adding motor and link friction, as one could expect.

6.1. Linear feedback design

A decomposition of our original system (2.3) - (2.4) into the two lower order slow and fast subsystems

$$\dot{x} = \mathbf{A}_{11} \mathbf{x} + \mathbf{A}_{12} \mathbf{z} + \mathbf{B}_1 u \tag{6.12}$$

$$\epsilon \dot{\mathbf{z}} = \mathbf{A}_{21} \mathbf{x} + \mathbf{A}_{22} \mathbf{z} + \mathbf{B}_2 u \tag{6.13}$$

enables us to design a feedback control for each of these subsystems separately. We can design the dynamics of the dominant slow system (6.12) to our desire while assuring through a feedback design for the fast subsystem (6.13) that it declines so fast that its overall influence on the system behavior remains insignificant.

As a first step to a separated design, a control of the form

$$u = \mathbf{G}_1 \mathbf{x} + \mathbf{G}_2 \mathbf{z} \tag{6.14}$$

is applied to system (6.12) - (6.13). This yields the closed-loop system

$$\begin{bmatrix} \dot{x} \\ \epsilon \dot{z} \end{bmatrix} = \begin{bmatrix} A_{11} + B_1 G_1 & A_{12} + B_1 G_2 \\ A_{21} + B_2 G_1 & A_{22} + B_2 G_2 \end{bmatrix} \cdot \begin{bmatrix} x \\ z \end{bmatrix} . \tag{6.15}$$

A transformation of system (6.15) into the block diagonal form

$$\begin{bmatrix} \dot{\zeta} \\ \epsilon \dot{\eta} \end{bmatrix} = \begin{bmatrix} A_s + B_s G_s & 0 \\ 0 & A_f + B_f G_f \end{bmatrix} \cdot \begin{bmatrix} \zeta \\ \eta \end{bmatrix} \tag{6.16}$$

would allow the separated design in an easy manner through parameters G_s for the slow subsystem and G_f for the fast subsystem.

Let us show in the following how the matrizes in (6.16) can be interpreted as separate system matrizes for slow and fast subsystems and make clearer at the same time why we refer to η as the fast variable.

By introducing the time scale modification

$$\tau = \frac{t - t_0}{\epsilon} \tag{6.17}$$

with an initial time t_0, the derivation

$$\epsilon \dot{\eta}(t) = \epsilon \frac{d\eta(t)}{dt} \tag{6.18}$$

becomes

$$\epsilon \dot{\eta}(t) = \epsilon \frac{d\eta(\tau)}{d\tau} \cdot \frac{d\tau}{dt} = \frac{d\eta(\tau)}{d\tau} \tag{6.19}$$

With (6.19) we can write (6.16) as

$$\dot{\zeta}(t) = (A_s + G_s G_s)\, \zeta(t) \tag{6.20}$$

$$\frac{d\eta(\tau)}{d\tau} = (A_f + B_f G_f)\, \eta(\tau) \tag{6.21}$$

Hence, the poles of the fast subsystem are those of $A_f + B_f G_f$ in the (fast) time scale τ. Through the parameter ϵ, this time scale is a stretched form of the real time scale t in which the slow system poles are found. A decline in τ will consequently be faster by the factor ϵ in the time scale t. Given pole locations of (6.21), $\eta(\tau)$ will decline the faster the smaller ϵ is. From this we can draw the conclusion that pole locations for the fast subsystem do not have to be placed much further left to the slow subsystem poles, provided ϵ is sufficiently small.

Kokotovic gives in [9] (pages 96-97) the transformation leading from (6.15) to the system representation in (6.16) as

$$\begin{bmatrix}\zeta\\ \eta\end{bmatrix} = \begin{bmatrix} I_n - \epsilon H L & -\epsilon H \\ L & I_m \end{bmatrix} \cdot \begin{bmatrix} x \\ z \end{bmatrix} \tag{6.22}$$

where the slow sub-system is of order n and the fast sub-system of order m. Matrices L and H in (6.22) are given by

$$0 = A_{22} L - \epsilon L (A_{11} + B_1 G_s) + \epsilon L A_{12} L - (A_{21} + B_2 G_s) \tag{6.23}$$

and

$$\begin{aligned} 0 = {} & \epsilon [A_{11} + B_1 G_1 - (A_{12} + B_1 G_2) L] H \\ & - H [A_{22} + B_2 G_2 + \epsilon L (A_{12} + B_1 G_2)] + A_{12} + B_1 G_2 . \end{aligned} \tag{6.24}$$

The system matrices A_s, B_s, A_f and B_f are determined from

$$\begin{aligned} A_s &= A_{11} - A_{12} A_{22}^{-1} [A_{21} + \epsilon L (A_{11} - A_{12} L)] \\ B_s &= B_1 - A_{12} A_{22}^{-1} (B_2 + \epsilon L B_1)] \\ A_f &= A_{22} + \epsilon L A_{12} \quad , \quad B_f = B_2 + \epsilon L B_1 \end{aligned} \tag{6.25}$$

and the design parameters G_1, G_2 are related to G_s, G_f through

$$G_1 = G_s + G_f L \qquad \text{and} \qquad G_2 = G_f . \tag{6.26}$$

Once G_s and G_f are found, the composite control applicable to the original system (6.12) - (6.13) can be determined from (6.14) with (6.26) as

$$u = (G_s + G_f L) x + G_f z \tag{6.27}$$

A problem in the actual design process is the dependency of transformation matrix L from the design parameter G_s in equation (6.23). Knowledge of L is necessary for the derivation of A_s and B_s, which lead to G_s. Hence, L cannot be determined without knowing G_s and vice versa. However, it is possible to calculate an approximation of L without knowing G_s.

In [9] (p. 94-95 and 99-100), the design procedure for a second order approximation is given:

The first step is to find the first order approximation G_s' of G_s through placing the eigenvalues of

$$A_s' + B_s' G_s' \tag{6.28}$$

at the desired pole locations of the slow subsystem. System matrices A_s' and B_s' in (6.28) are determined from

$$A_s' = A_{11} - A_{12} A_{22}^{-1} A_{21} \quad , \quad B_s' = B_1 - A_{12} A_{22}^{-1} B_2 . \tag{6.29}$$

The corresponding first order approximation of L is

$$L' = A_{22}^{-1} (A_{21} + B_2 G_s') . \tag{6.30}$$

In the next step, a second order approximation

$$A_s'' + B_s'' G_s'' \tag{6.31}$$

of the slow system is designed. Here we have

$$\begin{aligned} A_s'' &= A_s' - \epsilon A_{12} A_{22}^{-1} L' (A_{11} - A_{12} L') \\ B_s'' &= B_s' - \epsilon A_{12} A_{22}^{-1} L' B_1 \end{aligned} \tag{6.32}$$

The third step is to design the fast subsystem in its second order approximation

$$A_f'' + B_f'' G_f'' \tag{6.33}$$

by placing its poles at the desired locations through G_f'' where

$$A_f'' = A_{22} + \epsilon L' A_{12} \quad , \quad B_f'' = B_2 + \epsilon L' B_1 \tag{6.34}$$

With G_s'' and G_f'' determined in the preceding manner, we calculate the composite feedback control law (6.27) as

$$u'' = (G_s'' + G_f'' L'') x + G_f'' z \tag{6.35}$$

with

$$L'' = A_{22}^{-1} (A_{21} + B_2 G_s'') + \epsilon A_{22}^{-1} L' [A_s' + B_s' G_s'] \tag{6.36}$$

The approximate design leads to a non-exact block diagonal form of the system matrix of (6.16). Also, the actual pole locations of the system will only be approximations of the poles placed for the approximate slow and fast systems.

6.2. Simulation results

Simulations for the singular perturbation design are performed on the linear model for system parameters as in section 3.2. so that the results can be compared with the previous state space simulations. The control is designed with the second order approximate procedure described in (6.28) - (6.36).

For the first simulation shown in Figures 6.1 and 6.2, poles of the slow system (6.20) are placed at $s_1, s_2 = -30$ and the fast system poles of (6.21) at $s_3, s_4 = -45$. Through the approximate design the poles that were actually realized through the computed feedback gain (6.35) for the system (6.15) are dislocated from the desired pole locations and are at $s_1, s_2 = -7.37 \pm j36.92$, $s_3 = -16.55$, $s_4 = -77.67$. From plot 6.1 rise and settle times of $T_r = 0.120\,s$ and $T_s = 0.180\,s$ are measured which are a little more than half of the times obtained for the single state feedback PD-control simulations in 3.2. In addition to the improvement in response speed we can also see the approximate second order behavior. Except for the displacement between motor and link position in the beginning of the transient response, during which the fast states z still decline, the response is free from the oscillations observed for the PD-control design as well as for the simple state feedback design in section 4.2. Also, it is critically damped, that means it does not overshoot. The input torque, however has a relatively high initial value of 3.0 Nm. This is about two and a half times of the value observed for the state space design while the latter is twice as fast. On the other hand, the pole locations for the state space design were obtained through an optimization procedure. Optimizing the singular perturbation design (which is for example given in [9]) should yield better values for the input torque.

In the second simulation, which is shown in Figures 6.3 and 6.4, we see the influence that a placement of the fast system poles farther left at $s_3, s_4 = -80$ has on the system response. The slow system poles are kept at $s_1, s_2 = -30$. Realized pole locations are at $s_1, s_2 = -17.30 \pm j46.36$, $s_3 = -18.72$ and $s_4 = -125.66$. With $T_r = 0.113\,s$ and $T_s = 0.166\,s$, we do not obtain a response much faster than in the previous case but the input torque has now an initial value of 9.0 Nm. This is actually above an acceptable range because of the resulting high force on gears and arm.

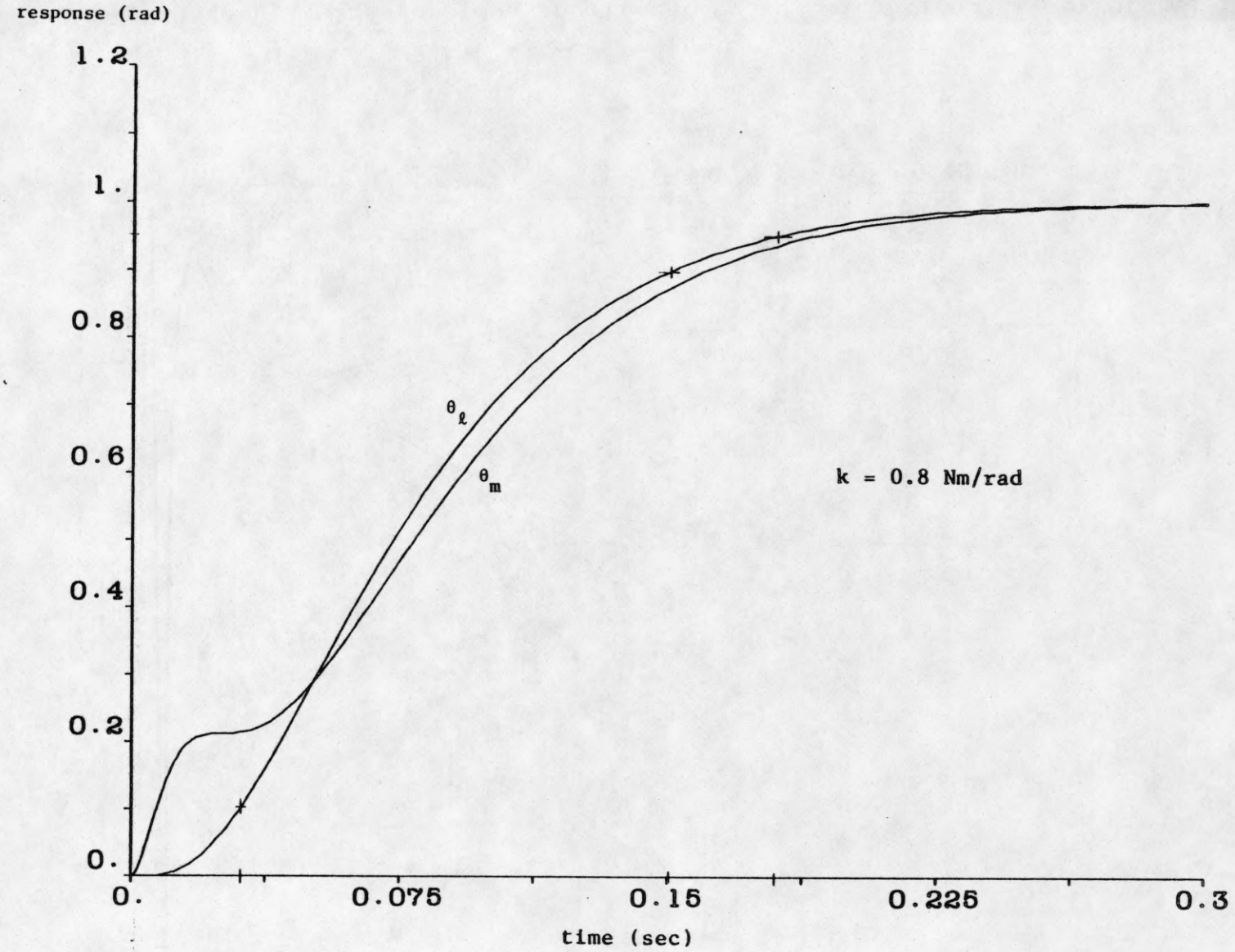

Figure 6.1 Step response for linear system with singular perturbation design

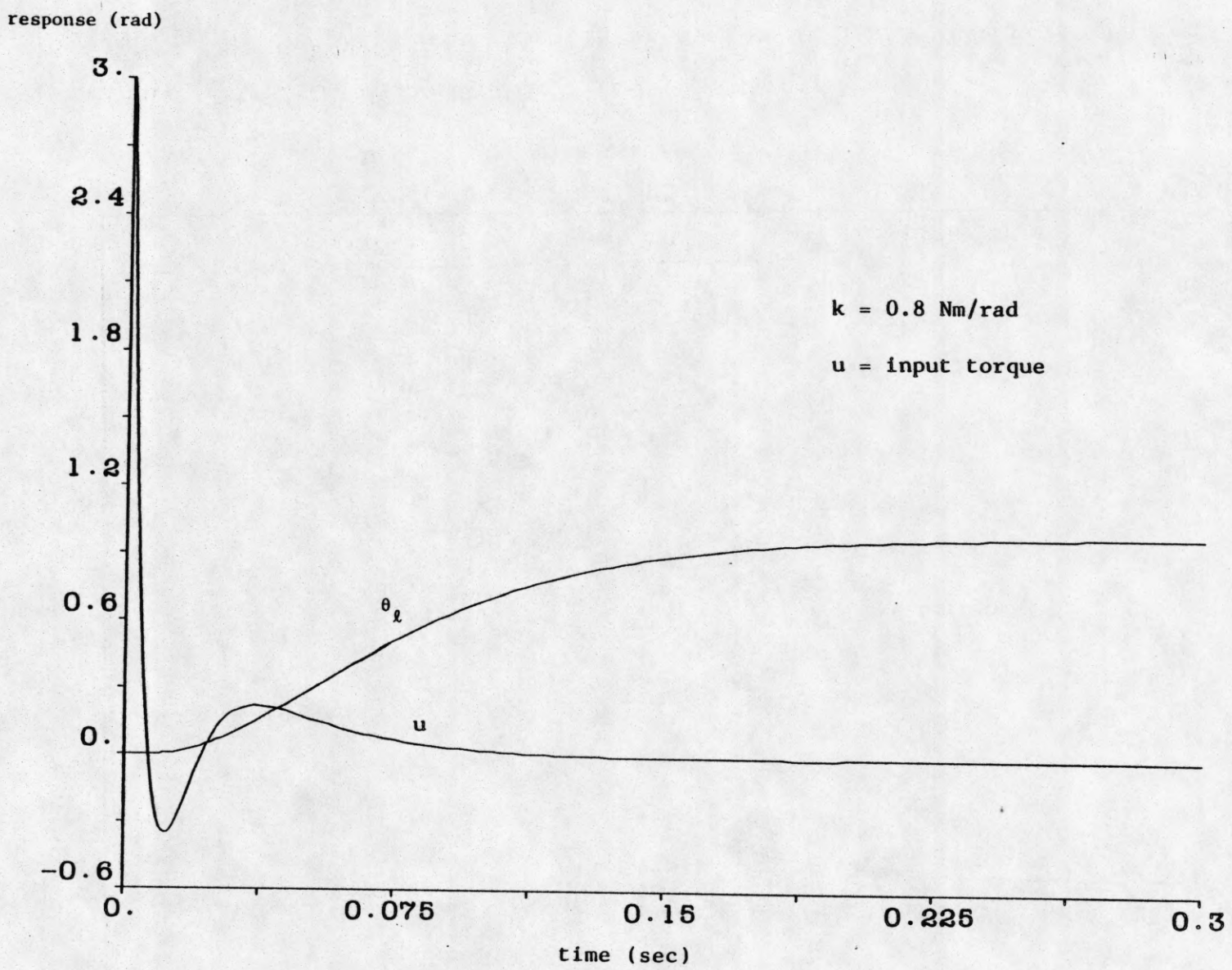

Figure 6.2 Input torque for linear system with singular perturbation design

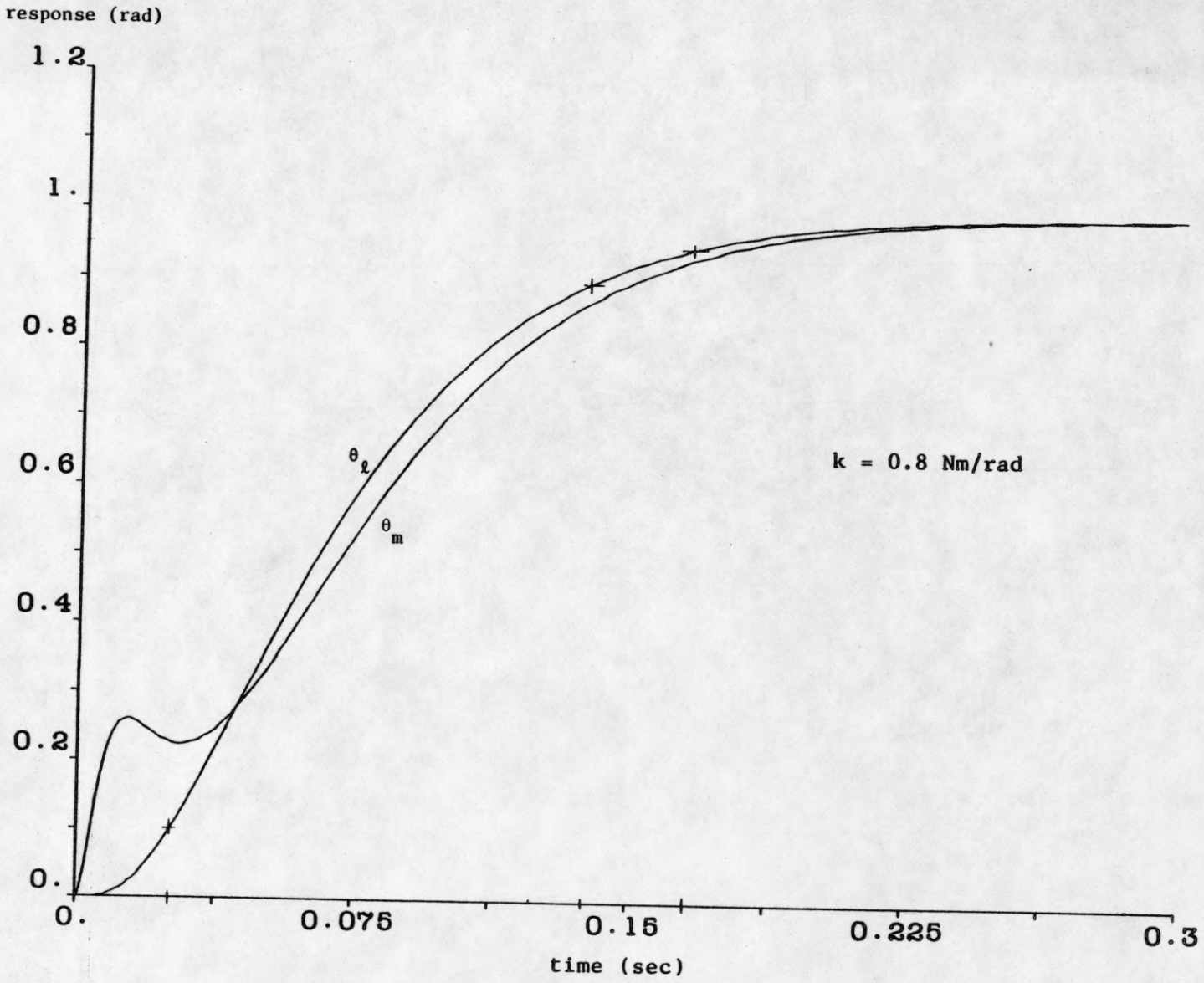

Figure 6.3 Step response for linear system with singular perturbation design

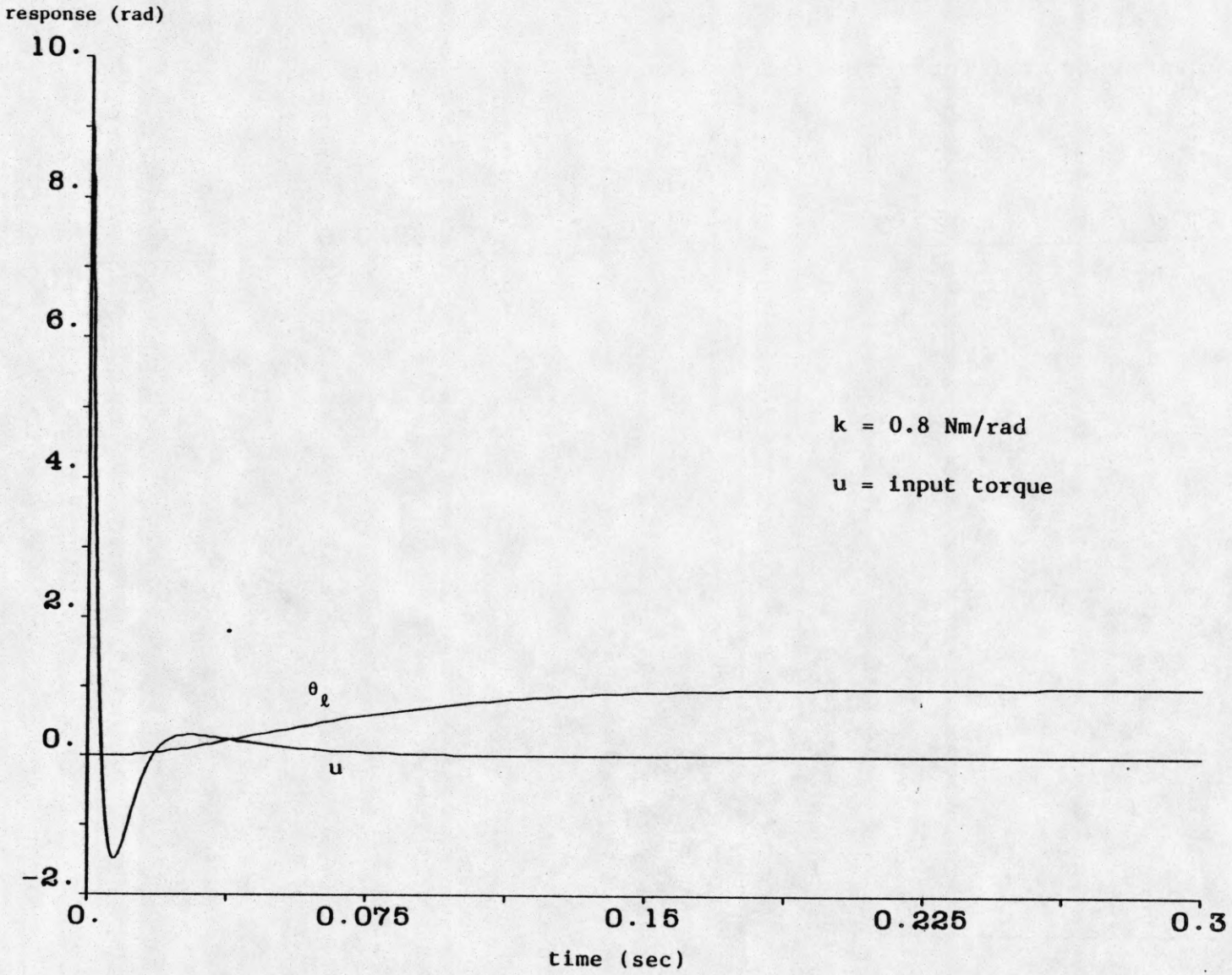

Figure 6.4 Input torque for linear system with singular perturbation design

7. SUMMARY AND CONCLUSIONS

A simulation of the transient response of our linear model with a simple PD-control reveals that the system behavior is largely dependent on inertia, compliance, and damping of the manipulator joint and link. A large inertia is helpful in decreasing oscillations of the link but slows down its motions. A small stiffness decreases the coupling between motor and link. Due to an improved capacity of storing and releasing energy, a small stiffness leads to more oscillations in the transient response of the system. A high damping of the link on the one hand contributes to a damping of the arm oscillations, but on the other hand, slows down the arm motions. The best results are obtained with a small inertia, large stiffness and large damping.

From the comparison of the simulations for the state space design with those for the PD-control we have been able to see that the former had in all cases the faster response. Since the poles can be placed arbitrarily in the case of a full state feedback we have also been able to eliminate higher frequency oscillations in the unit step response. The only limits to the increase in cycle-time are mechanical stability of the robot structure and power of the motors used.

A slight decrease in the response quality evolves when the initial states for the system and those for the observer are not equal. This occurs, for example, in the case of measurement errors. However, even with these displacements the responses are better than for the simple PD-control and with an observer optimization we can minimize these disadvantages.

Using a nonlinear observer in conjunction with a nonlinear state feedback controller we have been able to recover exactly the linear behavior from the nonlinear system.

Finally, applying a singular perturbation design has yielded that the flexible joint shows a behavior which is in the approximation similar to the behavior of a rigid link. In addition to an increased response speed, compared to the PD-controlled system, this eases the design in the end. However, the performed simulations showed relatively high values for the input torque, in comparison to the state space design. Optimization procedures can solve this problem and should be applied here.

We have not considered the robustness issue arising from parameter disturbances, external disturbances, and inexact cancellation of nonlinearities. As shown in [9] and the references therein, a number of techniques such as variable structure control or parameter estimation schemes can now be added to the design here to improve the system robustness.

REFERENCES

[1] E. I. Rivin, "Effective rigidity of robot structures: Analysis and enhancement," *Proc. 1985 American Control Conference*, Boston, MA, June 1985.

[2] L. M. Sweet and M. C. Good, "Re-definition of the robot motion control problem," *Proc. 23rd IEEE CDC*, Las Vegas, Vol. 2, p. 724-732, 1984.

[3] R. Marino and M. W. Spong, "Nonlinear control techniques for flexible joint manipulators: A single case study," *Proc. 1986 IEEE Conf. on robotics and automation*, San Francisco, March 1986.

[4] R. Su, "On the linear equivalence of nonlinear systems," *System and control letters*, 2, p. 48-52, 1982.

[5] A. J. Krener and A. Isidori, "Linearization by output injection and nonlinear observers," *System and control letters*, 3, p. 47-52, 1983.

[6] J. Y. S. Luh, "Conventional controller design for industrial robots - a tutorial," *IEEE Trans. Syst., Man, Cybern.*, Vol. SMC-13. No. 3, p. 304, May/June 1983.

[7] I. McCausland, Introduction to optimal control, New York, London: John Wiley & Sons Inc., p. 195, 1969.

[8] M. W. Spong, "Modeling and control of elastic joint robots," *ASME Journal of dynamical systems, measurement and control*, December, 1987.

[9] P. Kokotovic, H. K. Khalil, and J. O'Reilly, Singular perturbation methods in control: Analysis and design, London, New York, Tokyo: Academic Press Inc., 1986.

APPENDIX I

Derivation of stability boundary for PD-control and feedback of the link position θ_l

We derive the stability boundary for the system with PD-control and feedback of the link position θ_l with the Routh-Hurwitz criterion. Since our system is of fourth order, the coefficients $a_0, \ldots, a_4$ of the characteristic polynomial

$$Q(s) = a_0 s^4 + a_1 s^3 + a_2 s^2 + a_3 s + a_4 \tag{I.1}$$

must fulfill the following conditions:

1. All coefficients $a_0, \ldots, a_4$ have the same sign.

2. $a_1 a_2 - a_0 a_3 > 0.$

3. $a_1 a_2 a_3 - a_1^2 a_4 - a_0 a_3^2 > 0.$

For the coefficients $a_0, \ldots, a_4$ we obtain from $Q(s) = 1 + G_{0l}$ with equation (3.4) the values

$$\begin{aligned} a_0 &= J_m J_l & a_3 &= k\,[(B_m + B_l) + K_p T_D] \\ a_1 &= B_m J_l + B_l J_m & a_4 &= k K_p \\ a_2 &= k(J_m + J_l) + B_m B_l \end{aligned} \tag{I.2}$$

Hence, the first condition for asymptotic stability is fulfilled for all $K_p > 0$ because all coefficients have then a positive sign.

For the second condition we obtain

$$(B_l J_m + B_m J_l)\cdot[k(J_m + J_l) + B_m B_l] - k J_m J_l [(B_m + B_l) + K_p T_D] > 0 \tag{I.3}$$

from which follows

$$K_p < \frac{(B_l J_m + B_m J_l)\cdot[k(J_m + J_l) + B_m B_l]}{k T_D J_m J_l} - \frac{B_m + B_l}{T_D}, \tag{I.4}$$

and after some rearrangement

$$K_p < \frac{1}{T_D}\left|\left(\frac{B_m}{J_m} + \frac{B_l}{J_l}\right)\left(J_m + J_l + \frac{B_m B_l}{k}\right) - (B_m + B_l)\right| \tag{I.5}$$

For $J_m + J_l >> \frac{B_m B_l}{k}$, which can be assumed if either the stiffness k is large or the link damping B_l is small, expression (I.5) can be reduced to

$$K_p < \frac{1}{T_D}\left|\frac{J_l}{J_m} B_m + \frac{J_m}{J_l} B_l\right| = K_{p1} \tag{I.6}$$

This approximation is non-critical, which means that the exact boundary of (I.5) is always larger than the approximate boundary of (I.6).

When we plug in the coefficients which contain K_p into the third Hurwitz condition, we obtain

$$a_1 a_2 k\,[(B_m + B_l) + K_p\,T_D] - a_1^2\,k\,K_p - a_0 k^2[(B_m + B_l) + K_p\,T_D]^2 > 0\,, \qquad \text{(I.7)}$$

and after some rearrangement

$$0 > K_p^2(a_0 k^2 T_D^2) + K_p\,[2a_0 k^2 (B_m + B_l)\,T_D + a_1^2\,k - a_1 a_2 k\,T_D]$$

$$+ a_0 k^2 (B_m + B_l)^2 - a_1 a_2 k\,(B_m + B_l)$$

$$= K_p^2 + K_p \cdot \left| 2\,\frac{B_m + B_l}{T_D} + \frac{a_1^2}{a_0 k\,T_D^2} - \frac{a_1 a_2}{a_0 k\,T_D} \right| + \left| \frac{(B_m + B_l)^2}{T_D^2} - \frac{a_1 a_2}{a_0 k\,T_D^2}\,(B_m + B_l) \right| \qquad \text{(I.8)}$$

Because the highest order coefficient K_p^2 of this second order polynomial has a positive sign, the polynomial has values smaller than zero if K_p lies between its two zeros $K_{p_{01}}$ and $K_{p_{02}}$ given by

$$K_{p_{01}}, K_{p_{02}} = -\frac{p}{2} \pm \left| \frac{p^2}{4} - q \right|^{\frac{1}{2}} \qquad \text{(I.9)}$$

with

$$p = 2\,\frac{B_m + B_l}{T_D} + \frac{a_1^2}{a_0 k\,T_D^2} - \frac{a_1 a_2}{a_0 k\,T_D} \qquad \text{(I.10)}$$

and

$$q = \frac{(B_m + B_l)^2}{T_D^2} - \frac{a_1 a_2}{a_0 k\,T_D^2}\,(B_m + B_l) \qquad \text{(I.11)}$$

For large stiffnesses k or small dampings B_l we make again the above approximation

$$\frac{a_2}{k} = J_m + J_l + \frac{B_m\,B_l}{k} \approx J_m + J_l$$

and

$$\frac{a_1^2}{k} = \frac{(Bm\,J_l + B_l\,Jm)^2}{k} = 0\,.$$

This yields

$$p = \frac{1}{T_D} \left| 2(B_m + B_l) - \left| \frac{B_m}{J_m} + \frac{B_l}{J_l} \right| (J_m + J_l) \right| \qquad \text{(I.12)}$$

$$= \frac{1}{T_D} \left| (B_m + B_l) - \left| \frac{J_l}{J_m} B_m + \frac{J_m}{J_l} B_l \right| \right| \qquad \text{(I.13)}$$

and

$$q = \frac{1}{T_D^2} \left| (B_m + B_l)^2 - \left| \frac{B_m}{J_m} + \frac{B_l}{J_l} \right| (J_m + J_l)(B_m + B_l) \right|$$

$$= -\frac{1}{T_D^2}\left(\frac{J_l}{J_m}B_m + \frac{J_m}{J_l}B_l\right)(B_m + B_l) \tag{I.14}$$

For $K_{P_{01}}, K_{P_{02}}$ we obtain then

$$K_{P_{01}}, K_{P_{02}} = -\frac{1}{2T_D}\left[(B_m + B_l) - \left(\frac{J_l}{J_m}B_m + \frac{J_m}{J_l}B_l\right)\right] \pm \left(\frac{1}{4T_D^2}\left[(B_m + B_l) - \left(\frac{J_l}{J_m}B_m + \frac{J_m}{J_l}B_l\right)\right]^2 + \frac{1}{T_D^2}\left(\frac{J_l}{J_m}B_m + \frac{J_m}{J_l}B_l\right)(B_m + B_l)\right)^{\frac{1}{2}} \tag{I.15}$$

$$= -\frac{1}{2T_D}\left[(B_m + B_l) - \left(\frac{J_l}{J_m}B_m + \frac{J_m}{J_l}B_l\right)\right] \pm \frac{1}{2T_D}\left[(B_m + B_l) + \left(\frac{J_l}{J_m}B_m + \frac{J_m}{J_l}B_l\right)\right] \tag{I.16}$$

Equation (I.16) yields

$$K_{P_{01}} = \frac{1}{T_D}\left(\frac{J_l}{J_m}B_m + \frac{J_m}{J_l}B_l\right) \tag{I.17}$$

$$K_{P_{02}} = -\frac{1}{T_D}(B_m + B_l) \tag{I.18}$$

$K_{P_{01}}$ is equal to the approximate upper boundary of K_P from the second Hurwitz condition (equation (I.6)). Equation (I.18) is redundant since we determined in the first Hurwitz condition already that $K_P > 0$ which implies (I.18).

Hence, the final result for the stability boundary is

$$K_P < \frac{1}{T_D}\left(\frac{J_l}{J_m}B_m + \frac{J_m}{J_l}B_l\right) := K_P' . \tag{I.19}$$

The validity of this expression can be demonstrated on the example of the realistic parameter configuration of our model in section 3.2. Figure I.1 shows how the exact boundaries for K_P determined from the second and third Hurwitz condition approach the approximation K_P' for large stiffnesses k and/or small dampings B_l.

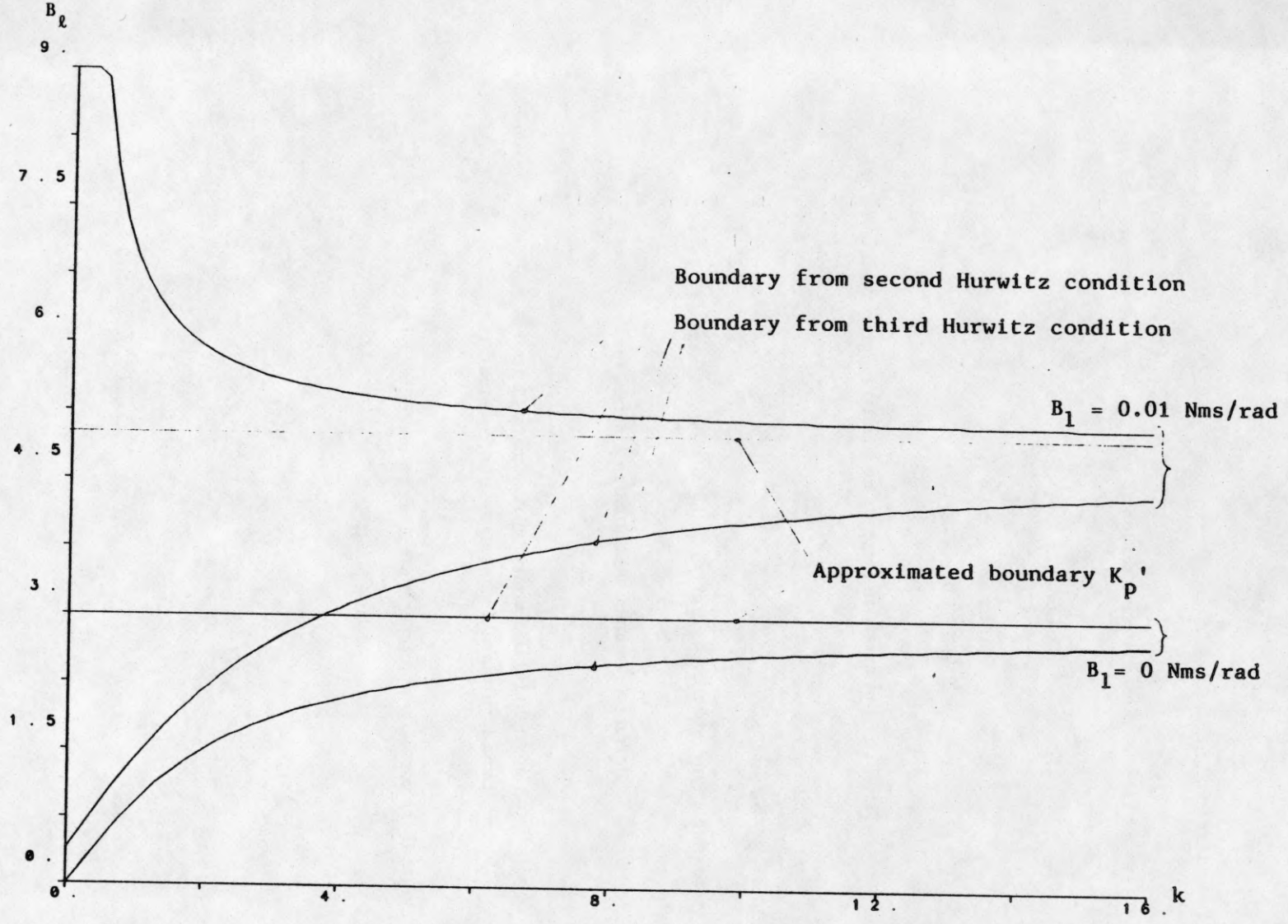

Figure I.1 Exact and approximated stability boundaries of K_p for PD-controlled system, feedback of link position

APPENDIX II

Simulation Procedures

The simulations for the PD-controlled system in section 3. were run with the software package

HR-Controls

Hunter Research Corp.
Cupertino, California

Since the program was used in on-line operation there are no simulation procedures given here.

For the state space simulations in section 4. through 6. the software package

Simnon - an interactive simulation program for
nonlinear systems. Version 4.

Copyright (c) Department of Automatic Control
Lund Institute of Technology, Lund, Sweden.

was used. Printouts of the simulation procedures are given on the following pages.

```
CONTINUOUS SYSTEM STAFEEDB
"
"
"    Simulation procedure for step response of
"    system in state space and pole placement
"
"
State x1 x2 x3 x4
Der dx1 dx2 dx3 dx4
Time t
r=if t<0 then 0 else 1
dx1=x2
dx2=-k/Jl*x1-Bl/Jl*x2+k/Jl*x3
dx3=x4
dx4=(k*x1-k*x3-Bm*x4+v)/Jm
v=-(K1*x1+K2*x2+K3*x3+K4*x4)+(K1+K3)*r
u=if v<ulow then ulow else if v<uhigh then v else uhigh
y1=x1
y2=x3
ulow:-9
uhigh:9
K1=ac4*Jm*Jl/k-K3
K2=(ac3*Jm*Jl-K3*Bl)/k-Bl-Bm-K4
K3=(ac2-k/Jl)*Jm-k-Bl*(Bm+K4)/Jl
K4=(ac1-Bl/Jl)*Jm-Bm
ac1=-ar-br-cr-dr
ac2=ar*br+ac^2+cr*dr+cc^2+(ar+br)*(cr+dr)
ac3=-((ar+br)*(cr*dr+cc^2)+(cr+dr)*(ar*br+ac^2))
ac4=(ar*br+ac^2)*(cr*dr+cc^2)
ar:-80
ac:0
br:-80
cr:-80
cc:0
dr:-80
Jm:0.0004
Jl:0.0004
Bm:0.015
Bl:0.0
k:0.8
END
```

```
CONTINUOUS SYSTEM OSTFEEDB
"
"
"    Simulation procedure for step response
"    of system in state space, optimized
"    pole placement and observer feedback
"
"    Observer poles at  ar+jac, br-jac, cr+jcc, dr-jcc
"
"
State x1 x2 x3 x4 xo1 xo2 xo3 xo4
Der dx1 dx2 dx3 dx4 dxo1 dxo2 dxo3 dxo4
Time t
r=if t<0 then 0 else 1
dx1=x2
dx2=-k/Jl*x1-Bl/Jl*x2+k/Jl*x3
dx3=x4
dx4=(k*x1-k*x3-Bm*x4+u)/Jm
dxo1=Ko1*(x1-xo1)+xo2
dxo2=Ko2*(x1-xo1)-k/Jl*xo1-Bl/Jl*xo2+k/Jl*xo3
dxo3=Ko3*(x1-xo1)+xo4
dxo4=Ko4*(x1-xo1)+(k*xo1-k*xo3-Bm*xo4+u)/Jm
u=-Kc1*xo1-Kc2*xo2-Kc3*xo3-Kc4*xo4+(Kc1+Kc3)*r
e1=x1-xo1
e2=x2-xo2
e3=x3-xo3
e4=x4-xo4
Ko1=ao1-Bm/Jm-Bl/Jl
Ko2=ao2-Ko1*(Bm/Jm+Bl/Jl)-Bm*Bl/(Jm*Jl)+k*(1/Jm-1/Jl)
Ko3=ao3*Jl/k-Ko1*(Bm*Bl/k/Jm-Jl/Jm)-Ko2*Bm*Jl/k/Jm-(Bm-Bl)/Jm
Ko4=ao4*Jl/k+Ko1*Bl/Jm+Ko2*Jl/Jm+Ko3*Bm/Jm
ao1=-ar-br-cr-dr
ao2=ar*br+ac^2+cr*dr+cc^2+(ar+br)*(cr+dr)
ao3=-((ar+br)*(cr*dr+cc^2)+(cr+dr)*(ar*br+ac^2))
ao4=(ar*br+ac^2)*(cr*dr+cc^2)
Kc1:-0.696037
Kc2:0.0264752
Kc3:2.11025
Kc4:0.0389741
ar:-200
ac:0
br:-200
```

cr:-200
cc:0
dr:-200
Jm:0.0004
Jl:0.0004
Bm:0.015
Bl:0.0
k:0.8
END

```
CONTINUOUS SYSTEM NONLINOB
"
"
"   Simulation procedure for step response of
"   nonlinear system with linearizing feedback
"   and nonlinear observer with output injection
"
"   System poles at   ar+jac,  br-jac,  cr+jcc,  dr-jcc
"   Observer poles at  aor+jaoc, bor-jaoc, cor+jcoc, dor-jcoc
"
"
State x1 x2 x3 x4 xo1 xo2 xo3 xo4
Der dx1 dx2 dx3 dx4 dxo1 dxo2 dxo3 dxo4
Time t
r=if t<0 then 0 else 1
dx1=x2
dx2=(-k*x1-M*g*l*sin(x1)-Bl*x2+k*x3)/Jl
dx3=x4
dx4=(k*x1-k*x3-Bm*x4+u)/Jm
dxo1=Ko1*(x1-xo1)+xo2
dxo2=Ko2*(x1-xo1)+(-k*xo1-Bl*xo2+k*xo3-M*g*l*sin(x1))/Jl
dxo3=Ko3*(x1-xo1)+xo4
dxo4=Ko4*(x1-xo1)+(k*xo1-k*xo3-Bm*xo4+u)/Jm
e1=x1-xo1
e2=x3-xo3
y1=xo1
y2=xo2
y3=-k/Jl*xo1-M*g*l/Jl*sin(xo1)-Bl/Jl*xo2+k/Jl*xo3
y41=-(k/Jl+M*g*l/Jl*cos(xo1))*xo2+k/Jl*xo4
y42=Bl/Jl*(k/Jl*xo1+M*g*l/Jl*sin(xo1)+Bl/Jl*xo2-k/Jl*xo3)
y4=y41+y42
v=-ac4*y1-ac3*y2-ac2*y3-ac1*y4+ac4*r
w=Jm*Jl/k*(v-u1-u2-u3-u4-u5-u6)
u1=M*g*l/Jl*(xo2^2+k/Jl-(Bl/Jl)^2)*sin(xo1)
u2=M*g*l/(Jl^2)*(2*Bl*xo2+k*(xo1-xo3))*cos(xo1)
u3=(M*g*l/Jl)^2*sin(xo1)*cos(xo1)
u4=k*Bl/(Jl^2)*(2*xo2+Bl/Jl*(xo3-xo1))
u5=((k/Jl)^2+k^2/(Jl*Jm))*(xo1-xo3)
u6=-k/Jl*(Bl/Jl+Bm/Jm)*xo4-(Bl/Jl)^3*xo2
u=if w<ulow then ulow else if w<uhigh then w else uhigh
ac1=-ar-br-cr-dr
ac2=ar*br+ac^2+cr*dr+cc^2+(ar+br)*(cr+dr)
```

```
ac3=-((ar+br)*(cr*dr+cc^2)+(cr+dr)*(ar*br+ac^2))
ac4=(ar*br+ac^2)*(cr*dr+cc^2)
Ko1=ao1-Bm/Jm-Bl/Jl
Ko2=ao2-Ko1*(Bm/Jm+Bl/Jl)-Bm*Bl/(Jm*Jl)+k*(1/Jm-1/Jl)
Ko3=ao3*Jl/k-Ko1*(Bm*Bl/k-Jl)/Jm-Ko2*Bm*Jl/(k*Jm)-(Bm-Bl)/Jm
Ko4=ao4*Jl/k+Ko1*Bl/Jm+Ko2*Jl/Jm+Ko3*Bm/Jm
ao1=-aor-bor-cor-dor
ao2=aor*bor+aoc^2+cor*dor+coc^2+(aor+bor)*(cor+dor)
ao3=-((aor+bor)*(cor*dor+coc^2)+(cor+dor)*(aor*bor+aoc^2))
ao4=(aor*bor+aoc^2)*(cor*dor+coc^2)
ulow:-9
uhigh:9
ar:-20.15
ac:54.28
br:-20.15
cr:-35.94
cc:0
dr:-58.69
aor:-200
aoc:0
bor:-200
cor:-200
coc:0
dor:-200
Jm:0.0004
Jl:0.0004
Bm:0.015
Bl:0.0
k:0.8
M:0.02
g:9.8065
l:0.5
END
```

```
CONTINUOUS SYSTEM SINGPPPL
"
"
"   Simulation procedure for step response of system
"   with singular perturbational control design
"
"
State x1 x2 z1 z2
Der dx1 dx2 dz1 dz2
Time t
r=if t<0 then 0 else 1
dx1=x2
dx2=-Bl/Jl*x2-1/Jl*z1
dz1=1/eps*z2
dz21=k2*(Bm/Jm-Bl/Jl)*x2-k2*(1/Jm+1/Jl)*z1
dz22=-eps*Bm/Jm*z2-k2/Jm*u
dz2=1/eps*(dz21+dz22)
v=G11*x1+G12*x2+G21*z1+G22*z2-G11*r
u=if v<ulow then ulow else if v<uhigh then v else uhigh
y1=x1
y2=x1-z1/k
k2=k/k1
eps=1/sqrt(k1)
ulow:-9
uhigh:9
Jm:0.0004
Jl:0.0004
Bm:0.015
Bl:0.0
k:0.8
k1:10
G11:-3.645
G12:-0.290029
G21:18.4631
G22:0.485576
END
```